ARMY RESEARCH LABORATORY

A Review of Heavy-Fueled Rotary Engine Combustion Technologies

by Chol-Bum M. Kweon

ARL-TR-5546 **May 2011**

NOTICES

Disclaimers

The findings in this report are not to be construed as an official Department of the Army position unless so designated by other authorized documents.

Citation of manufacturer's or trade names does not constitute an official endorsement or approval of the use thereof.

Destroy this report when it is no longer needed. Do not return it to the originator.

Army Research Laboratory
Aberdeen Proving Ground, MD 21005-5066

ARL-TR-5546 **May 2011**

A Review of Heavy-Fueled Rotary Engine Combustion Technologies

Chol-Bum M. Kweon
Vehicle Technology Directorate, ARL

REPORT DOCUMENTATION PAGE	Form Approved OMB No. 0704-0188

1. REPORT DATE *(DD-MM-YYYY)*	2. REPORT TYPE	3. DATES COVERED (From - To)
May 2011	Final	June 2010–January 2011

4. TITLE AND SUBTITLE
A Review of Heavy-Fueled Rotary Engine Combustion Technologies

5a. CONTRACT NUMBER

5b. GRANT NUMBER

5c. PROGRAM ELEMENT NUMBER

6. AUTHOR(S)
Chol-Bum M. Kweon

5d. PROJECT NUMBER
1VP2J1

5e. TASK NUMBER

5f. WORK UNIT NUMBER

7. PERFORMING ORGANIZATION NAME(S) AND ADDRESS(ES)
U.S. Army Research Laboratory
ATTN: RDRL-VTP
Aberdeen Proving Ground, MD 21005-5066

8. PERFORMING ORGANIZATION REPORT NUMBER
ARL-TR-5546

9. SPONSORING/MONITORING AGENCY NAME(S) AND ADDRESS(ES)

10. SPONSOR/MONITOR'S ACRONYM(S)

11. SPONSOR/MONITOR'S REPORT NUMBER(S)

12. DISTRIBUTION/AVAILABILITY STATEMENT
Approved for public release; distribution is unlimited.

13. SUPPLEMENTARY NOTES

14. ABSTRACT
The rotary engine has been used as one of the powerplants for unmanned aerial vehicles because of its many merits, such as higher power density, light weight, simple design, smooth operation, low vibration, and compact size. However, it also has demerits, such as high fuel consumption and higher maintenance requirements. This report reviews the current status of the heavy-fueled rotary engine combustion technologies and gains insights into the technology gaps that need further research and development to improve its efficiency, performance, and durability.
The major challenges for the rotary engine to use a heavy fuel such as JP-8 include its inherently low compression ratio, high heat loss due to high surface-to-volume ratio, and seal leaks. Up to now, the rotary engines have not been extensively researched and developed, particularly for heavy-fueled rotary engines, compared to the reciprocating engines. Therefore, significant opportunities in all respects exist to improve efficiency, performance, and durability of the rotary engines by using today's advanced technologies.

15. SUBJECT TERMS
rotary engines, heavy fuel, JP-8, fuel injection, fuel stratification, UAV

16. SECURITY CLASSIFICATION OF:			17. LIMITATION OF ABSTRACT	18. NUMBER OF PAGES	19a. NAME OF RESPONSIBLE PERSON
a. REPORT	b. ABSTRACT	c. THIS PAGE			Chol-Bum M. Kweon
Unclassified	Unclassified	Unclassified	UU	94	19b. TELEPHONE NUMBER (*Include area code*) 410-306-4734

Standard Form 298 (Rev. 8/98)
Prescribed by ANSI Std. Z39.18

Contents

List of Figures

List of Tables

INTENTIONALLY LEFT BLANK.

Executive Summary

In recent years, rotary engines have been used for various applications, including automobiles, motorcycles, and unmanned aerial vehicles (UAVs). The power range of the current rotary UAV engines around the world is between 20 and 90 hp. The UAVs that use a rotary engine as its powerplant include Harpy, Hermes, Shadow, and Searcher. The demand for UAVs is projected to dramatically increase around the world.[1–5] However, our knowledge of the rotary engine is surprisingly inadequate, particularly for heavy-fueled rotary engines. This report summarizes the understanding and finding from the currently available literature in rotary engines, more specifically heavy-fueled rotary engines.

A rotary engine has many advantages compared to a reciprocating engine, such as higher power density, smooth operation, simple design, low vibration, compact size, and light weight. But, it has also disadvantages like higher fuel consumption and more frequent maintenance requirements. However, these drawbacks have been steadily improved upon for gasoline-fueled rotary engines by some manufacturers, such as Mazda. Recently, the rotary engine has become attractive to some applications, where the merits are becoming more important. Today's advanced combustion control and sophisticated fuel injection system may make the rotary engines more efficient and quite. Manufacturing accuracy and materials technology may resolve the issues of sealing leaks.

Rotary engines, particularly heavy-fueled rotary engines, have not been extensively researched and developed compared to the reciprocating engines. Hence, considerable opportunities exist to improve the efficiency and performance of the rotary engines by implementing advanced fuel systems, ignition systems, control systems, and system optimization. In addition, the rotary engine configuration itself can be further optimized with the currently available sophisticated computational fluid dynamics tools.

Engine efficiency can be improved by improving combustion efficiency and reducing cooling, exhaust, and friction losses, while maintaining combustion noise levels below a threshold. Improving combustion efficiency requires a thorough understanding of fuel spray, fuel-air

[1]Institute for Defense and Government Advancement (IDGA) Web site. UAVs Becoming Big Business in Defense Industry. http://www.idga.org/military-aircraft/articles/uavs-becoming-big-business-in-defense-industry/ (accessed 9 March 2011).

[2]Federation of American Scientists (FAS) Web site. Unmanned Aerial Vehicles. http://www.fas.org/spp/starwars /docops/amd/Chapter-2.htm (accessed 9 March 2011).

[3]Bharat Book Bureau. *Opportunities for Composites in the Global UAV Market 2009–2014: Trends, Forecast and Opportunity Analysis*; Market Research Report, September 2009.

[4]Federation of American Scientists (FAS) Web site. Military Unmanned Aerial Vehicle Development Status and Trend. http://www.fas.org/ (accessed 9 March 2011).

[5]Market Research. The Unmanned Aerial Vehicles (UAV) Market 2010–2020: Technologies for ISR and Counter-*Insurgency*; Market Research Report, 18 June 2010.

mixing, ignition, and combustion processes. An inherently low compression ratio of the rotary engine requires external ignition sources, such as spark or glow plugs. Direct-injection fuel stratification would enable the rotary engine to improve combustion efficiency by keeping the fuel-air mixture from near the leading and trailing sides of the combustion chamber. This improved efficiency would reduce engine-out unburned and incompletely burned gases. Use of a turbocharger or supercharger would deliver higher airflow into the combustion chamber for lean combustion. As it is already proven in diesel engines compared to gasoline engines, lean combustion achieves higher combustion efficiency. Cooling heat loss can be reduced by an optimized combustion rate and the use of low thermal conductivity materials on the inner surfaces of the combustion chamber. Friction loss can be decreased by optimizing the seal loading and by using lower friction materials for the seals with minimal seal wear. Friction loss can also be decreased by reducing the seal area.

Various areas for further research and development are proposed in the conclusion and recommendations section to improve efficiency, performance, durability, and reliability of the rotary engines. Several of these areas were studied in the past; however, the scope of work was insufficient, and crucial conclusions were not made. Furthermore, most of these works were performed more than a decade or two ago. Thus, the currently available advanced technologies were not used in their research and development. It is worthwhile to more thoroughly research the rotary engines by using advanced systems and tools available today.

1. Introduction

This report reviews the current status of the heavy-fueled rotary engine combustion technologies. The details include the current understanding of combustion chamber design, fuel spray, ignition system, apex and side seals, heat loss and flame quenching, turbocharging, and supercharging for heavy-fueled rotary engines. The objectives of this report are as follows:

- To understand the state-of-the-art rotary engine combustion technologies.
- To gain insights into technology gaps that need further research and development.
- To document these findings by reviewing many technical papers, journals, and industry reports.

Rotary engines have been used for many different applications, including automobiles, aircraft, motorcycles, and power generators. Most of the applications have used spark-ignited gasoline fuel. A few companies, such as Curtiss-Wright Corporation and John Deere, Inc., developed spark-assisted stratified-charge rotary engines (SCREs) of heavy fuels for the general aviation community. Despite the advantages of rotary engines compared to reciprocating engines, most of these efforts were stopped because of reasons such as high fuel consumption. A few companies, such as Mazda and UAV Engines Ltd. (UEL), have continued to improve the efficiency and performance of rotary engines. Yet, these engines use gasoline fuel.

As the requirements for internal combustion engines have changed with time, a rotary engine is viewed as one of the most promising powerplants for UAVs and ground vehicles because of its high power density, compact size, light weight, and low vibration—characteristics that are becoming more important in advanced vehicles. Furthermore, the fuel economy of rotary engines can be improved by reducing seal leaks and heat losses; improving combustion with advanced fuel and ignition systems; and better controlling combustion with advanced electronic engine controllers. However, small-scaled internal combustion engines are challenging because the aforementioned systems are not fully developed yet. As the demand for small-scaled engines increases, those systems will then advance.

This report covers the following areas:

- The brief history and operating principles of the rotary engine and its advantages and disadvantages.
- The effects of compression ratio (CR) and ignition on rotary engine combustion and efficiency as well as direct-injection stratified-charge rotary engines (DI-SCREs) and small heavy-fueled rotary engines.

- The effects of combustion chamber design, fuel spray, ignition—including both spark and glow plug ignitions—apex and side seals, heat loss and flame quenching, and boosted intake pressure on heavy-fueled rotary engine performance and efficiency.
- The findings and recommendations for further research and development.

2. Brief History and Principles of the Rotary Engine

2.1 Brief History

The first patent of the Wankel piston machine was issued to Felix Wankel in 1933; he went on to collaborate with the German motorcycle manufacturer NSU (currently Audi) in 1954 (*1*). Since then, the Wankel rotary engine has been used in automobiles, motorcycles, aircraft, snow mobiles, power generators, trucks, lawn mowers, compressors, outboards, and chain saws (*1–19*). However, all of the applications had been based on spark-ignited gasoline with intake throttling. Major automobile manufacturers such as General Motors, Toyota, Ford, and Mercedes-Benz discontinued the Wankel engine development programs by the mid 1970s (*1, 20*), mainly because of its poor fuel economy, which was unacceptable after the Organization of the Petroleum Exporting Countries (OPEC) oil embargo in 1973 and the subsequent gasoline price increase. However, some programs have continued at companies such as Toyo Kogyo (currently Mazda) and Curtiss-Wright Corporation. Mazda has been very successful in improving the performance and efficiency of the Wankel rotary engine. They have produced numerous models of gasoline-fueled rotary engine automobiles, especially sports cars, starting from Cosmo Sport 110S in 1967 to RX-8 with a 232-hp RENESIS (Rotary Engine's geNESIS) rotary engine in 2004 (*1*, *20, 21*).

In the mid 1960s, the Curtiss-Wright Corporation, which owned the North American rights to the Wankel rotary engine, started researching spark-assisted SCREs to increase power and reduce fuel consumption (*5*). This research led to the development of multi-fuel-capable rotary engines (*6*). During the late 1970s and early 1980s, uncertainty over aviation gasoline prices and availability triggered the need for general aviation airplane engines that could burn kerosene. Kerosene or jet fuel was proposed by the general aviation community because it was used for commercial aircrafts at that time (*22*). The National Aeronautics and Space Administration's (NASA's) preliminary engineering program selected the Curtiss-Wright Corporation's SCRE as the best engine for this application among the candidates of gas turbines, diesel engines, and spark-ignition reciprocating engines (*7*, *22*, *23*). In 1983, the Curtiss-Wright Corporation was awarded for the NASA's Rotary Engine Technology Enablement Program. In 1984, the Curtiss-Wright Corporation sold its rotary engine business to John Deere, Inc. (*8*, *24*).

John Deere researched multi-fuel-capable rotary engines, and the design was proposed for several U.S. Marine combat vehicles in the late 1980s (*2*). In 1986, John Deere and NASA

demonstrated an SCRE with brake-specific fuel consumption (BSFC) of 310 g/kWh (0.51 lb/hp-h) at 160 hp at 8000 rpm. They set a BSFC goal of 213 g/kWh (0.35 lb/hp-h) by using turbo-compounding, adiabatic components, a lightweight rotor, and reduced friction (*5*). Their experimentation showed that a lean mixture could lower the BSFC (*25*).

Hydrogen has also been used in a rotary engine combined with a fuel cell, which is termed a Hydro Wankel Cell, with a goal to make a zero-emission engine (*26*, *27*). Mazda is one of the main players in developing a hydrogen rotary engine (*9*). Their research is focused on developing the RENESIS hydrogen rotary engine. Mazda commercialized the first-in-the-world hydrogen rotary engine, termed as the Mazda RX-8 Hydrogen RE, in 2006. The RX-8 Hydrogen RE uses a dual fuel system (i.e., hydrogen and gasoline).

A survey showed that a rotary engine is one of the most promising powerplants for hybrid vehicles because of its high power density, compact size, light weight, and low vibration—characteristics that are becoming more important in advanced vehicles (*10*, *28*). In recent years, several companies announced that they are considering rotary engines for their hybrid powerplants (*9*, *11*, *12*). Mazda already commercialized the Mazda Premacy Hydrogen RE Hybrid in 2009 (*9*). This hybrid combined the Mazda RX-8 Hydrogen RE with their hybrid system. Several other companies such as General Motors, AVL, FEV, Lotus Engineering, and Rotapower are considering a rotary engine as a range extender for their plug-in hybrid cars (*11*, *12*). In the plug-in hybrids, the engine is used as a power generator. The engine is easier to optimize because it can run on only optimal points.

Most of the current hybrid cars use the Atkinson cycle, which is a modified Otto cycle (i.e., conventional gasoline cycle) in which the intake valve is closed later than at a normal timing (*29*). Late intake valve closing leads to lower effective CR while the expansion ratio is unchanged. Late intake valve closing allows higher geometric CR, which is different from the effective CR, without causing engine knocking or detonation. Late intake valve closing also reduces pumping loss. Since expansion ratio is proportional to thermal efficiency, the Atkinson cycle allows higher thermal efficiency than conventional gasoline engines. When the Atkinson cycle is combined with a supercharger, it is called the Miller cycle. The Miller cycle improves power density by introducing more fresh air into the combustion chamber by increasing intake manifold pressure (*30*). Implementing the Atkinson or Miller cycle in rotary engines can improve efficiency and power; however, doing so will be difficult because the rotary engine does not have intake and exhaust valves. The method used by Mazda for side ports may be applied.

Other areas of interest for rotary engines are in small, mini, and microscale powerplants. Recently, the concept of the rotary engine has been used for Power MEMS (Micro Electro-Mechanical System) (*31–40*), which describes microsystems for generation of power or pumped heat (*31*). The University of California at Berkeley is the leading proponent of a rotary engine for Power MEMS.

In recent years, rotary engines have been used in small-scaled unmanned aerial vehicles (UAVs) in several countries. The main manufacturers of the UAV rotary engines include UAV Engine Ltd. (UEL), Moller International, Cubewano, and Plextek (*13*, *41–45*). The power range of current UAV engines around the world is between 20 and 90 hp (*45*). The UAVs that use a rotary engine as its powerplant include Harpy, Hermes, Shadow, and Searcher. The demand for the UAVs is projected to dramatically increase around the world.

Although rotary engines may not be as successful as reciprocating engines, rotary engines may be used in areas where size, weight, and vibration are critical. The fuel economy of rotary engines may be enhanced by improving combustion, reducing seal leaks and heat loss in the working chambers, and developing modified rotary engines, such as the rotary Atkinson or Miller cycle engines.

2.2 Operating Principles of the Rotary Engine

A rotary engine has fewer moving parts than a reciprocating engine, as shown in figure 1 (*19*). The main parts of the rotary engine include an eccentric shaft, a three-flank rotor, and a trochoid housing. In figure 2 (*19*), the three-flank rotor rotates about its center of gravity and at the same time rotates around the crankshaft centerline. The rotor turns at one-third of the crankshaft speed, driven by a gear on the crankshaft. The three corners of the rotor divide the trochoid-shaped rotor housing into three working chambers (i.e., trochoid chamber). Each working chamber executes a full four-stroke cycle on each rotation of the rotor. Thus, the engine achieves one power stroke per revolution of the crankshaft. The system is completely balanced by counterbalancing the crankshaft. As an example, unlike the four-stroke reciprocating engines, rotary engines do not have intake and exhaust valves to control flow through the intake and exhaust ports.

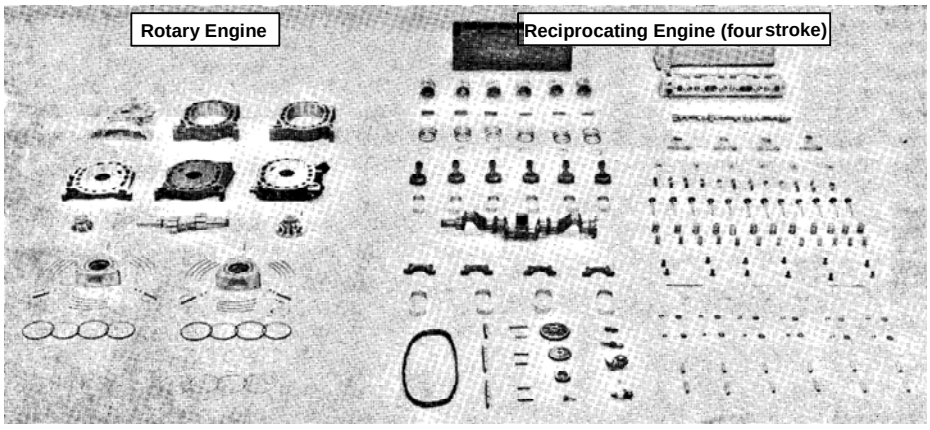

Figure 1. Main parts of rotary (left) and four-stroke reciprocating (right) engines (*19*).

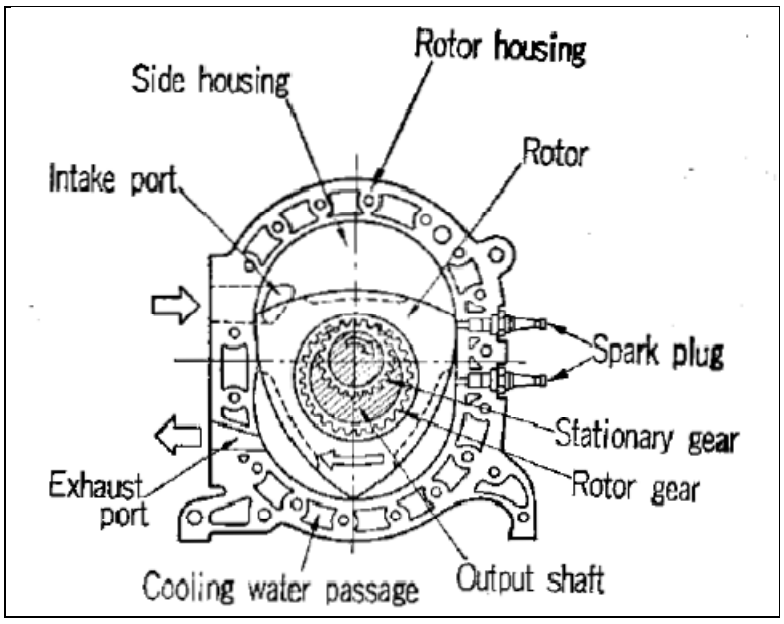

Figure 2. A rotary engine showing the three-flank rotor, trochoid housing, and crankshaft (*19*).

Figure 3 compares the basic principles of the Wankel rotary and reciprocating engines (*46*). The fuel-air mixture enters into the first chamber during the intake process for the rotary engine; the fuel-air mixture is then compressed as the rotor rotates during the compression process. For an SCRE, air enters into the combustion chamber, and fuel is injected and mixed with the air during the compression process. When the compressed fuel-air mixture reaches its target spark timing, a spark plug ignites the fuel-air mixture, and the combusted gases expand during the expansion process. The expansion continues until the rotor reaches the exhaust port where the combustion products exit. These processes take place in all three chambers at the same time. Three events of combustion are achieved in every rotation of the rotor within the housing. This leads to a flatter torque curve for the rotary engine compared with a one-cylinder reciprocating engine in which combustion occurs for every two revolutions of the crankshaft. Details of rotary engine operation can be found in the literature (*20*, *47*).

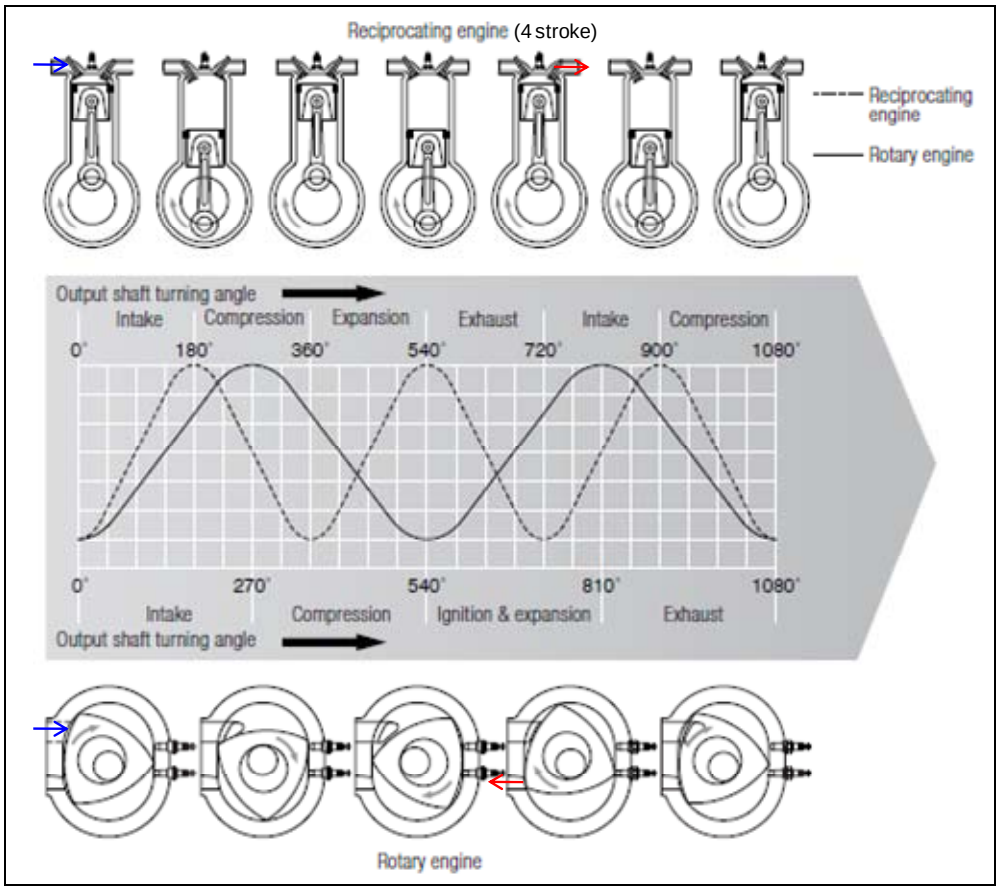

Figure 3. Comparison of basic operating principles of the rotary (top) and reciprocating (bottom) engines (*46*).

A significant difference between the two engines is the shape of the combustion chamber in all processes, as shown in figure 3. In the rotary engine, the combustion volume is traveling while the combustion process takes place. The main difference between the mechanisms of the two engines to get the turning force is in the expansion process, as shown in figure 4 (*46*). The combustion gases in the reciprocating engine force the piston down, and the mechanical force is transferred to the connection rod, which rotates the crankshaft. However, the combustion gases in the rotary engine exert force to the flank of the rotor. As a result, one of the three flanks of a triangle is forced toward the center of the eccentric shaft. This movement consists of two divided forces: one being the force toward the crankshaft center and the other being the tangential force that rotates the crankshaft.

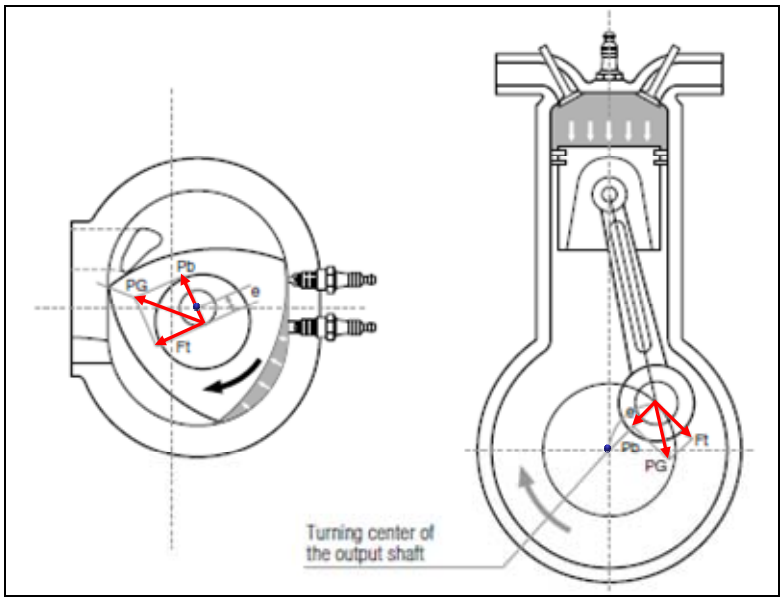

Figure 4. Comparison of force mechanisms of the rotary (left) and reciprocating (right) engines (*46*).

The trochoid chamber is always divided into three working chambers. Because of the rotation of the rotor, the three working chambers are always in motion and successively execute the four processes of intake, compression, ignition and expansion, and exhaust inside the trochoid chamber. Each process takes place in a different location in the trochoid chamber, whereas the four processes take place within each cylinder in the reciprocating engine.

2.3 Advantages and Disadvantages of the Rotary Engine

Rotary engines have many advantages compared to reciprocating engines. These advantages include higher power density, smooth operation, low vibration, simple design, compact size, and light weight. The main disadvantage of the rotary engine is inefficiency, which has made it less attractive to many manufacturers. Another major disadvantage of the rotary engine is frequent maintenance and overhaul. For example, the UEL (UAV Engine Ltd.) rotary engine used in the U.S. Army's Shadow requires a complete overhaul after about 250 h of operation (*48*). Low engine efficiency has been continuously improved upon by some manufacturers such as Mazda. The rotary engine is attractive to some applications where its merits are becoming more important. Today's advanced combustion control and sophisticated fuel injection system may make the rotary engines more efficient. Manufacturing accuracy and materials technology may resolve the issues of sealing leaks. Table 1 shows the advantages and disadvantages of the rotary engines with respect to four-stroke reciprocating engines, its main competitor.

Table 1. Advantages and disadvantages of rotary engines (*10*, *13*, *20*, *49*, *50*).

Advantages	
Effects	**Causes**
High specific power density High power-to-weight ratio High power-to-volume ratio	• Higher operating speed possible by rotation ➡more air in and more fuel in per time ➡more power output per engine total weight. • One power pulse per shaft rotation.
Smooth operation	• Continuous unidirectional motion. • No reciprocating parts such as connecting rods and conventional crankshaft with weight balances, only the rotor geared directly to the output shaft; eccentric shaft shape counterbalances the offset rotor to eliminate high-speed wobbling. • Ease of balancing. • One power pulse per shaft rotation.
Simple design	• Very few parts and no valves and valve trains. • Half the number of parts of reciprocating engine (four-stroke).
Compact size and lightweight	• Fewer parts. • Less volume occupation. • About a third of the bulk and weight of a reciprocating engine (four-stroke).
Low vibration levels	• Three power strokes per each rotation of eccentric output shaft, which leads to extremely low torque oscillation and vibration.
Lower noise	• Slower fuel burning rate and less mechanical noise. • Depends on engine calibration.
More mixing time	• One-third of output shafts speed (slow rotor speed) ➡suited for stratification. • Three power pulses per rotor rotation/three shaft rotations per rotor rotation.
Higher volumetric efficiency	• No valve restrictions.
Multifuel capability	• Separates combustion region from intake region, which prevents localized hot spots from forming; prevent preignition or detonation.
Lower cost	• Simple design and smaller size , which results in lower manufacturing costs.
Lower NOx	• Lower flame temperatures.
Easier design of emissions control devices	• Compact size.
Nonreversibility of seal paths	• One direction rotation.
Sizing flexibility	• Just add additional rotors.
Mechanical simplicity	• Fewer parts and reciprocation parts.
Reliability	• Fewer overall stress points. • Positive net torque through the shaft.
Disadvantages	
Higher fuel consumption	• Less efficient; however, improved as the technology evolves. • High fuel consumption at low speeds➡insufficient torque.
Lower thermal efficiency	• High surface-to-volume ratio➡high heat losses➡flame quenching. • Long and narrow combustion chamber➡longer flame travel time. • Particularly at low-end torque.
Higher oil consumption	• Rotary engine burns a lot of oil.
Coolant system weight	• For liquid-cooled rotary engine.
Maintenance	• Constant maintenance
Manufacturing	• Not well established; requires different tooling from reciprocating engines.

3. Rotary Engines for Heavy Fuels

Heavy fuels (Jet-A, Jet-A1, JP-5, JP-8, diesel, etc.) are defined as kerosene-based, commonly used in jet aircraft engines. These fuels are safer alternatives to gasoline and are more readily available and cost-effective both on land and sea. Among them, JP-5 and JP-8 are the preferred fuels in military applications because of reduced logistic burden and safety. Also, most heavy-duty military engines are developed to be operated on heavy fuels such as diesel. However, small engines have some technical challenges due to the large surface-to-volume ratio, which induces large heat loss leading to inefficient combustion or misfire.

3.1 Compression Ratio

Autoignition can be obtained with a heavy fuel when the chamber temperature reaches its autoignition temperature. In a reciprocating engine, a heavy fuel-air mixture is typically ignited by compression ignition (CI) because of its higher ignition quality (i.e., higher Cetane number) and higher CR. The CRs of the reciprocating engines vary widely from below 10:1 to over 20:1 with SI engines on the lower side (typically below 13:1) and CI engines on the higher side (typically above 14:1) (*51*). However, a rotary engine is limited for high CRs because of the geometric shape of the trochoid (i.e., small displacement volume) (*49*). The maximum CR is obtained when the flanks of the rotor are shaped exactly according to the inner envelope of the trochoid; however, this is not practical. The CR for a rotary engine is defined in equation 1.

$$\text{Compression ration} = \frac{V_{th,min} + V_t + V_d}{V_{th,min} + V_t} , \quad (1)$$

where $V_{th,min}$ is the theoretical minimum volume, V_t is the sum of the combustion chamber recess and spark plug hole volumes, and V_d is the displacement volume or stroke volume.

Another limiting factor for higher CR of a rotary engine is imperfect sealing of the apex and side seals. Perfect seals between the rotor and the housing walls are needed to keep the chambers isolated and to achieve its design CR. Lower CR will lead to incomplete combustion resulting in lower combustion efficiency. Unlike a piston engine that has a ring arrangement, the rotary engine has only one sealing line of contact; therefore, it cannot reach the same tightness as in the piston engine, which leads to sealing leaks. The rotary engine should be designed to achieve as high CR as possible to autoignite a heavy fuel-air mixture by optimally designing the geometric CR and minimizing the sealing leaks. As an example, figure 5 shows the effect of the engine CR on the engine performance (*52*). In this case, the CR range (7.5 to 8.92) is narrow, thus the engine performance is increasing all but linearly. However, this trend will not linearly increase as the CR continues to increase, as shown in figure 6. Real engines have other limiting factors, such as knocking for SI engines and heat loss; therefore, the efficiency increase is even lower with increasing CR.

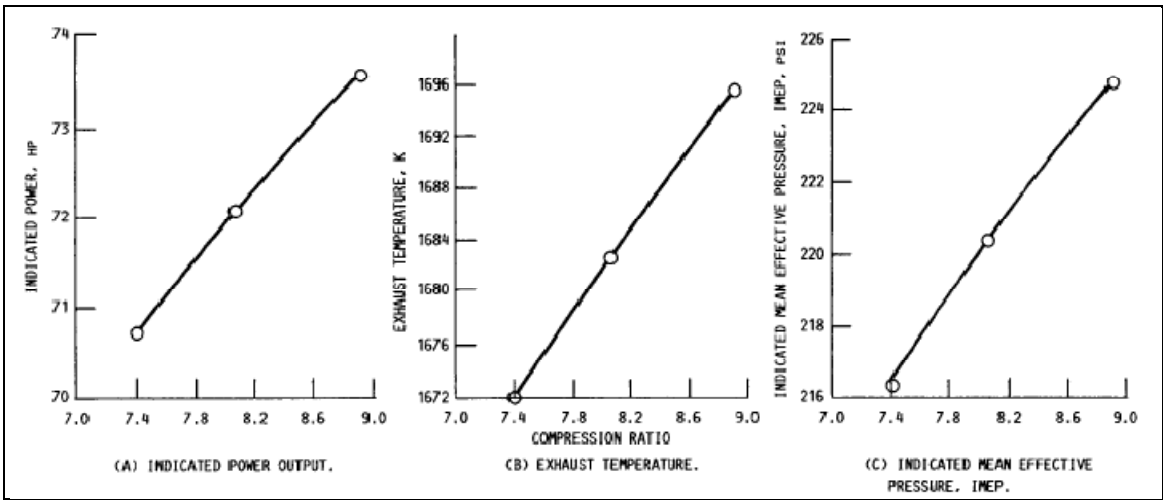

Figure 5. Indicated power, exhaust temperature, and indicated mean effective pressure (IMEP) with respect to CR (*52*).

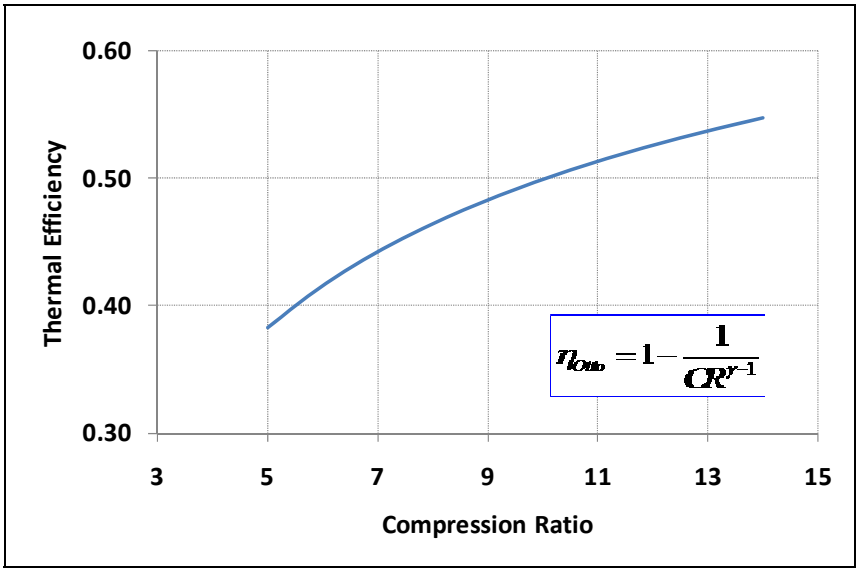

Figure 6. Thermal efficiency of an ideal Otto cycle engine with respect to CR (*51*).

3.2 Ignition

Even if the rotary engine has an optimal geometric CR and excellent apex and side sealing, it cannot reach the autoignition temperature of a heavy fuel because of its inherently small displacement. Therefore, the engine requires an additional ignition source to locally ignite the fuel-air mixture. Once a small volume of the mixture is ignited by the additional ignition source, combustion will take place with subsequent flame propagation into the unburned mixture. This additional local ignition energy (i.e., minimum ignition energy) has been obtained in the rotary engine from spark plugs or glow plugs (*2, 14, 15, 22, 52–58*). One, two, or three spark plugs have been used in the rotary engines depending on its applications (*2, 53, 54*). A pilot flame ignition system was also used to improve ignitability under lean conditions in which pilot fuel is injected toward the adjacent spark plug, and subsequently, flame propagates into the fuel-air mixture in the main chamber (*2, 54, 57, 58*), which is similar to an indirect diesel engine with a glow plug.

3.3 Direct-Injection Stratified-Charge Rotary Engine (DI-SCRE)

A major problem of the premixed SI Wankel engines is low fuel economy. DI-SCRE was developed by the Curtiss-Wright Corporation in the mid 1960s to improve fuel economy and reduce unburned hydrocarbon emissions (*20*). In a DI-SCRE rotary engine, fresh air is introduced into the working chamber through the inlet port. A circular swirl is generated as the fresh air passes through the intake port, and this swirl motion continues during the compression process. Liquid fuel injection starts at about 30° bTC (before top center). Injection duration and quantity are determined based on the required engine load. The combustion chamber is designed to provide a fuel-rich mixture (i.e., stoichiometric mixture) adjacent to a spark plug. The fuel-air mixture becomes more lean the farther it gets from the spark; eventually, the mixture consists solely of air near the walls. Right after the fuel injection starts, the spark plug ignites the fuel-rich mixture, and flame propagates. The swirling motion of the charged air continually provides air to the burning mixture. Therefore, the DI-SCRE rotary engine operates under lean conditions. As the engine speeds and loads increase, mixing time is insufficient and a locally fuel-rich mixture exists causing inefficient combustion. Insufficient mixing time can be overcome by a low equivalence ratio (or high excess air ratio) operation, increased turbulence intensity, and/or multiple injections.

Burley et al. (*59*) showed that the major causes of high hydrocarbon emissions in rotary engines were apex seal leaks, residuals (reduced flame temperature), and flame quenching due to cold-wall zones (i.e., long narrow combustion chamber) and the large surface-to-volume ratio of a rotary engine (radical removal and reaction zone cooling). Although the DI-SCRE rotary engine operated under lean conditions, combustion efficiency was poor at light load, which produced high unburned hydrocarbon emissions (*60*). One of the several possible reasons for high hydrocarbon emissions was poor in-cylinder fuel distribution, which might be caused by erratic fuel injection (*60*). The results show that the total individual cycle heat release at light

loads disagrees with the total fuel energy provided, which was caused by partial or incomplete combustion of individual cycles. The incomplete combustion would exhaust more unburned and partially burned gases; therefore, the energy released by combustion is lower than the energy provided by fuel supply. Today's sophisticated high-pressure fuel injection systems can be used to improve in-cylinder fuel distributions. This study can be done with advanced computational fluid dynamics (CFD) codes, which are presently available.

The rotary engine may be well suited for stratified-charge operation (*5*). As shown in figure 7, the waist of the rotor trochoid housing increases the air motion past a stationary injector, which enhances fuel-air mixing (*25*). Since fuel stratification is sensitive to fuel properties, especially fuel volatility (*14*), stratification is important for the rotary engine to burn heavy fuels. The Curtiss-Wright Corporation demonstrated the feasibility and advantages of the DI-SCRE rotary engine (*5*). The following attributes are the most significant advantages to using the DI-SCRE rotary engine over a premixed rotary engine (*2, 25*):

- Multifuel capability: improved fuel tolerance.
- Higher thermal efficiency.
- Lower hydrocarbon emissions except at light loads.
- Reduced throttling losses.

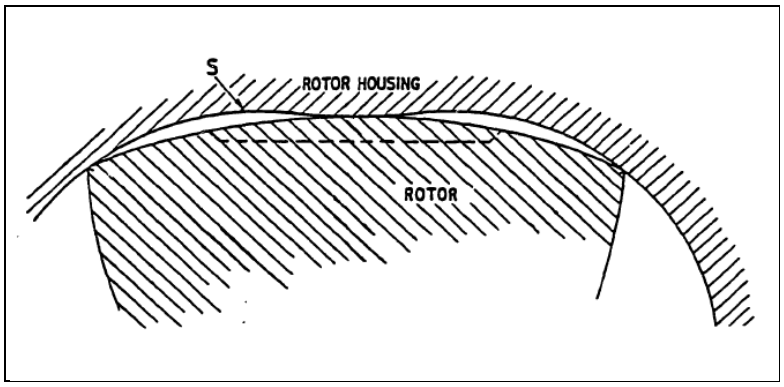

Figure 7. Rotary engine rotor and trochoid housing (*25*).

Fuel stratification is an excellent method to control combustion, which is especially beneficial for rotary engines (*14*). The realization of the DI-SCRE rotary engine depends on the better understanding of the effect of engine design and operating parameters on unsteady, multidimensional fluid flow, fuel injection, fuel-air mixing process, and combustion inside the engine's combustion chambers (*60*).

3.4 Small Heavy-Fueled Rotary Engines

A small rotary engine is defined as an engine with rotor displacement <500 cc and a generating radius smaller than 100 mm (*53*). In the past, good performance was obtained in medium and large rotary engines with rotor displacement >500 cc by using a high-pressure dual-injector configuration with a pilot-main injection sequence (*61, 62*). However, the dual-injector sequential injection system is not suitable for a small rotary engine because of space constraints. Also, for small rotary engines, the local air-fuel ratio (AFR) around the spark plug is much more dependent on engine load (i.e., fuel injection quantity) at a constant speed (*53*). Air swirl induced during the intake process is substantially decayed during the compression process for small rotary engines. As the rotor approaches the top center (TC) position, the induced swirl is extinguished (*53*). This might be caused by reduced space at the TC position.

Rotor speed plays a more distinct role in the small displacement engines because of confined spaces available for the combustion chamber. A high mixture velocity induced by rotor motion and the shape of the combustion chamber are drastically changed by the transfer between combustion chamber leading and trailing pockets (or recesses). This transfer alters the entire spectrum of the fuel-air mixture.

Spark plug characteristics such as gap geometry, energy, orientation, position relative to the spray, and spark timing play a more significant role in the combustion process of the small rotary engine. The injector spray pattern plays a major role in combustion stability, which depends on engine load and speed. Misfiring can be caused by improper mixture composition in the vicinity of the spark plug electrode at the ignition time, particularly at low loads (*15*). In contrast, in a large rotary engine with a dual injection system, pilot injection is much less dependent on engine load (*15*).

As discussed previously, a small-scale rotary engine has a host of different characteristics from a medium or large rotary engine. And improving the performance and efficiency of a small-scale rotary engine is more challenging and requires a thorough understanding of fuel injection, fuel-air mixture formation, ignition, combustion, and emissions formation processes.

4. Review of Heavy-Fueled Rotary Engine Research

One of the best spray strategies for heavy-fueled rotary engines would be fuel stratification. This study has been done in the past mostly for medium to large rotary engines and with limited success. This section discusses what is found from the literature until now for each major control variables and/or the components.

4.1 Combustion Chamber Designs

The combustion chamber design is critical in any internal combustion engine because it eventually determines the combustion efficiency of the engine. In a rotary engine, the basic geometric design parameters include the rotor radius, the eccentricity of the shaft, the depth or height of the rotor housing, and the rotor pocket (or recess) volume. Engine displacement and CR are determined with these measurements.

Shih et al. (*63*) performed a numerical analysis of the unsteady multidimensional flow inside the combustion chamber of an idealized two-dimensional (2-D) rotary engine (i.e., a rotary engine of infinite width) under motored conditions to investigate the flow patterns during intake, compression, gaseous fuel injection, expansion, and exhaust. A K-ε model was used for turbulence flow analysis. Gaseous fuel was injected during the compression process. No leaks across the seals were assumed. Wall temperatures were assumed to be 300 K, and the intake pressure was slightly higher than the exhaust port to prevent back flow from the exhaust port to the intake port through the apex seal. Figure 8 (left) shows the geometry of the 2-D rotary engine. The results show that the general motion of the entire combustion chamber is in one direction in figure 8 (right), which may not be true. Their conclusion is that the 2-D engine cannot account for all the factors occurring inside a real engine, such as a cross-flow and Taylor vortices. Another observation is that the grid is too coarse and cannot capture all the detailed small-scale flows.

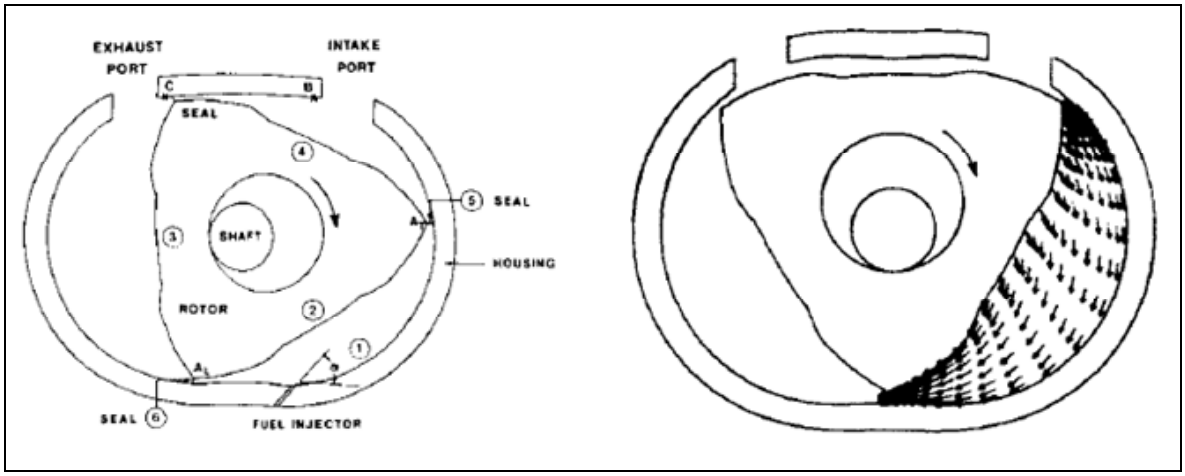

Figure 8. Geometry of a 2-D rotary engine (left) and flow pattern at 357° (right) (*63*).

Nagao et al. (*64*) used a high-speed photo-technique and a one-directional flame propagation model to clarify the relationship between squish and flame propagation in a rotary engine. Two quartz windows were located between the two spark plugs, as shown in figure 9 (left). Although

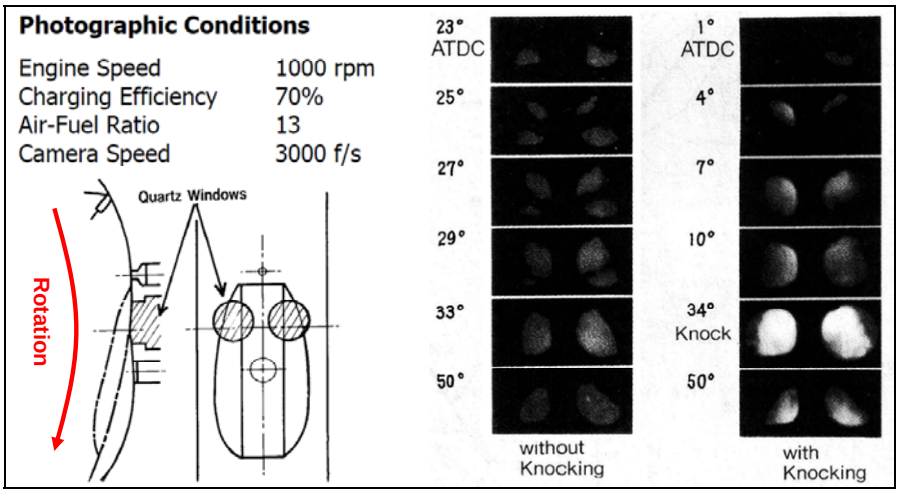

Figure 9. Quartz windows for photo technique (left) and photograph of flame propagation (right) (*64*).

the view areas were limited with the windows, the two flame fronts approached each other in figure 9 (right). A trailing flame propagated rapidly toward the leading direction, while the leading flame moved slowly in the trailing direction. This photograph shows that the squish flow is dominant in the direction of rotation.

Yoshioka et al. researched the effect of squish flow on flame propagation (*64*). They used a spark-tracing technique in a transparent rotary engine to visualize the patterns of squish, as shown in figure 10 (right). Figure 10 (left) shows that the squish flow patterns have a convex shape in the rotating direction, and the flow pattern in the vicinity of the trailing end of the rotor pocket (or recess) is strongly impacted by the pocket (or recess) shape. Therefore, the propagating flame in the trailing direction from the trailing spark plug presents a complicated phenomenon because the flame is strongly influenced by the squish flow.

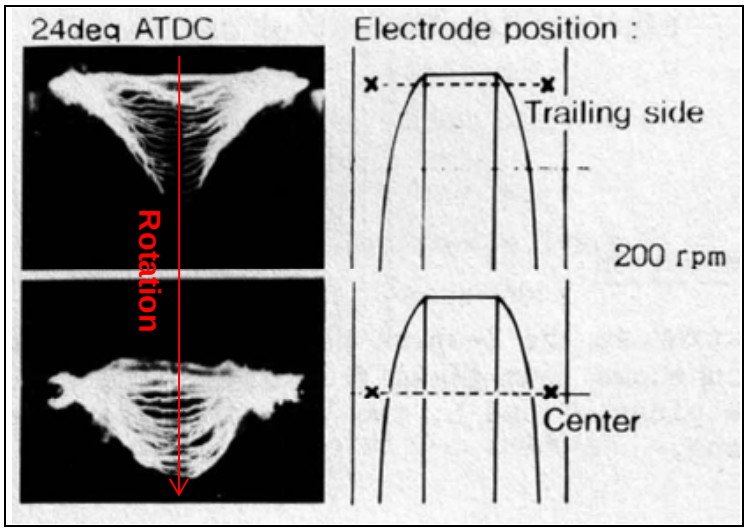

Figure 10. Patterns of squish flow (*64*).

Kamo et al. (*65*) converted a single-stage low CR Wankel rotary engine (Yanmar R450, 450 cc, CR = 8.0:1) to operate on diesel fuel (CR = 10.5:1) by using a properly designed combustion chamber and a variable heat input combustion aid to overcome cold starting issues. A spark plug was not used as an additional energy source in this investigation. Instead, an external combustion aid was used to supply the variable heat input to the intake port of the engine. They tested five different types of rotors, as shown in figure 11 (left). They selected type E as the best rotor design based on time to start. As shown in figure 11 (right), the optimal AFR was 55:1. When AFR was >85:1, the charge air temperature was too low for diesel spray autoignition. For AFR <35:1, the O_2 concentration was insufficient for a good start. The engine started in <5 s for an AFR of 55:1 and the charge air temperature of 200 °C. The engine even started in 15 s at the inlet air temperature of –10 °C. Obviously, it would be beneficial to optimize the combustion chamber and fuel spray. The injector used in the study will be discussed in section 4.2.

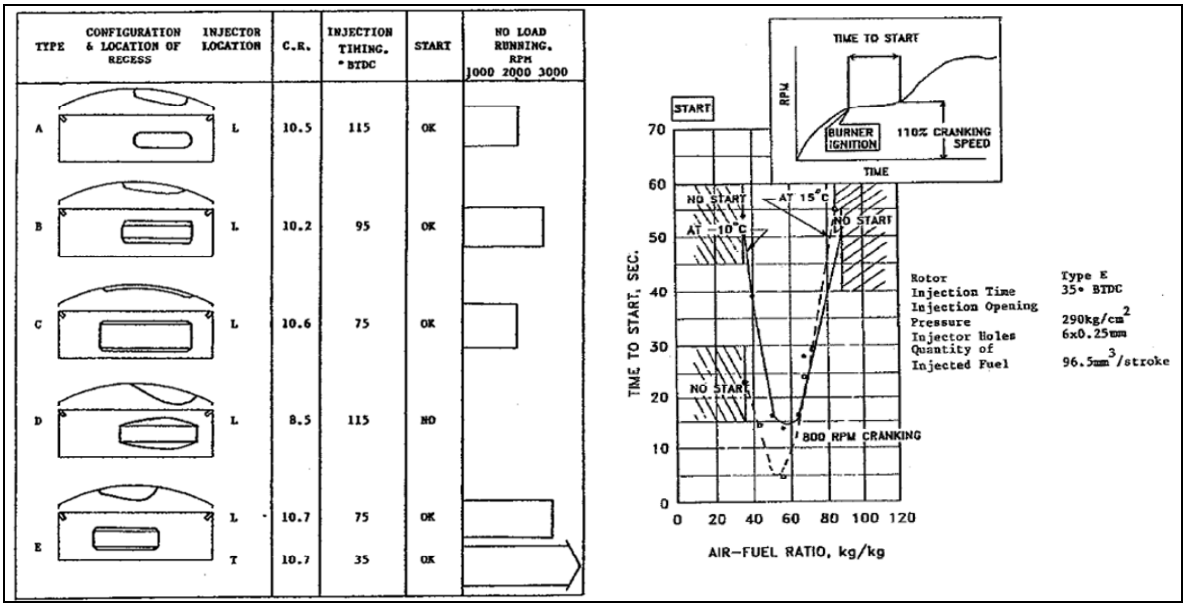

Figure 11. Types of rotors tested (left) and time to start vs. AFR for type E (right) (*65*).

Abraham and Bracco (*66*) showed that the turbulence diffusivity of the rotary engine at top center is smaller than in a corresponding reciprocating engine. Slow mixing, which is in part due to low turbulence diffusivity, may lead to slow burning rate. Also, pressure nonuniformity is caused by large fluid acceleration around the top center, which can reduce the indicated thermal efficiency. The rotary engine can be more efficient by improving the combustion rate and controlling pressure nonuniformity.

Irion and Mount (*24*) used a catalytic rotor to improve combustion rates and engine efficiency. The catalytic coating on the rotor surface (applied to the rotor flank and pocket [or recess]) was to promote combustion in close proximity to the rotor surface and pocket (or recess). The catalytic coating would reduce fuel ignition delay and promote combustion stability at lower

temperatures compared with noncatalytic surfaces. The catalytic coating was applied over a thermal barrier coating (TBC), which was intended to increase the rotor surface temperature. The observed BSFC of the catalytic rotor engine was 260 g/kWh (0.427 lb/hp-h) at 11.4 bar brake mean effective pressure (BMEP) and 6000 rpm. Engine power output was 100 bhp (75 kW), which is 50% cruise power at 6000 rpm. However, the results were similar to the thermal barrier rotor without the catalytic coating, as presented in figure 12.

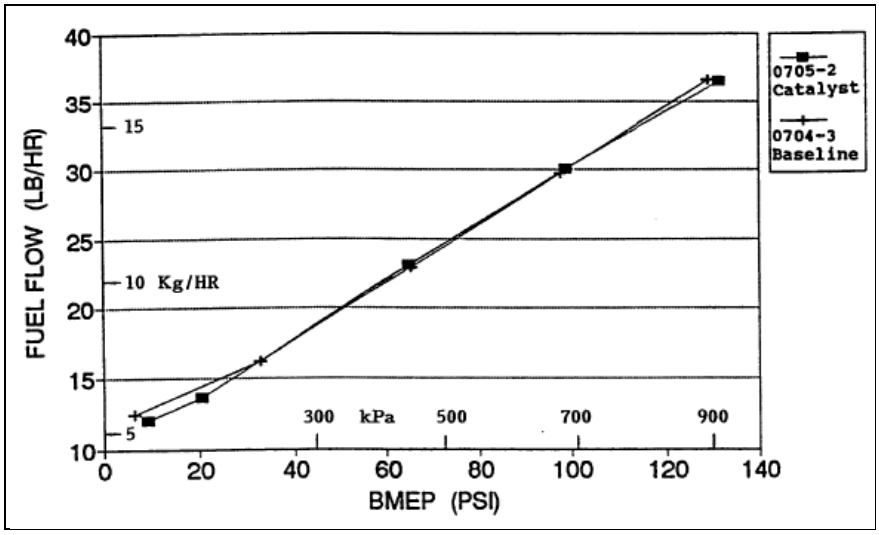

Figure 12. Comparison of fuel flow between the catalytic rotor and non-catalytic rotor (*44*).

Iron and Mount (*24*) also used a CFD analysis to generate four types of rotor combustion pocket (or recess) shapes, as shown in figure 13 (left). The purpose of this design was to increase gas recirculation within the rotor pocket (or recess) during the compression and combustion processes of the engine cycle because increased gas recirculation was predicted to improve fuel-air mixing, hence increasing combustion rates. The leading re-entrant pocket (or recess) rotor was not produced because of concerns about hardware durability caused by hot spots at the thin cross-sectional areas around the re-entrant shape. Instead, the leading rectangular (LR) pocket (or recess) was used to emulate the characteristic behavior of the re-entrant pocket (or recess). In addition, a dual pocket (or recess) rotor was produced but not tested because of the foreshortening of the NASA contract. The CR of each rotor pocket (or recess) design was 8.5:1. Figure 13 (right) shows the location of injectors and the spark plug in the standard rig engine.

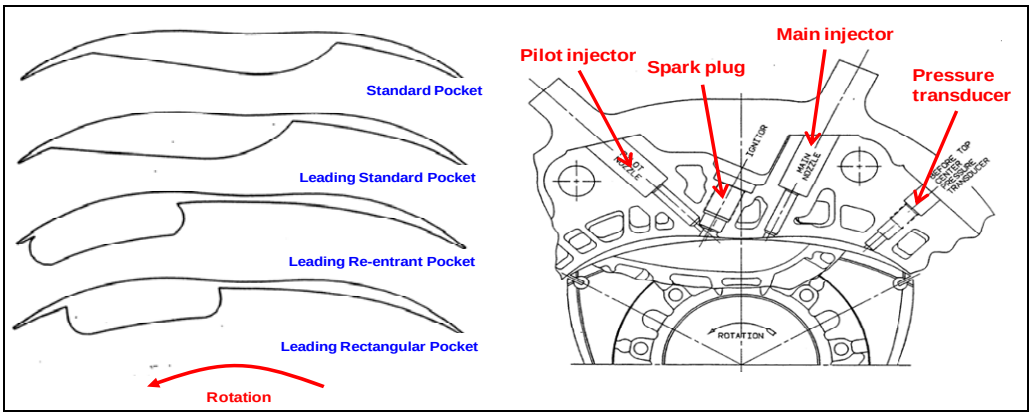

Figure 13. Four rotor geometries tested (left) and cross section of standard rig engine at top center position (*24*).

The leading standard (LS) pocket (or recess) rotor was used to increase diffusivity to enhance fuel-air mixing in the rotor pocket (or recess). This diffusivity was driven by the squish flow from the trailing flank of the rotor. The LS pocket (or recess) was identical to the standard pocket (or recess) but moved toward the leading flank. The LS pocket (or recess) rotor showed slightly higher BSFC (267 g/kWh or 0.439 lb/hp-h at 14 bar BMEP and 4400 rpm) compared to the standard pocket (or recess) rotor. The LS pocket (or recess) design had difficulty operating at engine speeds above 4400 rpm because of the high frequency of engine misfire.

The LR pocket (or recess) rotor was predicted by CFD to increase both gas recirculation and diffusivity, leading to improved fuel-air mixing in the rotor pocket (or recess). This phenomenon was induced by the squish flow from the trailing flank of the rotor. The LR pocket (or recess) rotor showed slightly higher BSFC (293 g/kWh or 0.481 lb/hp-h at 7.9 bar BMEP and 4400 rpm) and was limited in engine load due to a pressure wave in the combustion chamber, which generated conditions exceeding the hardware design pressure limits. The observed peak firing pressure was 110 bar at 7.72 bar BMEP and 6000 rpm. The high firing pressure resulted from the rapid combustion rate.

Abraham and Magi (*50*) used a three-dimensional (3-D) CFD to investigate the effects of ignition cavity flows on the performance of an SCRE. The coupling of the cavity and the main chamber was handled with an unsteady generalized curvilinear coordinate system. The main chamber grid was generated by using an algebraic grid generator and solving an elliptic equation in the cavity, as shown in figure 14. Cavity flows were calculated for different arrangements of the pilot injector and spark plug, and for different timings and fuel injection quantities of pilot and main injectors. Figure 15 (left) shows that the main characteristic of the cavity flow was the presence of a vortex, which was induced by the flow in the main chamber. The vortex in the cavity controlled the distribution of fuel, thus the burning rate in the cavity. The computed chamber pressures are compared for different pilot injector locations in figure 15 (right). The results clearly show that the location of the pilot injection and pilot injection timing are important for better efficiency. The combustion process and engine performance were sensitive to the variables in the ignition cavity.

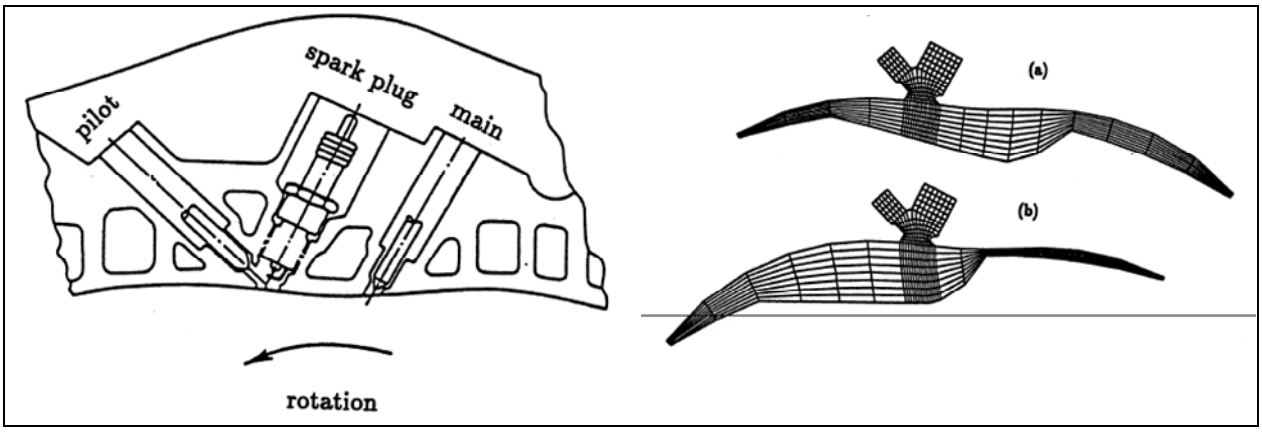

Figure 14. Ignition cavity arrangement (left) and cross section of engine showing numeric grid at (a) –280° crank angle (CA) and (b) –240° CA (*50*).

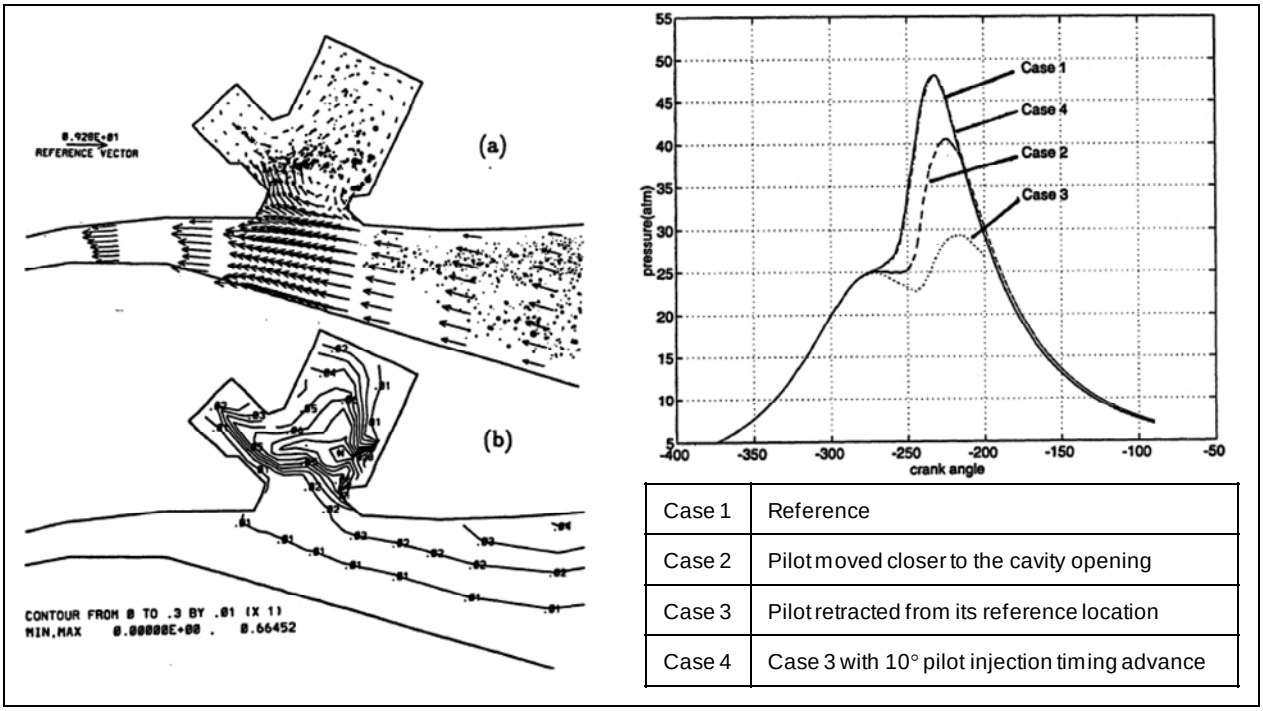

Case 1	Reference
Case 2	Pilot moved closer to the cavity opening
Case 3	Pilot retracted from its reference location
Case 4	Case 3 with 10° pilot injection timing advance

Figure 15. (a) Flow field and (b) fuel mass fraction contours at –295° CA (left) and computed chamber pressure showing effects of pilot injector location (right) (*50*).

Abraham et al. (*67*) performed a 3-D CFD to study the effect of the rotor pocket (or recess) geometry on the SCRE efficiency. They used two modified designs of the rotor recesses (or pockets): (1) a pocket (or recess) is located toward the leading edge of the rotor and (2) a two-pocket (or recess) rotor with two injectors and two spark plugs. The purpose of these modifications was to improve charge air utilization, thus improving efficiency of the DI-SCRE rotary engine. Abraham et al. could not make final conclusions and specific recommendations but mentioned that this research requires further extensive computations.

Yasuaki and Kouichi (*68*) visualized the flow fields inside the Wankel rotary engine for five different rotor pocket (or recess) shapes, as shown in figure 16. Figure 17 shows that rotor pocket (or recess) shape had little impact on the flow vortex patterns, but the vortex position was impacted by the pocket (or recess) location.

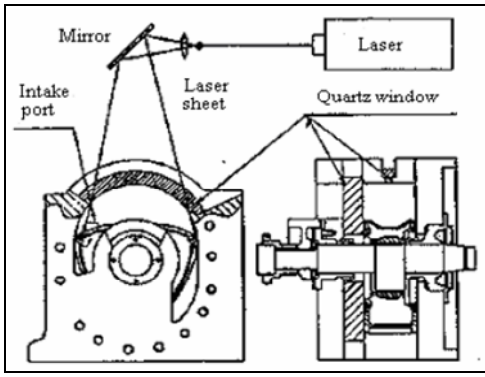

Rotor types

Rotor Type	Compression ratio	Recess Shape
MDR	9.4	
MDR-2D	7.1	
LDR1-2D	7.1	
LDR2-2D	7.1	
LDR2	9.0	

Figure 16. Transparent rotary engine bench setup (left) and rotor types tested (right) (*68*).

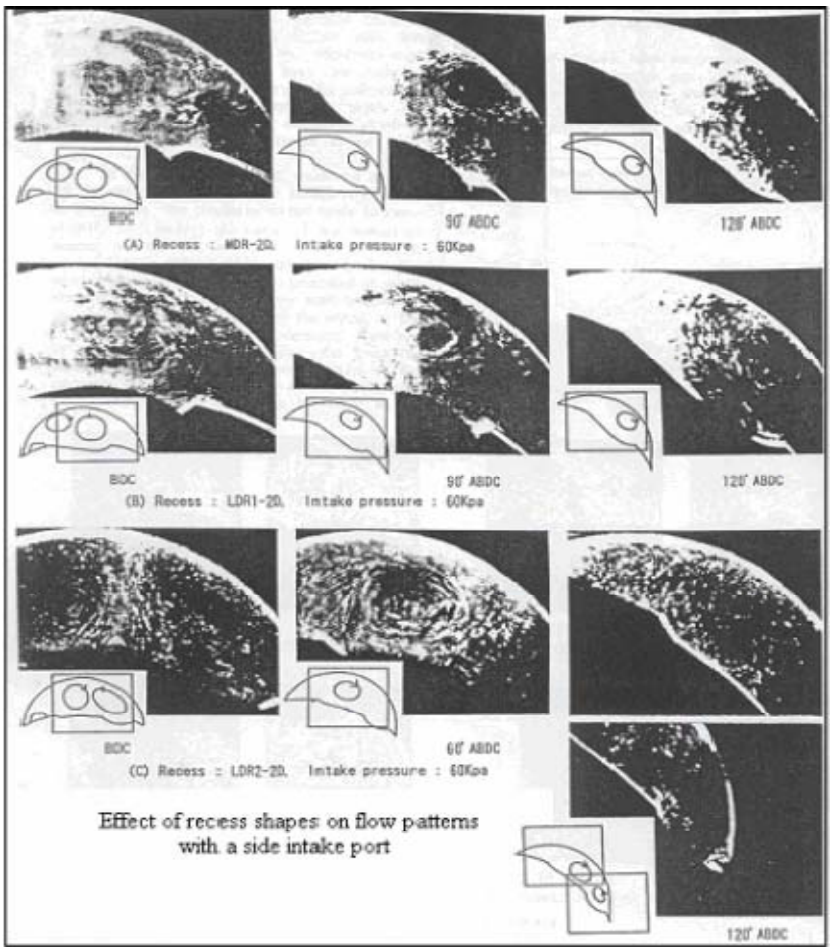

Figure 17. Effect of pocket (or recess) shapes on flow patterns with a side intake port (*68*).

Sprague et al. (*40*) developed small-scale rotary engines whose displacement ranges from 0.078 (P348) to 1.5 cc (S1500). The P348 is a 1/64th scale version of the smallest commercially available rotary engine, the 5-cc Graupner/OS 49-PI. The P348 was made to study the effect of scale on combustion and performance. The rotor recesses (or pockets) are shown for P348 and S1500 in figure 18. The S1500 has a pocket (or recess) depth of 1.5 mm, while the depth of the P348 is 0.67 mm. As the rotor pocket (or recess) depth was increased from 0.67 to 1.5 mm, combustion efficiency increased because of less quenching effect, which was caused by longer travel distance of the combustion heat flux. This result implies that even rotor pocket (or recess) depth has a significant impact on the combustion efficiency in small-scale rotary engines.

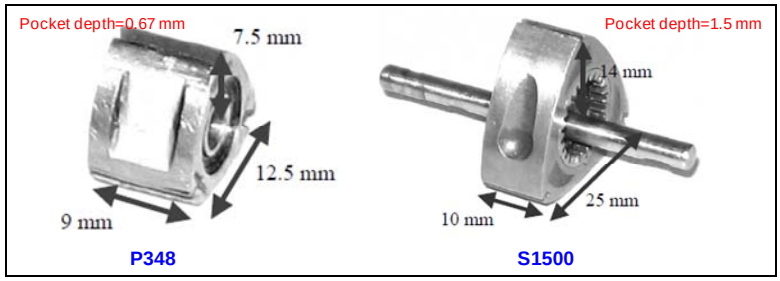

Figure 18. P348 and S1500 rotors with combustion recesses (or pockets) (*40*).

Izweik (*20*) used a CFD to investigate the effects of the rotor pocket (or recess) shape on the flow fields, as shown in figure 19 (left). Comparisons were made among the five-pocket (or recess) shape designs plus the KKM 407 pocket (or recess) design. The KKM 407 was on the market for light aircraft applications and was running on diesel and kerosene. Its power is 37 kW at 5700 rpm. The AVL FIRE CFD code was used to make the surfaces of the chamber, and the Hexahedral volume grid topology was used for grid generation. Figure 19 (right) shows the flow fields in the chamber at the engine speed of 2000 rpm for different rotor pocket (or recess) shapes. The flow field exhibits two regions: one behind the inlet port with a counterclockwise circulation and another in the leading flow part in the direction of rotation, which shows a clockwise circulation at the rotor pocket (or recess) end. All the pocket (or recess) shapes showed the same circulation effects but in different intensities.

Figure 20 shows that another flow circulation was developed across the flow space soon after the inlet cycle started. This circulation started near the inlet port and rotated counterclockwise upward near the fixed sidewall and rotated to the center of flow. The result showed that the rotor shape has no impact on the cross circulation, and the intensity was similar at the same engine speed. Inlet port velocity has a significant effect on the flow-field development in the chamber. The maximum velocity at the top center was significantly influenced by the rotor pocket (or recess) width and depth in figure 21. For instance, the KKM-407 rotor shows the lowest flow velocity because it has a wider and deeper rotor pocket (or recess). Rotor 1 shows the highest flow velocity because it has the smallest and narrowest rotor pocket (or recess).

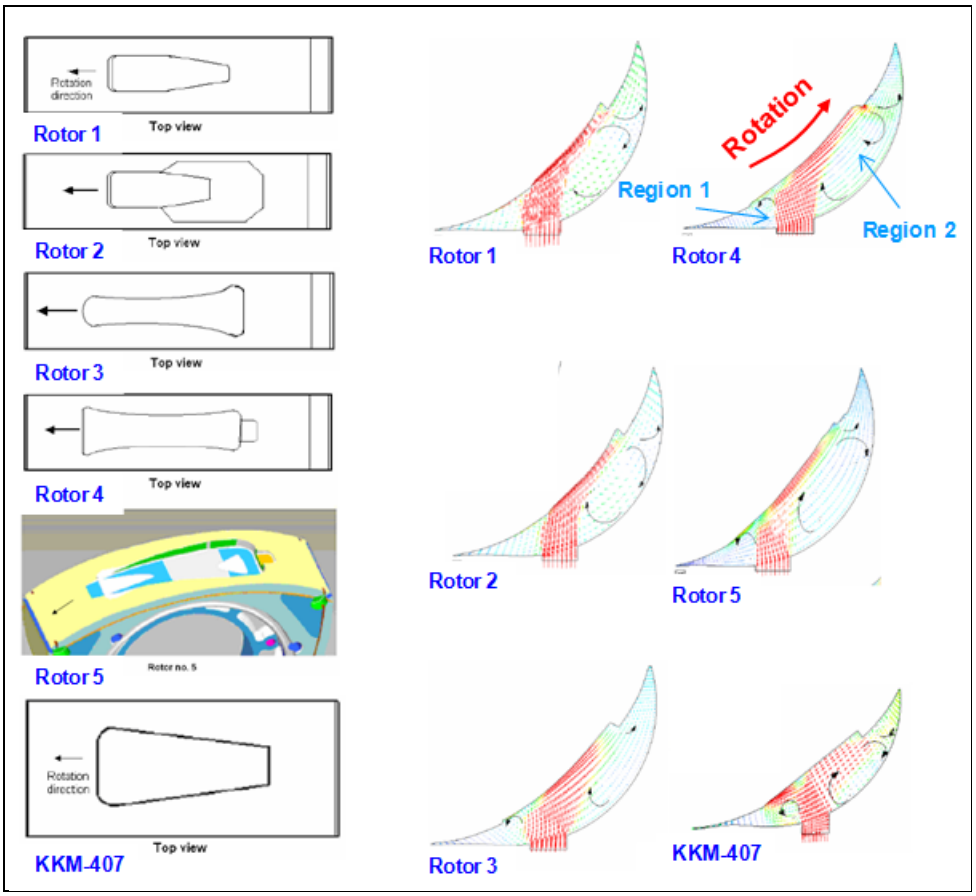

Figure 19. Different rotor pocket shapes (left) and velocity vectors during the inlet cycle (2000 rpm, Re = 53733.6) (right) (*20*).

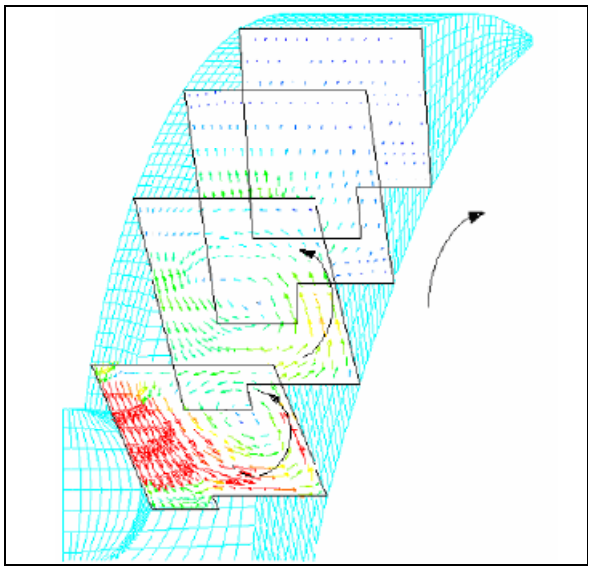

Figure 20. Cross-sectional cut planes (*20*).

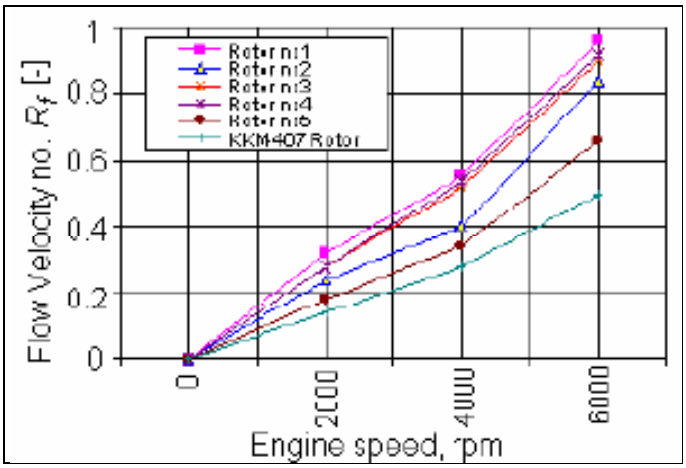

Figure 21. Maximum flow velocity vs. engine speed at top center, 540° (*20*).

Figure 22 shows the total pressure at 4000 rpm. The total pressure difference between the leading and trailing regions was higher for the rotor with the small and narrow pocket (or recess) than that with the deeper and wider pocket (or recess). Rotor 1, which has the smallest and narrowest pocket (or recess), showed the highest pressure difference (about 5.5 bar at 4000 rpm). Rotor 2 and the KKM-407 rotor showed almost equally distributed pressure along the chamber because both rotors have a wider and deeper rotor pocket (or recess) than the other rotors. This result implies that flow velocity and chamber pressure can be optimized by controlling the rotor pocket (or recess) width and/or depth while maintaining the same CR.

The pocket (or recess) volume increases both minimum and maximum mixture volumes by the same amount. Therefore, the pocket volume has no influence on displacement; however, it decreases the CR. Figure 23 shows the influence of flank rounding on clearance (i.e., smooth flank and recessed flank) and CR for an eccentricity ratio (e/R) of 0.16 (*47*). While rotor pocket (or recess) reduces the CR for a given included angle (θ) and e/R, it improves the shape of the long, narrow combustion pocket forming the minimum capture volume. Thus rotary engines, typically, equipped with more than one spark plug to improve combustion problems associate with this elongated pocket (or recess) shape.

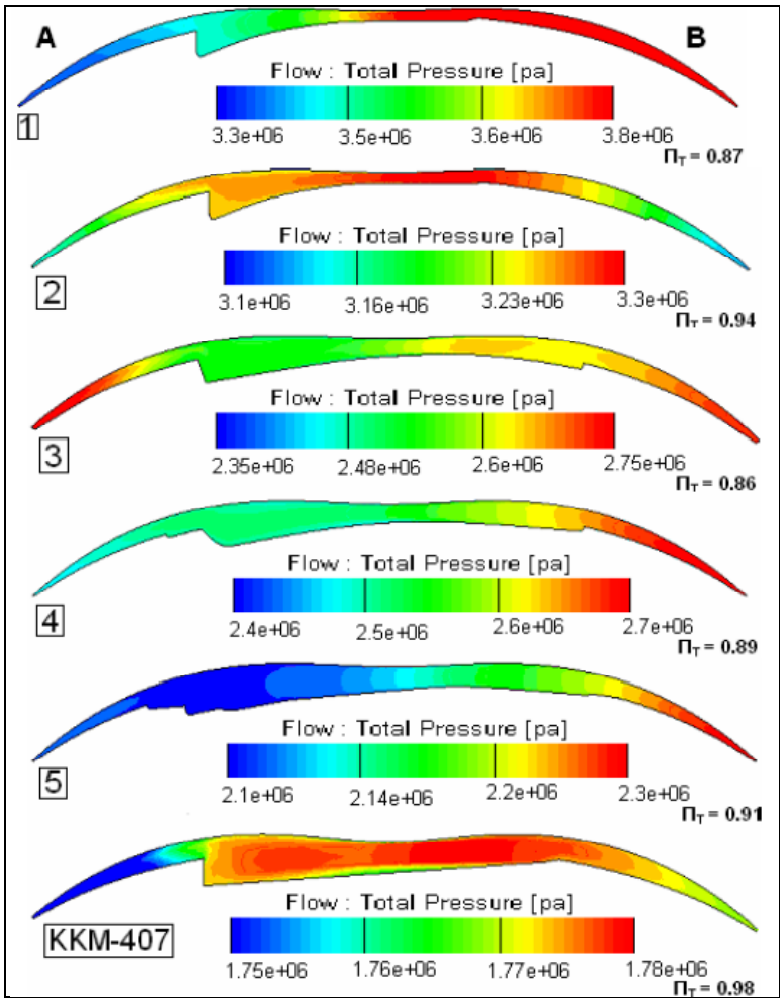

Figure 22. Fluid mean total pressure (Pa) at 4000 rpm (*20*).

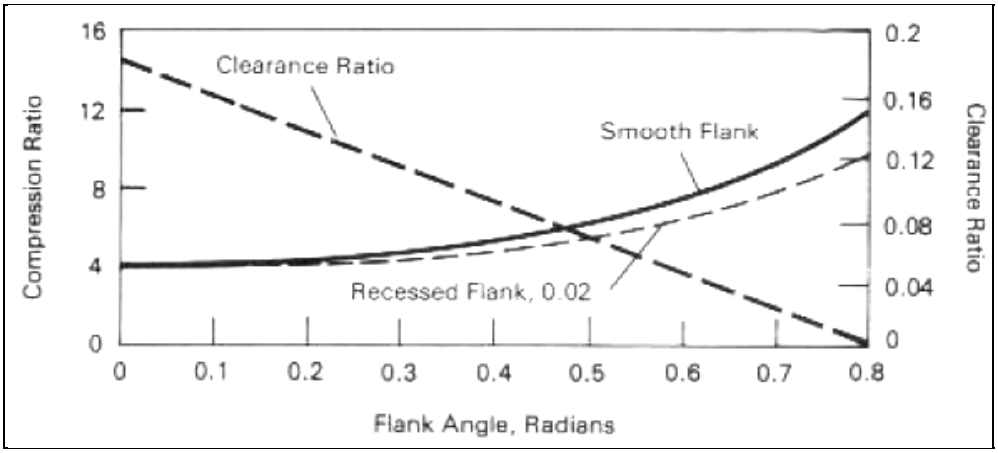

Figure 23. Influence of rotor rounding on clearance (i.e., smooth flank and recessed flank) and CR for an eccentricity ratio of 0.16 (*47*).

Ma et al. (*69*) used Fluent CFD software to evaluate the flow structure of the rotary engine combustion chamber designs. Figure 24 shows the trochoid housing outlines for a different trochoid constant, K (= R/e). As the K value decreases, the minor axis becomes smaller and presents the concave profile. Intake and exhaust ports are typically located on the concaved sides in a peripheral port system. Typical values of the trochoid constant, K, are between 6 and 8. As the K value increases, the CR also increases accordingly because the shape of the combustion chamber becomes longer and narrower. This change in shape may cause poor combustion because of uneven fuel distribution and poor flame propagation. Therefore, the K value needs to be optimized for efficient combustion.

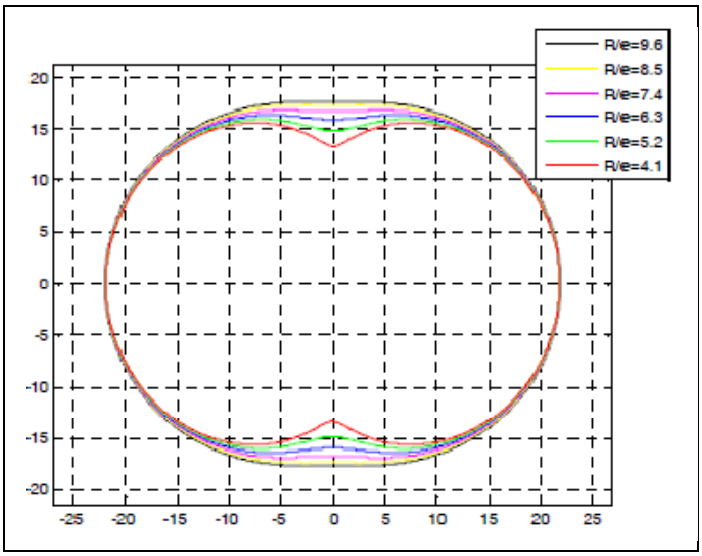

Figure 24. Trochoid housing outlines for different trochoid constant, K (= R/e) (*69*).

Figure 25 shows the flow lines and pressures at two different crank angle degrees at the engine speed of 3000 rpm. Air was introduced into the chamber naturally, and the exhaust port was at ambient pressure. During the intake process, air is jetted into chamber A and hits the rotor surface. The flow is divided into two regions: one forming a small recurrent flow in the area between the inlet port and the rotor apex and the other flowing against the surface of the rotor in the direction of rotation by forming a clockwise circulation. These results are similar to Izweik (*20*). As the compression process started, the small counterclockwise circulation disappeared, and another counterclockwise circulation developed at the leading region. The original clockwise circulation became less intense. Pressure at the top center in chamber B showed higher at the trailing region, but it was almost evenly distributed across the chamber.

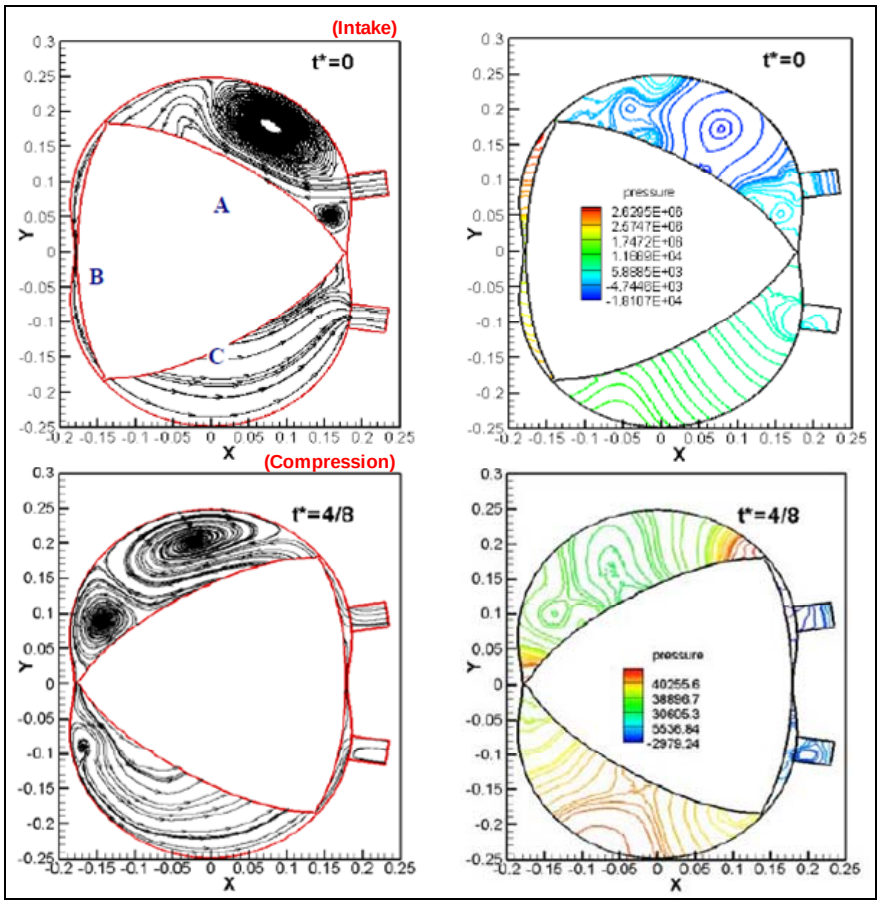

Figure 25. Flow lines (left) and pressure (right) at 3000 rpm (*69*).

4.2 Fuel Spray

The direct injection of liquid fuel is important for stratified combustion, and fuel injection and its control are critical parameters for efficient stratified combustion. High-pressure fuel injection systems have drastically evolved, especially over the last decade. DI-SCRE rotary engines have one or two injectors, located typically at or near the top center. Early work at Curtiss-Wright used a multihole nozzle injector with one of its sprays directed toward the spark plug (*2*). The major issue was to maintain the correct fuel-air ratio in the vicinity of the spark plug for various operating conditions. Various single injector stratified-charge combustion concepts, as shown in figures 26 and 27, were evaluated with varying degrees of success (*70*).

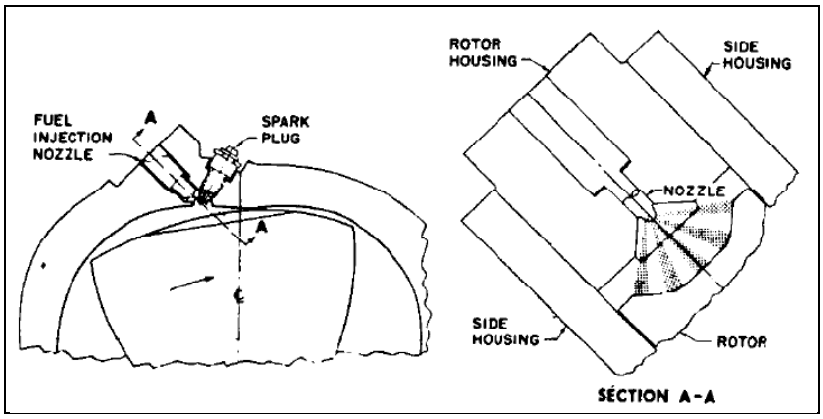

Figure 26. Coplanar single injector design (*70*).

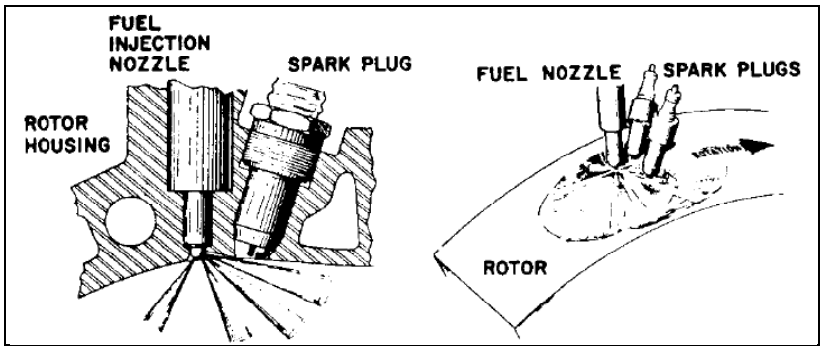

Figure 27. Shower head single injector design (*70*).

Subsequently, a dual-injector stratified-charge configuration was developed at Curtiss-Wright, which is shown in figure 28 (*2*). The pilot injector has a single hole (or nozzle) and injects a constant quantity of fuel, which is optimized for producing an ignitable mixture in the vicinity of the spark plug. The main injector has multiple holes, and its quantity is determined based on the load requirement of the engine. The dual-nozzle SCRE was successfully demonstrated on gasoline, methanol, diesel, and jet fuel without any engine adjustments. Therefore, multifuel capability was possible with direct-injection and spark assistance.

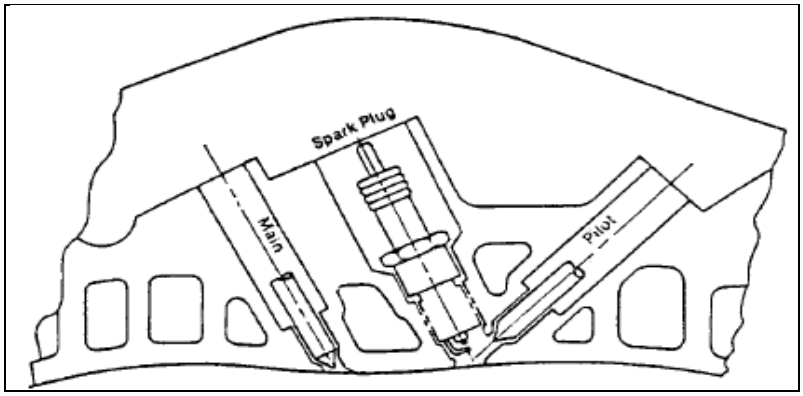

Figure 28. Curtiss-Wright dual-nozzle stratified charge configuration (*2*).

Kamo and Hamada (*65*) investigated the relationship between the location of the rotor pocket (or recess) and the injector during the cold start of diesel fuel in a rotary engine: trailing and leading injector locations are relative to the top center, as shown in figure 29. Fuel injection timing was varied from 5° to 55° bTC. They selected the trailing injector location with the type-E rotor shape, which was discussed earlier. They also designed two different nozzle sizes (0.15 and 0.25 mm) of a six-hole injector to control white smoke, which results from unburned fuel under cold conditions. (White smoke in a tailpipe is generated by fuel injection in the misfired cycles in cold conditions.) They used a visual evaluation for the white smoke level from the engine exhaust stack. The result shows that the smaller nozzle-size injector helped suppress the white smoke.

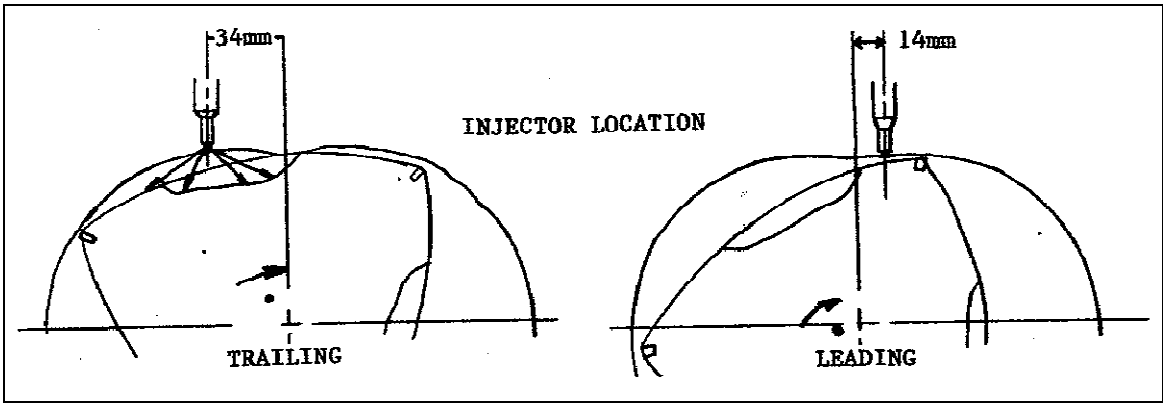

Figure 29. Relationship between location of rotor pocket (or recess) and injector (*65*).

Abraham and Bracco (*71*) used a 3-D CFD model to identify the main parameters for controlling combustion rate in a DI-SCRE rotary engine. They concluded that the orientation of the six-hole sprays of the main injector with respect to the air stream is important to enhance fuel vaporization and produce flammable fuel-air mixture. Particularly, no spray should be in the wake of any other sprays, which would deteriorate the fuel-air mixing. In controlled spray conditions, the indicated thermal efficiency was predicted to be 6% higher at higher loads and 2% higher at lower loads than the baseline. A new injector tip was designed based on the CFD results, and the experimental results showed slightly better efficiency than the CFD.

Abraham and Bracco (*55*) also used the 3-D CFD model to investigate the effect of design changes in the pilot injector on engine efficiency. The results showed that a two-hole "rabbit-ear" pilot injector can achieve higher thermal efficiency (about 5%) than the baseline single-hole pilot injector. The rabbit-ear pilot injector was predicted to increase the surface area of the early flame because of better fuel distribution, which led to increased burning rate.

The dual-orifice pilot nozzle tested in the NASA research rig engine (CR = 7.5:1) showed a 4.3% reduction in BSFC at 4400 rpm, and the best efficiency was observed at 5500 rpm (*24*). The achieved BSFC was 257 g/kWh (0.422 lb/hp-h) at 98 bhp (73.1 kW) at 5500 rpm. The first

version of the dual-orifice engine experienced poor hardware durability because of high temperatures generated within the pilot-igniter cavity. These temperatures eroded the spark plug electrodes and caused carbon to build up in the injector nozzle tip. The improved version of the dual-orifice engine showed 242 g/kWh (0.398 lb/hp-h) at 11.64 bar BMEP at 5500 rpm (95 bhp or 71 kW). The BSFC of 249.4 g/kWh (0.41 lb/hp-h) was observed for the load range of 10 and 12.4 bar BMEP at 6000 rpm.

Figure 30 shows the ranges of the pilot and main fuel injection quantities over the engine speeds. As the engine speed increases, the ranges of the fuel injection quantities narrow down, particularly for pilot fuel injection quantities. Figure 31 presents the pilot injection quantities, which range between 3 and 4.5 mm^3/injection, over the engine speed for the rig engine tested. Rotary engine performance was sensitive to various fuel injection systems, particularly for various fuel injection rate profiles. The results show that a high-pressure common-rail fuel system has the potential to provide the fuel injection characteristics favorable for the SCRE.

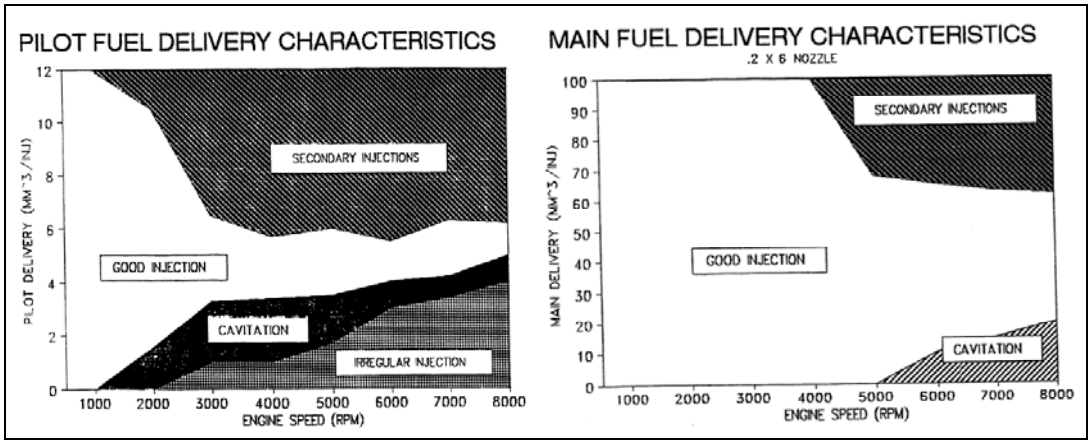

Figure 30. Pilot fuel delivery characteristics (left) and main fuel delivery characteristics (right) (*24*).

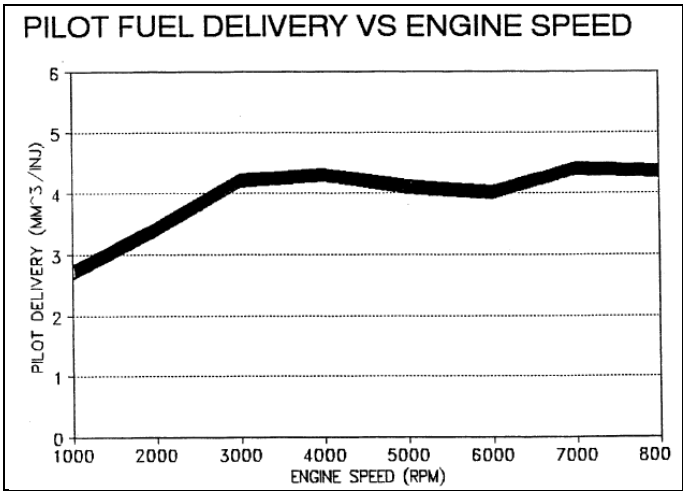

Figure 31. Pilot fuel delivery vs. engine speed (*24*).

Eiermann et al. (*53*) designed a small rotary engine (displacement: 400 cc) from an existing gasoline rotary engine with a spark-assisted direct injection of heavy fuels such as diesel and jet fuels. Unlike the previous studies that used a small ignition cavity for pilot injection, this study used a single injector with an open combustion chamber, as shown in figure 32. This engine showed BSFC lower than 335 g/kWh (or 0.55 lb/hp-h) at 5–12 kW and 3000–4000 rpm, which is higher than the medium and large dual-injector SCRE engines. This engine needs further improvement in BSFC, engine power density, and flexibility of operation in a broader range of speeds and loads.

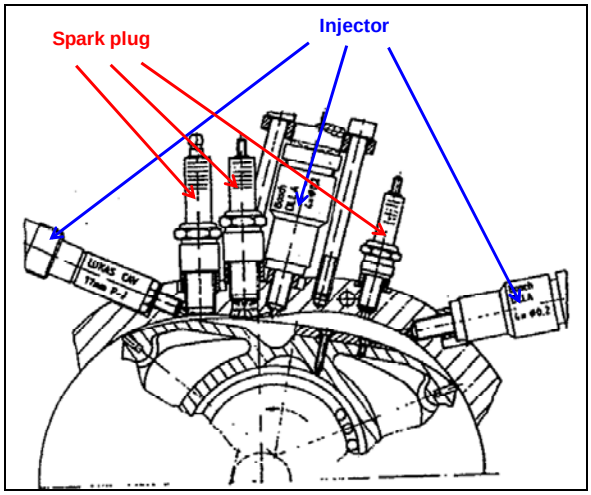

Figure 32. Locations of various injectors and spark plugs (*53*).

Kagawa et al. (*15*) investigated a DI-SCRE rotary engine for a motor vehicle application. In this study, the Curtiss-Wright dual-nozzle system (*2*) is named as the spray ignition system. Kagawa et al. developed a subchamber ignition system. The subchamber, which is defined as the area around the spark plug, was designed to secure a fuel-air mixture suitable for ignition around the spark plug. Figure 33 shows the schematic of the subchamber and spray ignition systems. The location of the nozzle was determined such that the injected fuel reaches the main combustion chamber without colliding into the walls of the subchamber. The subchamber hole was made to control the flow by throttling such that the fuel vapor and a small amount of fuel droplets remains in the subchamber. As shown in figure 34, AFR in the subchamber was slightly impacted by the absolute intake pressure (left) and engine load (right); therefore, most of the air-fuel mixture in the subchamber was ignitable. This more uniform AFR in the subchamber resulted in continuous stable ignition without being influenced by fuel injection rate, injection timing, or combustion chamber pressure. Figure 35 (left) shows that the uniform AFR in the subchamber led to improved and consistent BSFC, which is compared with the spray ignition system. Figure 35 (right) shows that the deterioration in BSFC in terms of intake pressure for various subchamber volumes. The result shows that the subchamber needs at least 12 cc. This result indicates that the shape of the subchamber is more important than the chamber volume.

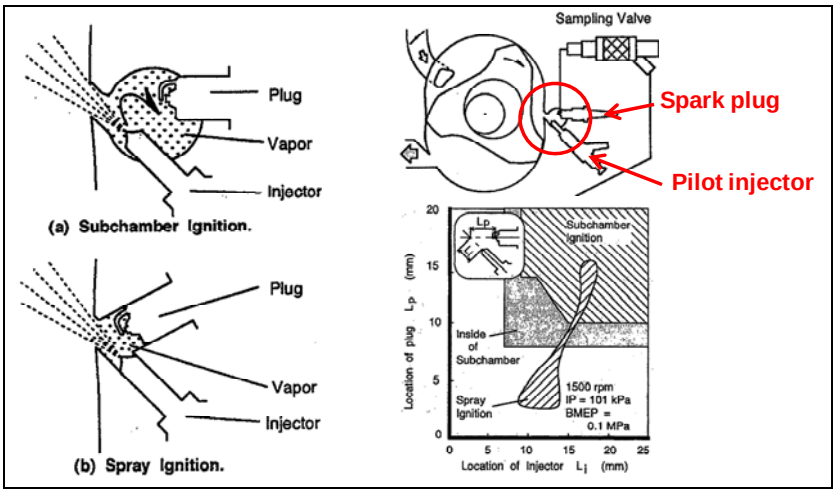

Figure 33. Ignition method (left) and ignition performance (right) (*15*).

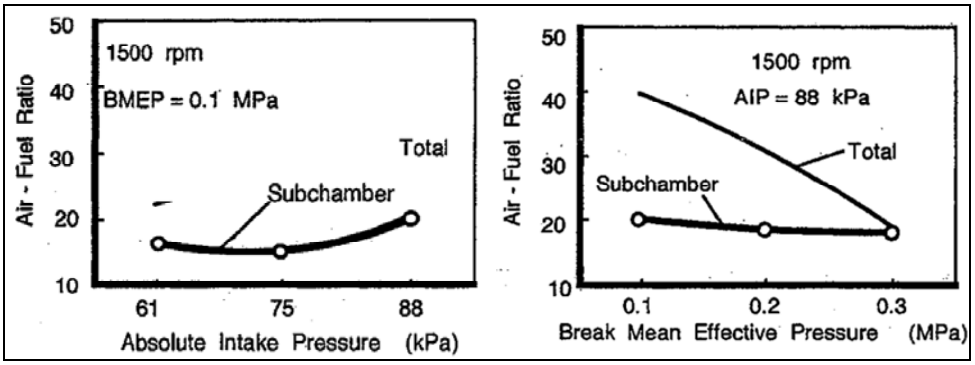

Figure 34. AFR vs. intake pressure (left) and BMEP (right) (*15*).

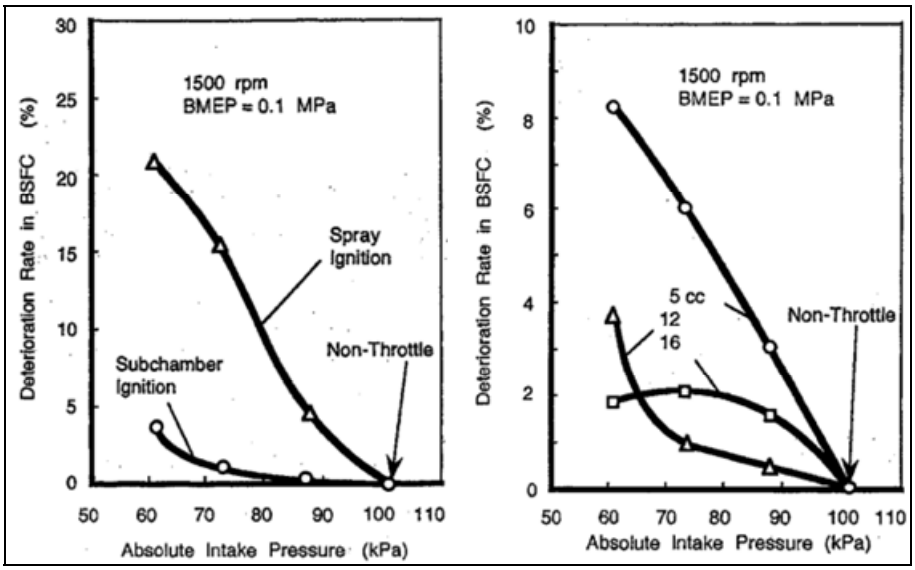

Figure 35. Deterioration in BSFC vs. intake pressure for different ignition systems (left) and different chamber volume of the subchamber ignition system (right) (*15*).

In addition, Kagawa et al. (*15*) studied the effect of the location of the main fuel injector to improve air utilization in the combustion process. They used main injection only to clarify mixture stratification. Fuel spray behavior was predicted by using a simplified 2-D calculation, as shown in figure 36. The simplified calculations were not accurate but were acceptable for relative comparisons. Figure 36 shows that the downstream injection has insufficient time for mixing, and that the injected fuel collided with the rotor surface. Conversely, the upstream injection has sufficient mixing time and reaches the nearby top center (TC) with considerable evaporation. Figure 36 (right) shows that the upstream injection achieved about 60% evaporation, while the downstream injection achieved about 38% evaporation. This calculation assumed that there was little evaporation after the collision.

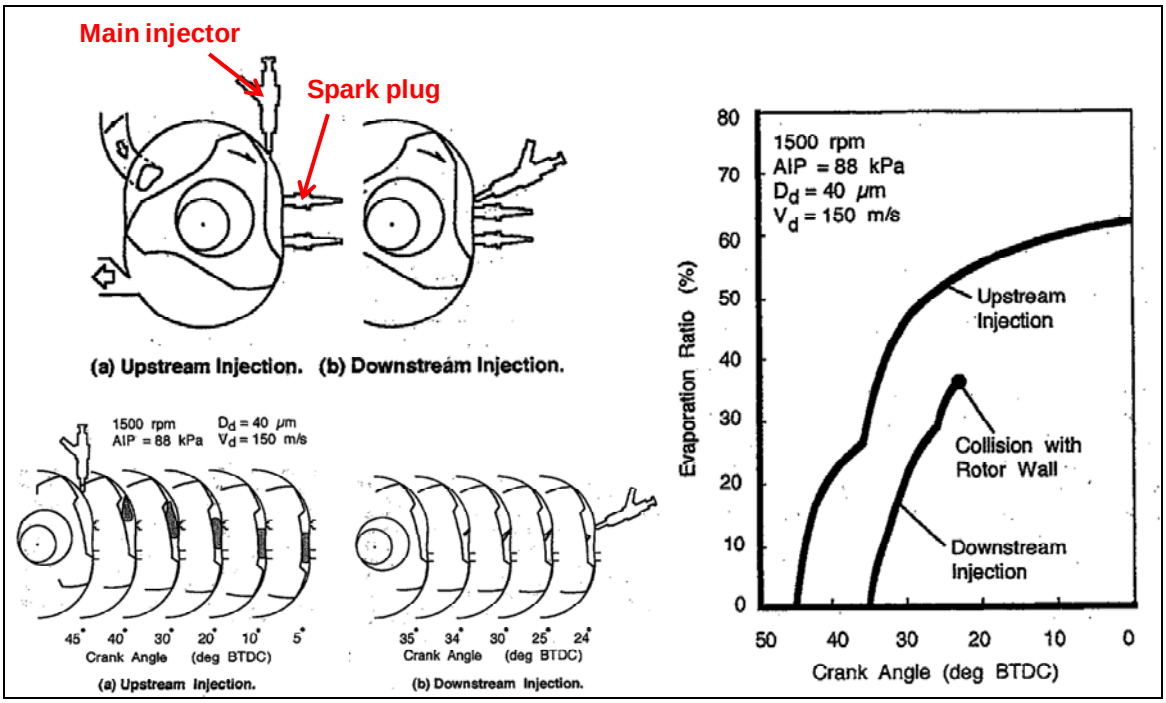

Figure 36. Downstream and upstream injections (left) and fuel evaporation during flight (right) (*15*).

Kagawa et al. (*15*) also used a 1.5-mm-diameter sampling hole in the trochoid surface to measure the fuel distribution in the main combustion chamber for the upstream fuel injection. Figure 37 shows that the upstream fuel injection stratifies the fuel on the leading side of the combustion chamber, and the trailing side is pretty lean. Since it is difficult to burn fuel on the trailing side of the combustion chamber, stratification on the leading side would be beneficial. Therefore, the upstream injection would enable ideal fuel distribution (due to wide flight range) with good stratification on the leading side.

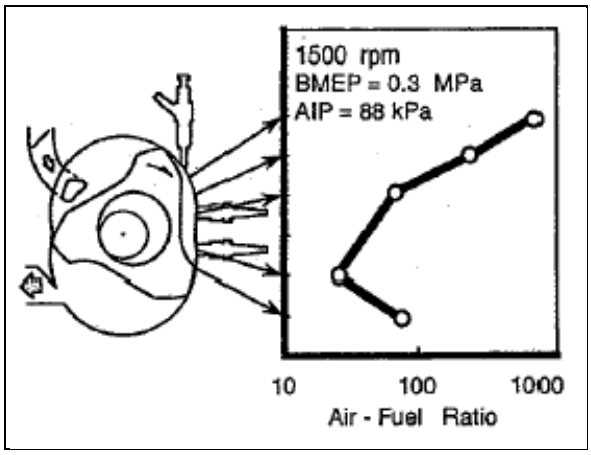

Figure 37. Fuel distribution in main chamber of upstream injection (*15*).

The maximum fuel injection rate depends on the orifice area of the main injector and the pressure difference between the fuel and combustion chamber. Hoffman et al. (*72*) compared the increased nozzle orifice area (6 × 0.254 mm) with the baseline (6 × 0.203 mm) for the same spray pattern. As shown in figure 38, the larger nozzle area of the main injector had higher peak firing pressure (PFP) than the baseline with similar fuel consumption (i.e., BSFC). The main injection timing was 5° advanced, and the duration was 4° reduced for the larger main nozzle area. The pilot injection timing was also advanced in the same amount for the larger main nozzle area. It was not clear whether this PFP increase was due to the increase in the main nozzle diameter or the injection timing advance.

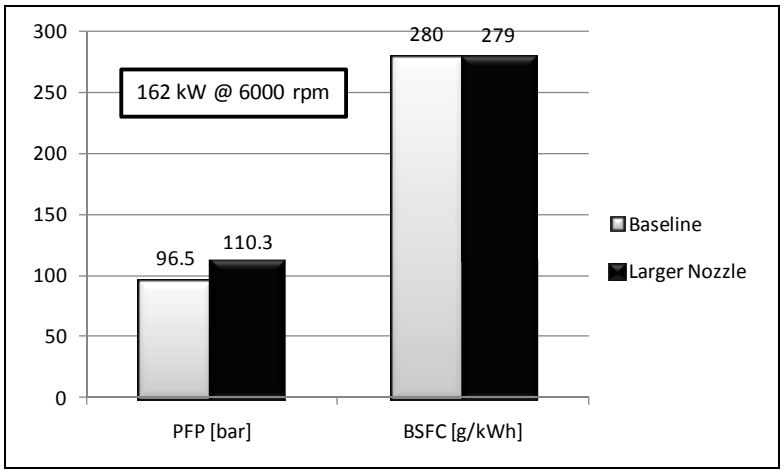

Figure 38. Comparison between baseline and larger nozzle area of main injectors (reproduced from Hoffman et al. [*72*]).

Izweik (*20*) used the AVL FIRE CFD code to investigate the best angle between the nozzle holes and the declination angle of the spray cone to the injector axis to achieve better penetration and mixture formation. A common-rail fuel system was used with three- and four-hole injectors (each hole diameter = 0.15 mm). The injector was located at the center position of the housing short axis. Diesel fuel was used because the experimental data was available; the fuel was injected between 15° and 40° bTC. The trochoid housing was made with fixed mesh while the rotor was made with moving mesh. All wall temperatures were fixed at 300 °C. Only 54° before engine TC to the end of compression (i.e., TC) was simulated as moving mesh. Initial conditions of pressure (P), temperature (T), and velocity were obtained from the separate flow model analysis. Parameters included three spray angles, three angles between the holes, and three fuel injection timings, as shown in figure 39. Fuel injection quantities were varied from 8 mm^3/injection to 50 mm^3/injection. Engine speed was set at 2000 rpm. Three different injections were evaluated: pilot injection (or preinjection), main injection, and both pilot and main injections. The wave breakup model was used to calculate diesel engine nozzle flow as recommended by AVL. The diesel nozzle model was validated by using a separate single-hole spray model. The model was validated for only liquid and vapor penetration, and spray angle.

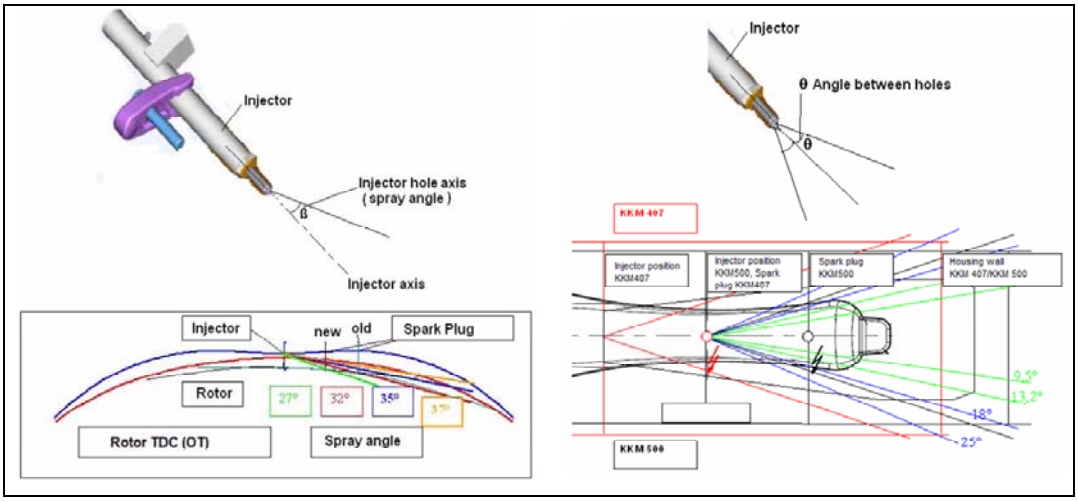

Figure 39. Different declination angles and spray angles (left) and possible angles between holes (right) (*20*).

The results show that angles between the holes below 13° are too small, for the spray cones will be interfaced together and may act like one bore injector. One the other hand, the angles between the holes >25° will inject the fuel directly to the combustion chamber walls because of the narrow rotor width. The spray angle is also constrained because of the small combustion chamber height. Spray angles <27° will spray the fuel directly to the rotor surface and will be reflected from the rotor surface to the housing and the rotor pocket (or recess) walls. This spray may produce a liquid film on the surfaces that is difficult to evaporate when the engine is cold.

Spray angles >35° may be a good choice. However, since the injector is normally recessed some millimeters from the housing surface, the injector may produce a liquid film on the housing surface that reaches the spark plug causing hard ignition.

The left side of figure 40 shows the plane cut distances from the nozzle center, and the right presents the mixture formation: the spray angle is 32°, the angle between the holes is 25°, and the injection timing is at 29° bTC.

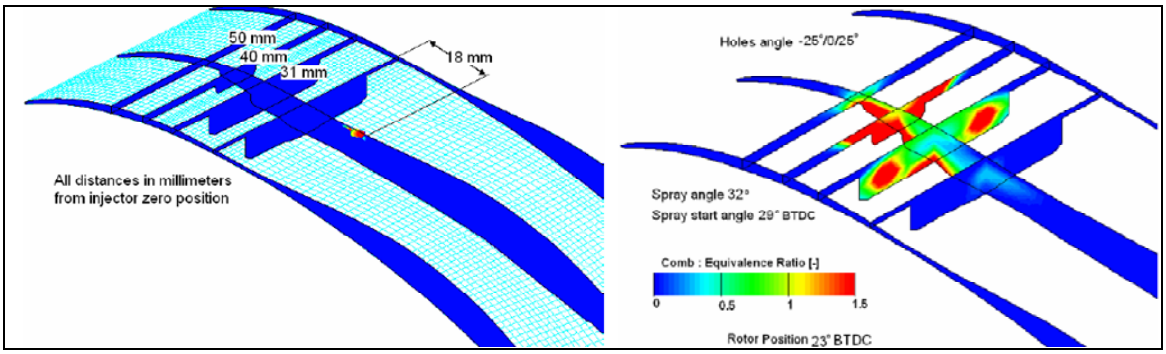

Figure 40. Plane cut distances from nozzle center (left) and mixture equivalence ratio (right) (*20*).

Fuel injection timing has a significant impact on the mixture formation and ignition timing. Figure 41 shows the equivalence ratio at four different crank angles at the preinjection timing of 39° bTC and the main injection timing of 20° bTC for the angle between holes of 18° and spray angle of 32°. The result shows that the preinjected fuel was so lean at the spark plug that it was difficult to ignite at the ignition time (normally 10°–20° bTC). Reduced separation time between the preinjection and main injection was needed to improve ignition of the pre injection fuel.

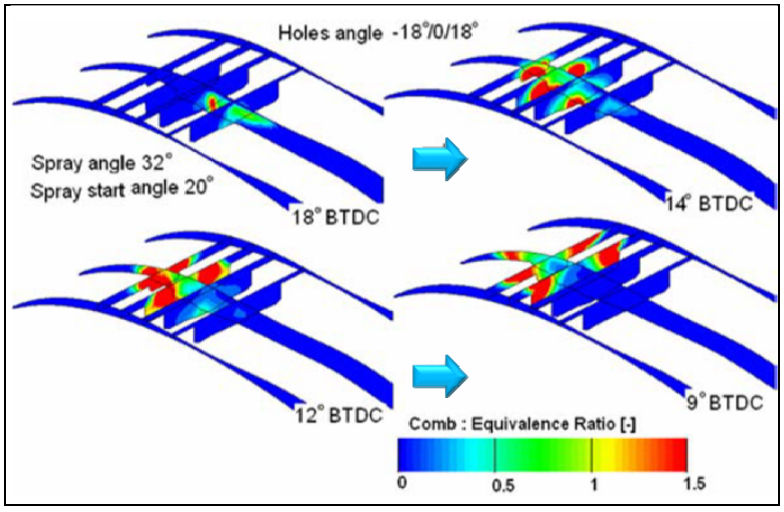

Figure 41. Equivalence ratio at fuel injection timing of 20° bTC (*20*).

Heavy fuel injection systems for light to heavy-duty engines have evolved significantly over the last three decades. However, electronically controlled heavy fuel injectors for small-scale engines have not been developed until recently. Several U.S. Army and U.S. Air Force–funded projects are developing injectors for small-scale engines fueled with heavy fuels. Enabling Energy Systems (Crown Point, IN) (*73*) is working with the U.S. Army Research Laboratory's Vehicle Technology Directorate in Cleveland, OH, to develop a pulsed electrohydrodynamic atomization injector for heavy fuels under funding from the U.S. Army Research Office. They are using a low-pressure (~1 barg) atomization system with multiple orifice designs to enhance small mean drop diameters at low-pressure drops. Kinetic BEI (South Elgin, IL) (*74*, *75*) is developing microfuel injectors and micro fuel pumps for small heavy-fuel engines up to 100 hp. The microfuel injectors are based on a common-rail fuel system and designed for compression and spark ignition engines. The target of the individual microinjector is 2.5 to 25 hp with potential maximum fuel pressure of 2000 bar. The third-generation prototype injector operates from 100 to 414 bar, and the target specification of the microfuel pumps is 276 bar. These injectors are still under development and have not been tested in engine systems.

Figure 42 shows the hollow-cone spray images of gasoline direct injection (GDi) piezo injector (*76*). The injection strategy of this system is to keep the fuel-air mixture near the spark plug. As shown in the figure, the spray penetration becomes shorter as the number of injections increases, while the fuel and air mixing increases with the increasing number of injections. A multihole GDi injector was also developed and used in Ford production engines (*77*). In this combustion system, one spray was directed toward the spark plug electrode for spark ignition, as shown in figure 43.

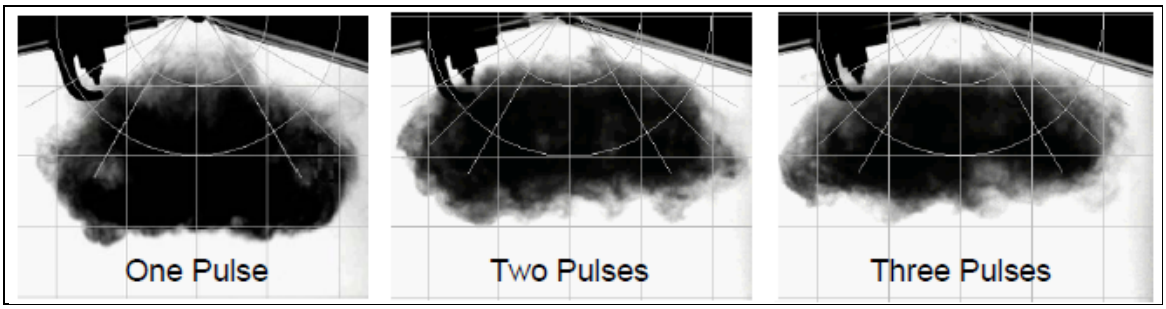

Figure 42. Pressure chamber spray comparison between single, double, and triple pulses with the same total fuel mass delivered (*76*).

Figure 43. Schematic of the 3.5-L V6 EcoBoost combustion system with multihole GDi injector (*77*).

4.3 Ignition System

Rotary engines have a long, narrow combustion chamber that constraints the fuel spray angles. It also has a large surface-to-volume ratio, as shown in figure 44 (*49*), which increases heat loss. In addition, the compression of the rotary engine is limited because of its geometric configuration. This constraint may be reduced by using a supercharger or turbocharger, which will be discussed later. Therefore, burning a heavy fuel in a rotary engine is inefficient. In order to increase the combustion efficiency, external ignition sources such as spark plugs or glow plugs have been employed in rotary engines (*53*). Stratified rotary engines favor a stoichiometric fuel-air mixture near the spark plug for efficient ignition; however, it is inconvenient to keep a consistent fuel-air mixture near the spark plug for various operating conditions. Thus, various subchamber designs were developed to make the fuel-air mixture consistent. In these applications, a single- or double-hole pilot injector was used in the small chamber to generate a fuel-air mixture for spark ignition. For small-scale rotary engines, space availability is limited in the trochoid housing to employ the subchamber or spray ignition methods. Hence, it is preferable to use an open combustion chamber. Since the fuel-air mixture moves quickly down the long, narrow combustion chamber, two or three spark plugs were implemented to improve combustion efficiency (*64*, *17*, *78*). As an alternative, glow plugs were also used to ignite the heavy fuel-air mixture in a rotary engine (*16*, *57*, *58*, *72*).

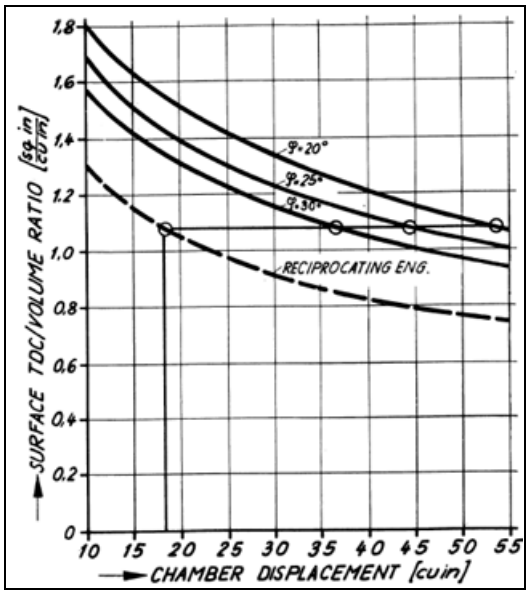

Figure 44. Surface-to-volume ratio vs. combustion chamber displacement (*49*).

Figure 45 shows a schematic flame propagation model for the two-spark-plug rotary engine (*64*). This model is based on a premixed gasoline SI rotary engine for Mazda passenger and sports car applications. However, this model may be used to better understand the combustion processes in the direct-injection spark-assisted heavy-fueled rotary engines. The flame propagation model has four flame fronts (i.e., TT, TL, LT, and LL) generated by two spark plugs (i.e., T and L), two burned gas regions, and three unburned gas regions. The flame propagation is influenced by the strong squish flow generated in the direction of the rotor rotation. For direct-injection spark-assisted stratified rotary engines, the combustion processes will be more impacted by the strong squish flow because it will influence the spray, stratification, mixture formation, and ignition.

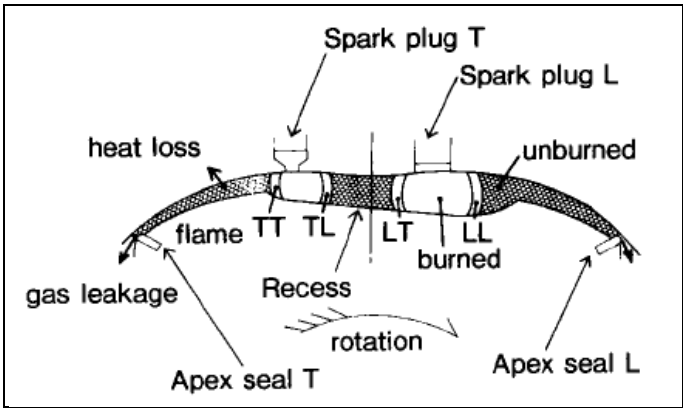

Figure 45. Flame propagation model for two-spark-plug rotary engine (*64*).

Figure 46 shows an arrangement of dual spark plugs for large rotary engines, which was tested at Deere (*79*). The spray ignition was used, which is when a pilot injector injects a small amount of fuel and generates a fuel-air mixture near the spark plug in the cavity. An additional spark plug (i.e., auxiliary igniter) is used to provide immediate ignition of a secondary region of the fuel-air mixture. The dual-ignition concept was based on the CFD analysis that showed very nonuniform mixture distributions near the TC, with two combustion regions being separated by a region of overly rich, slow-burning mixture. One igniter resulted in the delayed ignition of the second combustible region, which was delayed well beyond TC (*8*). Dual ignition was thought to provide simultaneous ignition in two regions, which would enhance the overall rate of heat release. As expected, the dual ignition system resulted in a faster pressure-rise rate, higher peak pressure, and improved thermal efficiency (see figure 47) (*8*). The single-igniter case shows two pressure peaks representing the sequential burning of the two combustible regions. The achieved BSFC was about 231 g/kWh. However, this improvement of 8%–10% in BSFC was achieved at low to medium loads (*8*).

Abraham and Bracco (*80*) also predicted a 7%–10% efficiency improvement when two ignition sources were used in their 3-D combustion model for a direct-injection stratified-charge rotary engine. At higher loads, a dual igniter at advanced timing resulted in a detonation type of combustion instability, leading to local overheating, seal lockup, and excessive blowby of hot combustible mixture into the following chamber. This also increased the possibility of detonation in that chamber. When the spark timing was retarded, the second igniter was not able to provide consistent ignition. This led to substantial deterioration of the engine performance at high loads. The researchers needed to optimize the spark timing as more fuel was injected. Furthermore, they needed to optimize the locations of the spark plugs for the given engine configuration.

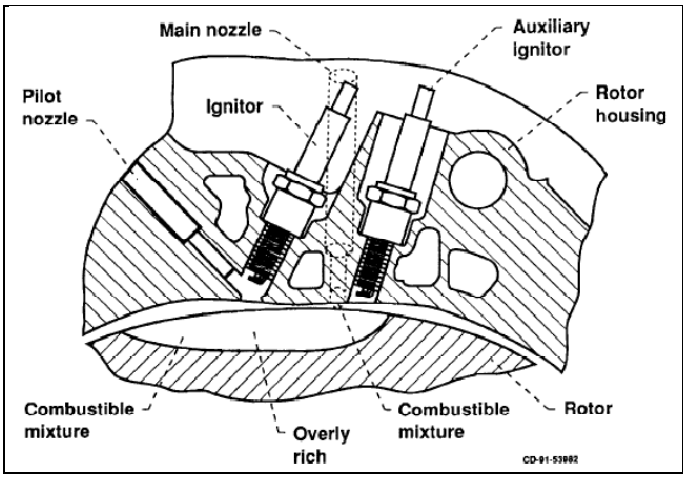

Figure 46. Dual spark ignition arrangement (*79*).

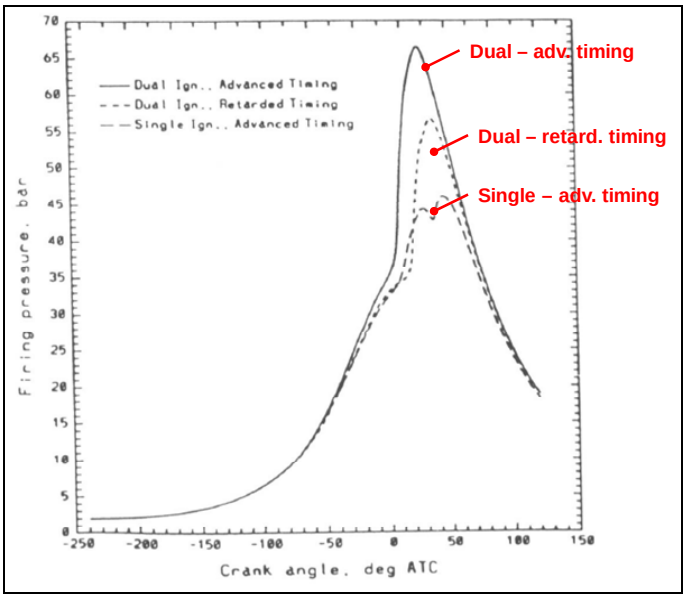

Figure 47. Comparison of predicted dual and single-ignition pressures with validated Sverdrup Technology AGNI-3D code (*8*).

The trailing side of the combustion chamber in a rotary engine generates a strong squish flow, which pushes back the flame front (i.e., TT), as shown in figure 48 (left) (*17*). This can be a problem for a premixed fuel-air mixture with the two-plug ignition system because flame cannot reach the trailing side, especially at mid to high engine speeds, which would exhaust a significant amount of unburned hydrocarbons. The same is true for the leading side of the combustion chamber. However, this can be an advantage for the stratified-charge combustion system because only fresh air will be in the trailing and leading sides.

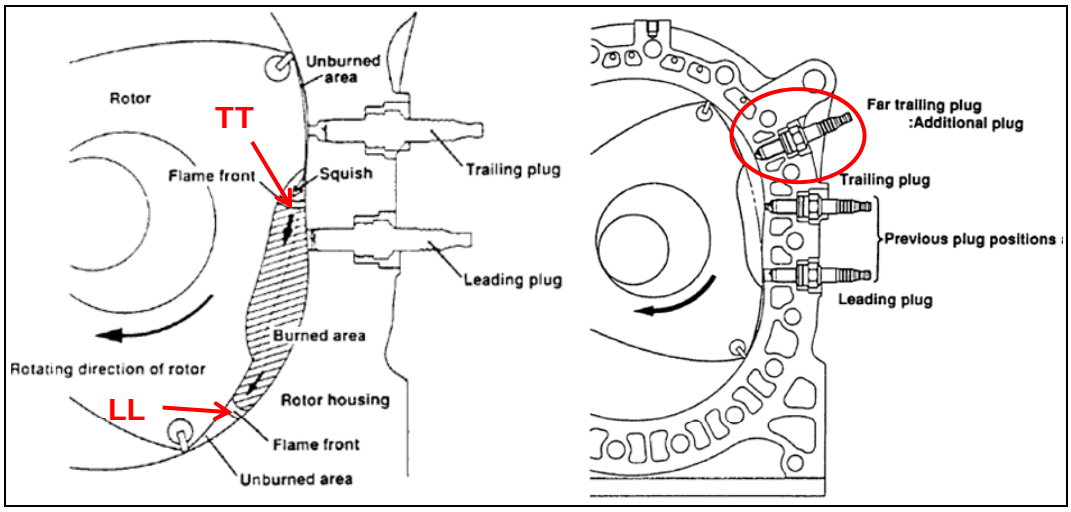

Figure 48. Push-back of flame front by squish flow (left) and three-plug ignition system (right) (*17*).

Mazda introduced a three-plug ignition system in their R26B racing car engine, as shown in figure 48 (right) (*17*). They employed an additional spark plug in the trailing side. The intent was to ignite the fuel-air mixture before the squish flow is generated. In this way, the mixture in the squish area would burn more completely and accelerate the flame propagation, which will lead to improved fuel economy. The volume of the spark plug hole was made as small as possible to prevent any gas flow from the high-pressure chamber to the following low-pressure chamber when the apex seal is partially across the plug hole. However, the size of the plug hole should not be too small as to affect the combustion. Figure 49 shows the improvements in load and fuel consumption relative to the two-plug system. Fuel consumption decreased about 3%, while load increased more than 2% at most of the engine speeds. Fuel consumption improvement decreased at lower engine speeds, while load improvement was reduced at higher engine speeds. Although it needs to be verified, the three-plug ignition system may not be beneficial for the stratified-charge rotary engine.

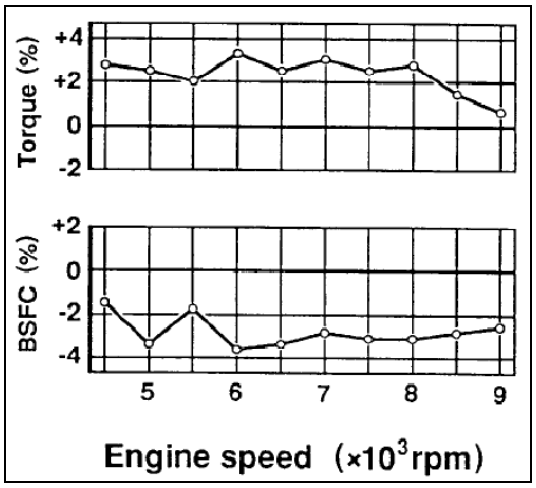

Figure 49. Comparison of torque and BSFC between two- and three-plug systems (*17*).

A single injector with the open combustion chamber will be one option for small-scale rotary engines because of the space constraints. Eiermann et al. (*53*) used a single injector in an open combustion chamber of a small spark-assisted direct-injection rotary engine fueled with diesel and a variety of jet fuels (shown in figure 32). The engine was successfully demonstrated at constant speed and various loads for multiple fuels. The fuel consumption measured was below 330 g/kWh at various operating regimes. Further work was proposed to improve engine power, fuel consumption, and operation flexibility over a broader range of speeds and loads. Eiermann et al. evaluated the spark plug location relative to the injector nozzle in the fuel spray visualization rig and refined the spark plug location based on the performance data from the engine bench. The effect of the spark depth on engine startability was evaluated by testing various spark plug depths with gaskets of varying thicknesses; the result is shown in figure 50.

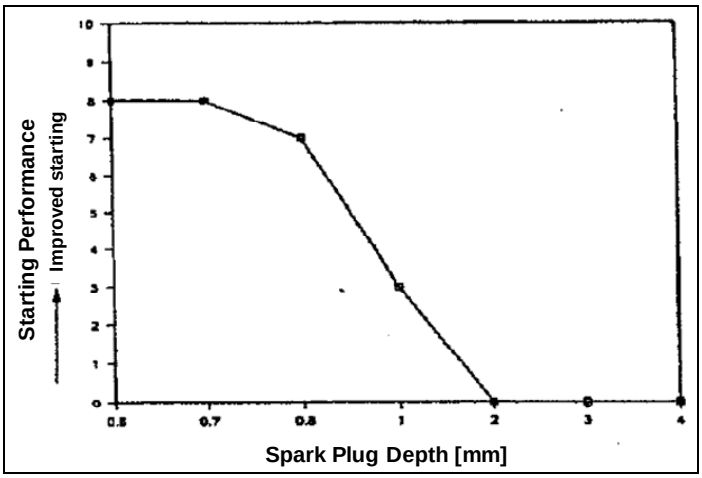

Figure 50. Influence of spark plug depth on engine startability (*53*).

Clearly, the spark plug depth should be at least 1 mm or lower in order to have good startability. In general, one of the most critical factors affecting the combustion processes in the single-injector open chamber SI small rotary engine was the ignition delay of the fuel-air mixture. One simple way to improve startability would be to use an ignition system with sufficient energy, which would easily ignite lean fuel-air mixture. The use of higher ignition energy is becoming common in modern GDi engines.

Hoffman et al. (*72*) compared the glow plug and spark ignition systems in a stratified-charge rotary engine (2013R SCORE). The maximum power of the engine was 340 hp at 8000 rpm and its CR was 7.5:1. It was equipped with the dual fuel injection system (i.e., pilot and main injectors), a TD08H-23K-33 cm^2 turbocharger, and a glow plug ignition system with two Nihon Gaishi Kaisha (NGK) CZ02 glow plugs. The engine was first tested with the glow plug ignition system as its baseline, and then the glow plug ignition system was replaced with a D&V (predecessor of FOE, both are company names) spark ignition system. The switch to the spark ignition system resulted in improved fuel consumption, engine startability, and combustion quality, as shown in figure 51 (*72*). The observed BSFC improvement for the spark ignition system was as high as 4% compared to the glow ignition system. One of the reasons for lower performance of the glow ignition system could be that the glow plugs were recessed too much in the housing, which was restricting the flow in and out of the pilot cavity.

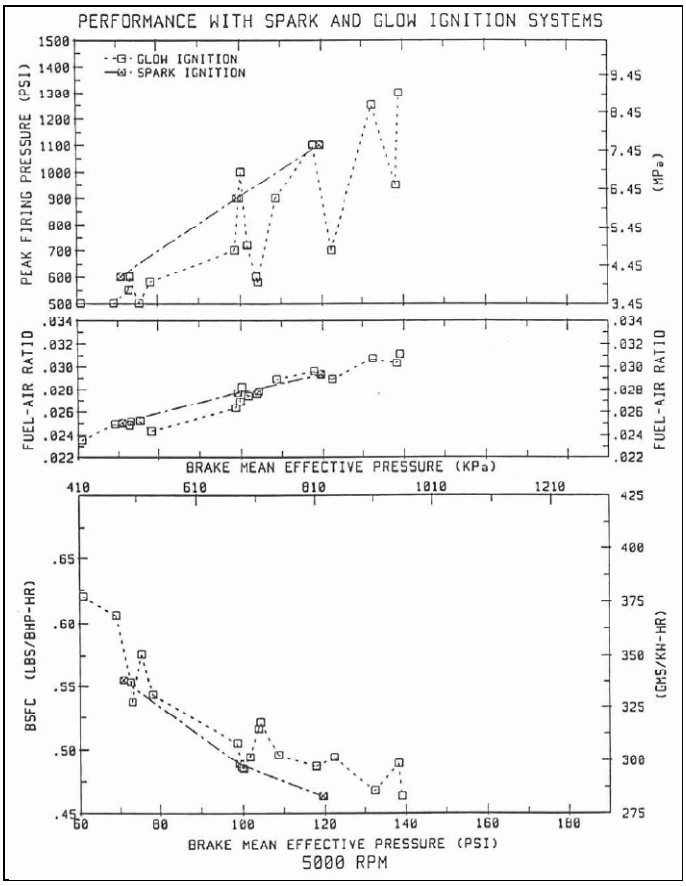

Figure 51. Performance comparison of spark and glow ignition system (*72*).

However, the D&V spark ignition system was unable to fire the engine at the engine speeds above 6500 rpm. This result was referred to an inability of a certain component in the ignition system and led to the evaluation of several different spark ignition systems. Prior to this evaluation, the FOE ignition system was used to study the effects of ignition timing and duration of the spark ignition system at two engine speeds (i.e., 4000 and 7000 rpm) by using a variable ignition start and duration control system. The results show that the ignition start time could be tolerated up to 10° delay, and the required ignition duration was at least 35°. It was also observed that the engine was unable to tolerate any spark timing later than pilot injection timing at 7000 rpm and light load. The optimal ignition timing was found to be the same as the start of the pilot injection timing. The summary of the finding from the tests are shown in table 2.

Table 2. Fining of major ignition parameter setting (*72*).

Spark Duration	40° CA desired for 150 to 10,000 rpm
Spark Energy	5000 mJ at 150 rpm and 50 mJ at 10,000 rpm Varying linearly between 50 and 10,000 rpm at constant spark duration
Spark Voltage	35 kV for 1.78-mm spark gap at combustion pressure of about 21 bar

Four different ignition systems were assessed in the bench testing for the 70 series NASA rotary engine development, which is summarized in table 3. The FOE ignition system was selected for the continuous work, and two ignition systems were built based on the FOE ignition system by ABB (Asea Brown Broveri) Process Analytics.

Table 3. Major ignition system parameters affecting the combustion (reproduced from Hoffman et al. [*72*]).

Ignition System	Feature	Engine Speed (rpm)	Spark Duration (°CA)	Spark Energy (mJ)	Spark Voltage (kV)
FOE (Autotronic)	Continuous spark	150	80	6900	41
		10,000	40	50	41
MSD 7 (Autotronic)	Capacitive multiple spark discharge	150	28	280	35
		10,000	28	40	35
HiFire (Mallory)	Inductive single spark	150	1.8 (2 ms)	200	35
		10,000	72 (1.2 ms)	110	35
Plasmachine	Continuous spark	Not tested			

Table 4 shows the comparison of the FOE and ABB spark ignition systems. The ABB ignition system shows slightly lower spark duration, spark energy, and spark voltage compared to the FOE ignition system. The spark voltage difference was thought to be the result of the variation in the simulated combustion pressure. The two tests were performed at significantly different time intervals in the test pressure vessel. The ABB ignition system exhibited misfiring at 5000 rpm. The FOE ignition system presented slightly better engine operation than the ABB system. It was postulated that the slightly poor engine operation with the ABB ignition system was due to the slightly shorter spark duration because the two systems were essentially the same. The task was not continued due to other priorities, and the result was inconclusive.

Table 4. Comparison of FOE and ABB ignition systems (reproduced from Hoffman et al. [*72*]).

Ignition System	Feature	Engine Speed (rpm)	Spark Duration (°CA)	Spark Energy (mJ)	Spark Voltage (kV)
FOE (Autotronic)	Continuous spark	150	80	6900	41
		10,000	40	50	41
ABB	Continuous spark	150	78	6700	38
		10,000	36	44	38

In contrast to the findings of Hoffman et al. (*72*), Muroki and Moriyoshi (*57*) observed that a glow plug pilot flame ignition system showed better ignitability and improved combustion characteristics, particularly in the lean mixture range, compared to the spark ignition system. Although they used a model Wankel combustion chamber in a two-stroke diesel engine, as shown in figure 52, this result implies that the use of a glow plug ignition system can give a different outcome for different engine configurations and test methods. Thus, a glow plug ignition system should not be excluded for further assessment. Muroki et al. (*58*) performed further research on the comparison of the glow plug and spark plug ignition systems in a

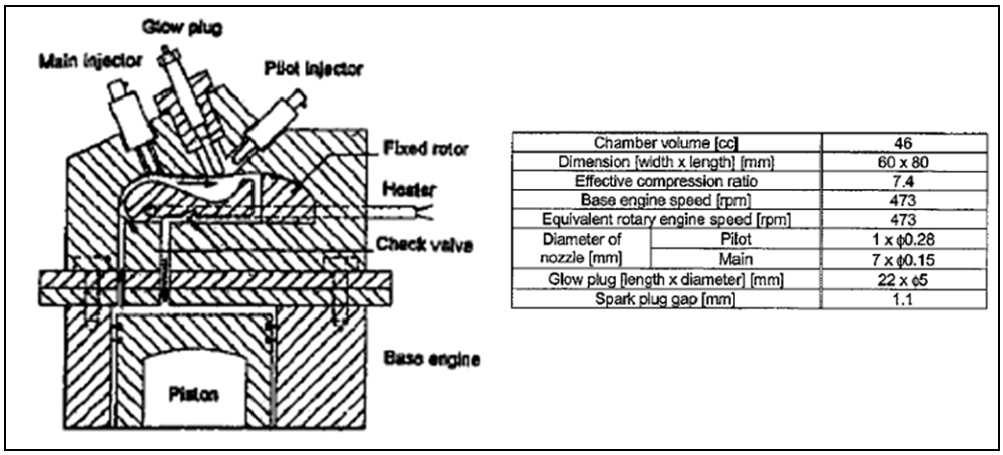

Chamber volume [cc]		46
Dimension [width x length] [mm]		60 x 80
Effective compression ratio		7.4
Base engine speed [rpm]		473
Equivalent rotary engine speed [rpm]		473
Diameter of nozzle [mm]	Pilot	1 x ϕ0.28
	Main	7 x ϕ0.15
Glow plug [length x diameter] [mm]		22 x ϕ5
Spark plug gap [mm]		1.1

Figure 52. Model Wankel combustion chamber in a two-stroke diesel engine (left) and engine specification (right) (*58*).

simulated direct-injection stratified-charge rotary engine by using both the experiment and numerical simulation. The high-speed images in figure 53 (left) show that flame propagated to the leading and the trailing corners of the combustion chamber with the glow plug ignition system; however, the flame could not reach the squish areas of the combustion chamber with the spark plug ignition system. In figure 53 (right), the glow plug ignition system presents significantly higher accumulated heat release than the spark plug ignition system. This indicates that the glow plug ignition system had more ignition energy than the spark plug ignition system, as shown in figure 53. Consequently, it was not a fair comparison between the spark and glow plug ignition systems. Evidently, the amount of ignition energy has a significant impact on the ignition of the stratified-charge fuel-air mixture. Therefore, more ignition energy would enable combustion initiation of leaner mixtures.

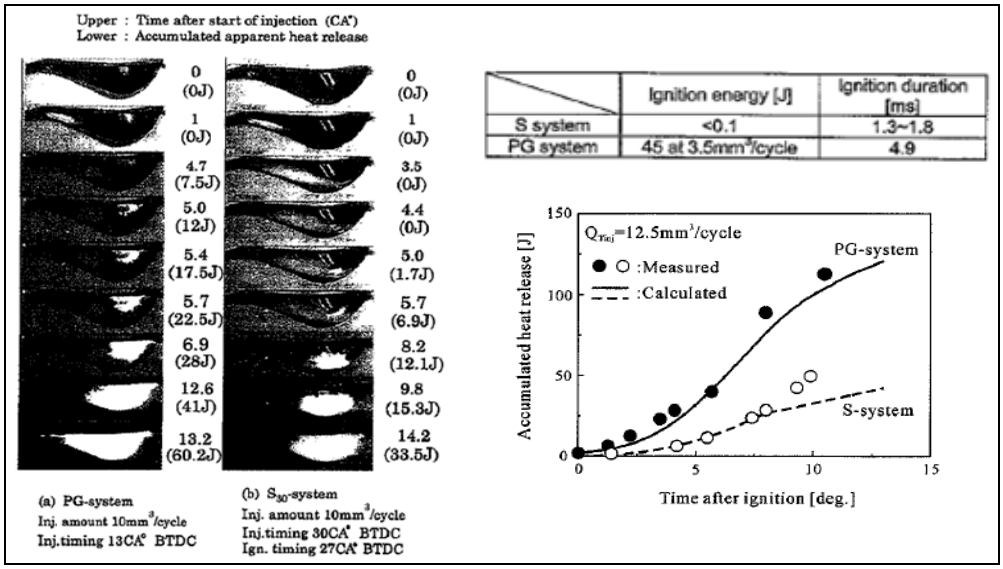

Figure 53. Comparison of high-speed images (left) and accumulated heat release (right) between glow and spark plug ignition systems (*58*).

Muroki et al. (*58*) used a prototype direct-injection stratified-charge rotary engine equipped with a glow plug ignition system to assess its multifuel capability, as shown in figure 54. The preliminary results show that the direct-injection stratified-charge rotary engine can be operated with the glow plug ignition system. Also, the engine is multifuel capable. In this research, they tested gasoline, light oil, and kerosene. Figure 55 demonstrates the performance of the DI-SCRE engine with light oil. The observed indicated specific fuel consumption (ISFC) was below 240 g/kWh at light loads. Optimization of the fuel injection timings, quantities, and fuel injector location would improve the engine performance.

The Mazda's RENESIS engine employed the microelectrode spark plug ignition system to improve fuel economy (*78*). The microelectrode spark plug uses a small side electrode and a thick gauge central electrode with an extremely thin tip, which promotes stable ignition of lean fuel-air mixtures. In addition, the spark plug was able to achieve high heat resistance by keeping lower temperatures for side and central electrodes. The tip material of the central electrode was also replaced from platinum to longer-lasting iridium.

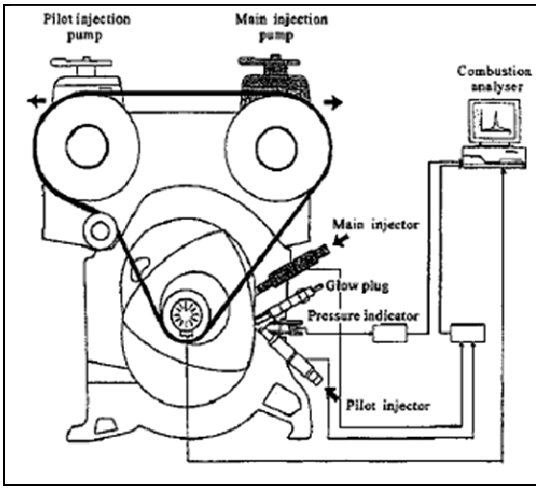

Engine		Rotary Engine
Displacement		654 cc ×1 Rotor
Compression ratio		9.4 : 1
Port timing	I.O.	45 °ATDC
	I.C.	50 °ABDC
	E.O.	75 °BBDC
	E.C.	50 °ATDC
Fuel injection pump	Type	Distributor type
	Inj. press.	13 MPa
Injection nozzle	Pilot inj.	1 φ 0.28 mm
	Main inj.	7 φ 0.15 mm
Injection timing	Pilot inj.	48 °BTDC
	Main inj.	30 °BTDC
Glow plug		9 Volt ×10.5 Amp.

Figure 54. Prototype of the direct-injection stratified-charge rotary engine (left) and its specification (right) (*58*).

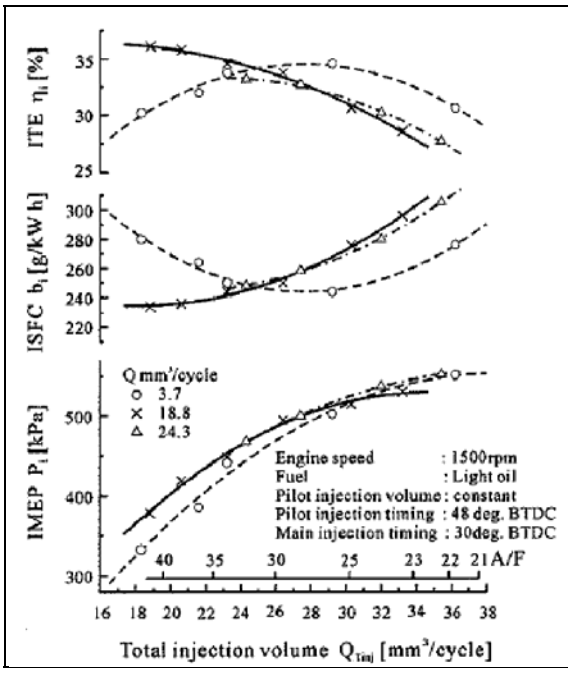

Figure 55. DI-SCRE engine performance vs. total fuel injection quantity with dual injections (*58*).

4.4 Apex and Side Seal Designs

Sealing has been one of the major problems of the rotary engine and is critical for efficient operation. However, unlike the issues with the higher fuel consumption, sealing problems can be improved by using advanced materials technologies (i.e., materials, heat treatment, and surface coating) in some degrees (*81*). As described earlier, the shape of the rotary engine combustion chamber is designed to make the three tips of the rotor stay in contact with the walls of the chamber (i.e., apex seals), along the edges of the rotor (i.e., side seals), and at the junctions between the apex and side seals (i.e., corner seals), which forms three sealed volumes of gas. Oil seals are used to control oil consumption. Significant pressure differences between the three chambers of the rotor in different phases of the cycle require efficient seals. These are demanded to avoid leaks between the adjacent volumes to reduce a performance loss. Typically, oil is introduced into the intake system to lubricate these gas seals. One or two springs are provided on the backside of each seal to keep close contact with the surface and remain sealed even when it is worn, as shown in figure 56 (*20*, *22*).

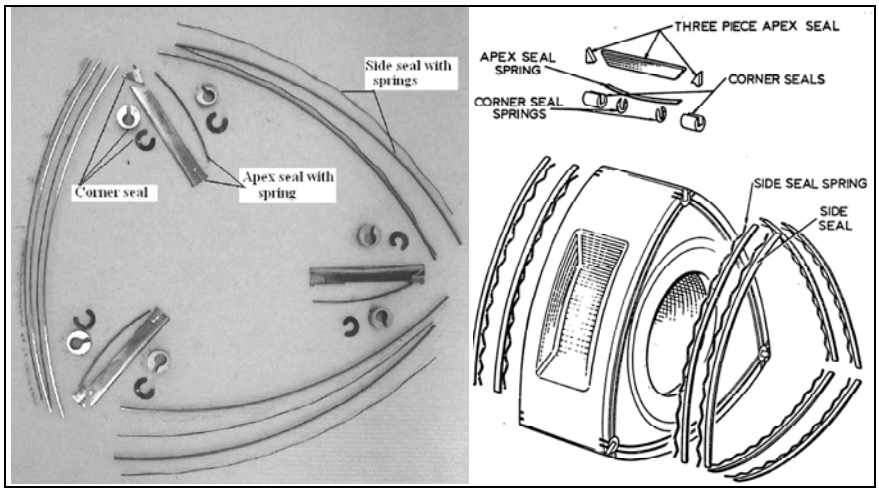

Figure 56. Gas sealing with springs (left) (*20*) and exploded view of typical engine gas seals (right) (*22*).

The major crevices (i.e., narrow open areas in the combustion chamber) are around the apex and side seals, along with smaller volumes in spark plugs and fuel injectors. The total crevice volume is about 3% of the clearance volume, and as much as 10% of the total cylinder mass (i.e., mixture mass of air and fuel) is pushed into the crevice at peak pressures for typical reciprocating engines. The measured total crevice volume of the Wankel engine, which is shown in figure 57, was 5% of the clearance volume (*22*). The volume associated with the side seals was roughly one-half that of the volumes of the apex and corner seals (*22*). The crevice volume incurs a large amount of heat transferred to the engine components and the removal of charge from the combustion chamber, which results in a performance loss.

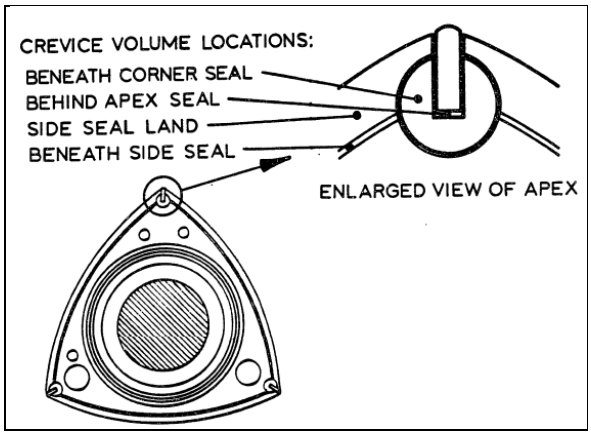

Figure 57. Schematic of crevice volume locations in the Wankel engine (*22*).

Insufficient sealing would allow the gas to flow from a high- to a low-pressure chamber. Leakage decreases volumetric efficiency (both real and effective) and allows unburned fuel energy and sensible enthalpy to pass to other chambers, which leads to decreased engine performance (*25*, *52*). Real volumetric efficiency is decreased by burned products entering the induction chamber from the adjacent combustion and exhaust chambers. On the other hand, effective volumetric efficiency is reduced as the charge escapes from the combustion chamber to the exhaust and intake chambers prior to combustion.

The primary differences of the side seal leaks from apex leaks are as follows:

- Burned gas will pass through the side seal during combustion in proportion to the surface area wetted by the burned gas volume.
- Leaks pass through the side seal to the rotor side, to the side intake port (only for a rotary engine with side ports), and to the intake chamber. Thus, most of the side seal leakage ends up in the intake chamber and is not evenly distributed between the leading and trailing chambers.

A major issue with the leaks is reduced effective CR, which worsens the ignition of the fuel-air mixture (*16*, *18*, *40*). Figure 58 compares the components of the seal arrangement between the rotary and reciprocating engines (*49*, *82*). As being distinct in the figure, the rotary engine has only one sealing line of contact, compared to the reciprocating engine that usually consists of two to five rings, including at least one compression ring. Although the piston engine has ring gaps compared to the rotor engine with almost no gap, it is easier to compensate the compression loss by controlling the clearance or displacement volume. Therefore, the piston gaps in the piston engine are not a serious issue. Furthermore, the blow-by gases are redirected to the intake manifold to remove any evaporative emissions. In contrast, the rotary engine has less flexibility in controlling the CR to compensate the compression loss due to the seal leaks. In general, it is believed that the poor fuel economy of the rotary engines is caused by the leaks of unburned fuel-air mixture through the seals during compression and combustion to the neighboring chambers (*20*). These leaks are also the main contributor of the high hydrocarbon emissions of the Wankel engine (*59*). Another major contributor of the unburned hydrocarbons would be lower combustion efficiency. A zero-dimensional combustion model by Norman (*22*) showed that the leakage of the apex seal had the major impact on the engine performance. At low loads, both low thermal energy utilization and crevice volume showed minor influence on the engine performance; however, they would have significant effects at high loads.

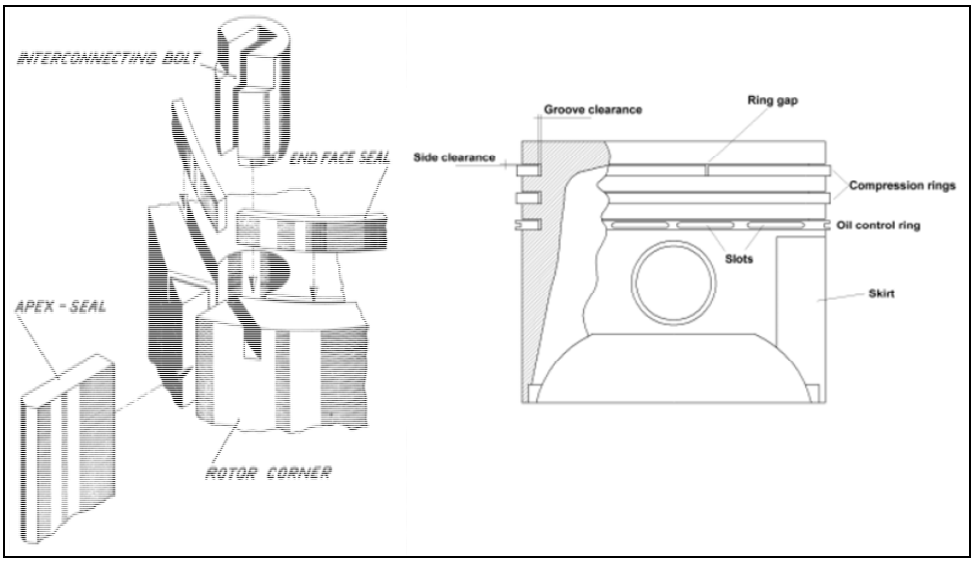

Figure 58. Components of seal arrangement (left) (*49*) and piston and piston rings (right) (*82*).

Eberle and Klorap (*83*) used a rotary engine analytical model to calculate apex and side seal leaks, and they used the model in conjunction with experimental data to estimate the relative importance of apex and side seal leaks. Their estimated apex seal leakage was 66%–75% of the total leaks. This apex seal leakage increased as the engine speed decreased. The same phenomenon is observed in the blow-by leakage in a reciprocating engine, in which blow-by increases as the engine speed decreases. It was concluded that a potential gain can be made by reducing the leakage area. They predicted that a reduction in leakage area of 5% at 2000 rpm could reduce BSFC by 6.5%.

Nguyen (*52*) used a computer simulation of the direct-injection stratified-charge Wankel engine for a John Deere model 1007R engine (CR tested from 7.5 to 8.92) to assess the effect of the leakage area on the engine performance. The model combined the apex and side seal leaks into three side seal leakage areas. Figure 59 shows that the indicated power increased by 12.4%, IMEP increased by 12.8%, and ISFC decreased by 15.7% as the leakage area changed from 0.02 to 0 cm^2 per apex. Although a complete elimination of leakage (i.e., zero leakage area) is not practically possible, even a modest reduction in the leakage could result in significant performance improvements.

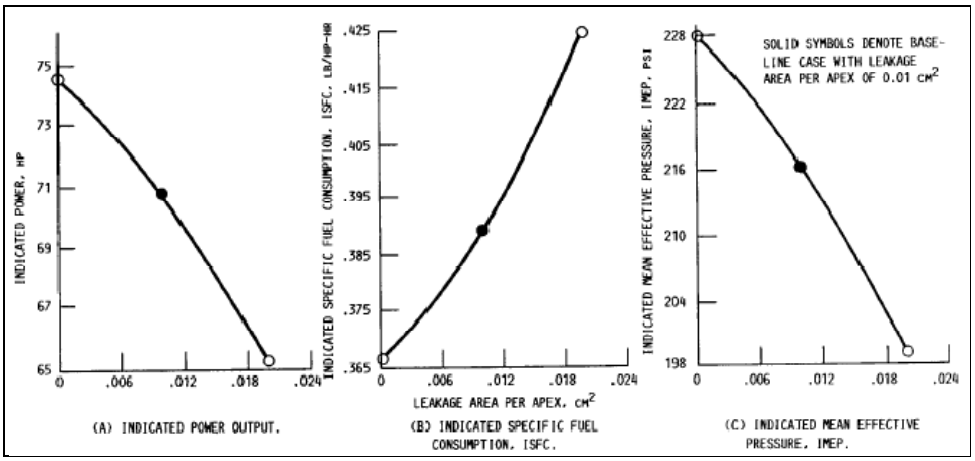

Figure 59. Indicated power, ISFC, and IMEP with respect to leakage area per apex at 4000 rpm and 8.9 bar BMEP (1007R turbocharged engine) (*52*).

Nguyen et al. (*84*) used the computer simulation for an Outboard Marine Corporation (OMC) rotary engine (CR = 12.94) to evaluate the influence of the leakage area on the engine performance, which was similar to Nguyen (*52*) and shows the same trend. However, this study shows additional engine performance data, such as the exhaust temperature and the volumetric efficiency, as shown in figure 60. As the leakage area reduced from 0.02 to 0.005 cm^2/apex, both the exhaust temperature and the volumetric efficiency increased almost linearly. In this case, the power increase was 40%, the rotor and housing temperature increase was 6.4%, the volumetric efficiency increase was 11%, and the ISFC decreased 45%. The better fuel economy for the OMC engine than the John Deere 1007R engine would be mainly due to its higher CR.

Kohno et al. (*85*) identified that the combustion misfires at light loads are mainly due to excess internal exhaust gas recirculation (EGR) gases, which was in this case caused by the leaks during the unique intake-exhaust mechanism of the rotary engine. In addition, it is possible that the leaks through the apex and side seals could contribute to the higher internal EGR rates in the trailing and leading chambers.

Knoll et al. (*86*) performed a dynamic analysis of rotary engine seals that accounts for apex seal separation from the trochoidal bore, apex seal shifting between the sides of its restraining channel, and apex seal rotation within the restraining channel. Their result shows that the apex seals separate from the trochoidal bore and shift between the sides of their channels, which are similar to what was observed in the experiment. They also showed that at high engine speeds, the apex seal was not separated from the rotary housing.

Since the rotary engine has almost no gap in the apex and side seals, seal loading and wear are the major design factors. Furthermore, typical rotary engines run at high speeds compared to reciprocating engines. This higher speed results in significant wear on the contact surfaces and has led to the development of the new apex seal materials, coating materials, and spray methods, which are resistant to wear (*17*, *87*).

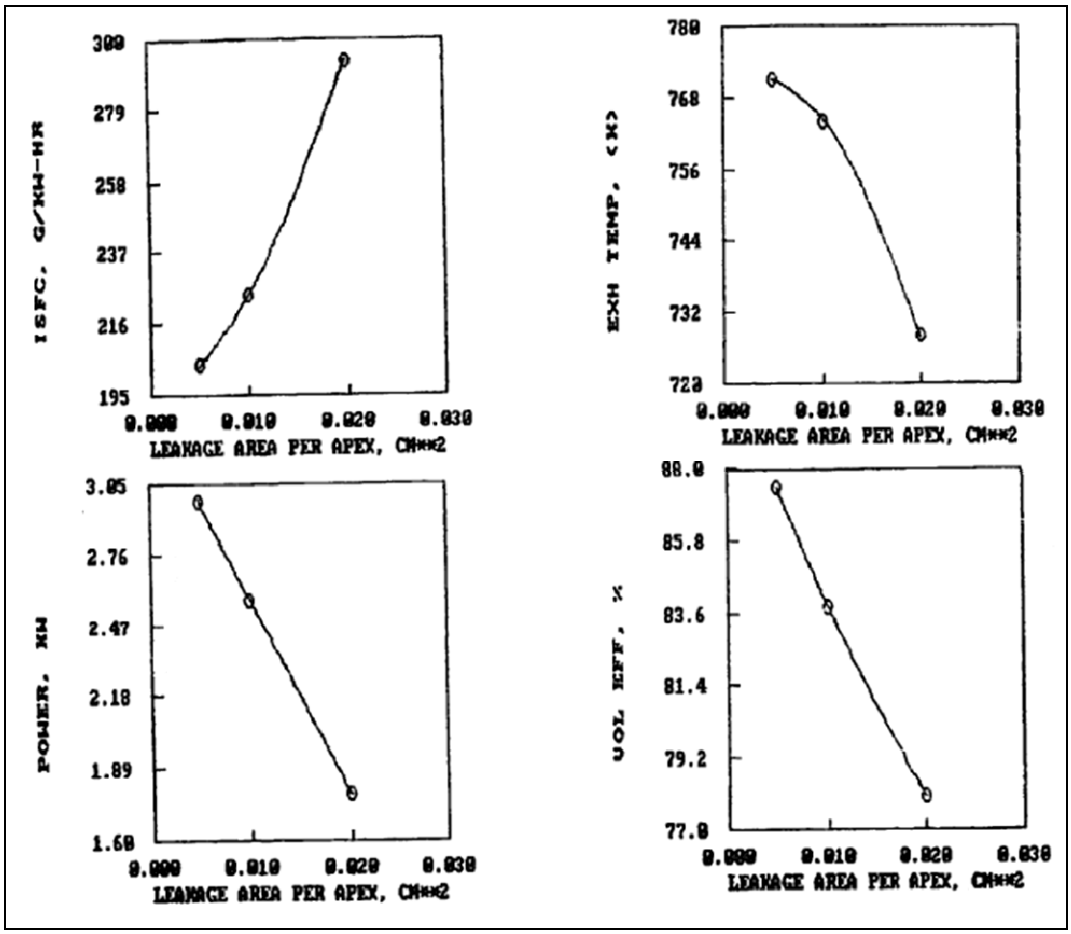

Figure 60. ISFC, exhaust temperature, power, and volumetric efficiency with respect to leakage area per apex at 3200 rpm and $\phi = 0.39$ (OMC engine) (*84*).

A fiber-reinforced silicon-nitride (Si3N4)-based ceramic material was used in the Mazda R26B racing car engine (*17*). The tough seal materials allowed the development of new apex seal designs, which provide tighter sealing (*17*, *88*, *89*). Figure 61 (left) shows an example of the redesigned apex seal compared with the original design for the Mazda R26B racing car engine. The new design presents a two-piece apex seal spring for better gas sealing compared to the original design with a one-piece apex seal spring. In figure 61 (right), the two-piece apex seal shows a consistent increase in torque throughout the entire speed range. However, fuel consumption showed little improvement. For miniscale engines (1–20 hp), spring-loaded apex seals could significantly improve the engine performance because of tight gas sealing (*89*).

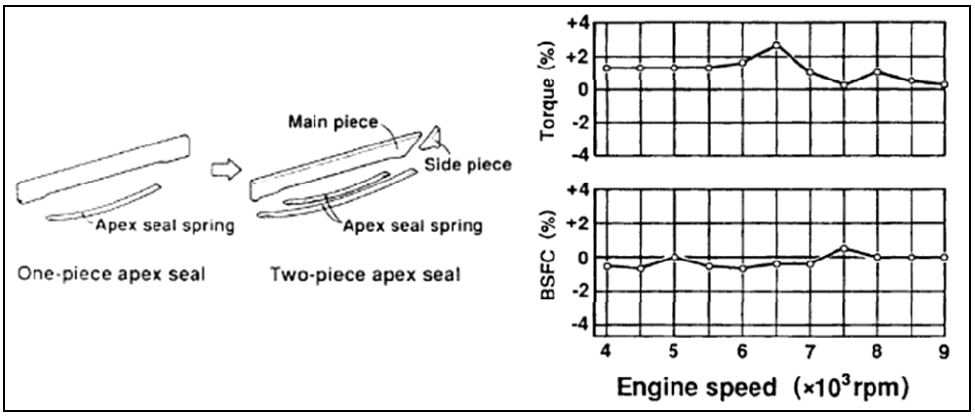

Figure 61. Comparison of apex seals between one and two pieces (*17*).

The internal surfaces of the rotor housing and side housings experience significant wear due to the apex seals, side seals, and oil seals, which are sliding at high speed and high load. Various coating materials and coating methods (*17*, *87*) have been developed to increase wear resistance and to reduce friction. Figure 62 presents a cermet coating (left) and its performance comparison with the soft-nitrided cast iron (right), which was used in the Mazda R26B racing car engine. A cermet is a composite material composed of ceramic (cer) and metallic (met) materials. Carbide-based cermet coating is known to provide superior wear resistance in high-temperature environments. A chrome carbide-based coating was applied with the detonation gun spray on the surfaces of the engine, as shown in the figure (left). The result shows that the detonation gun spray coating of the chrome-carbide cermet had less wear than the soft-nitrided cast iron.

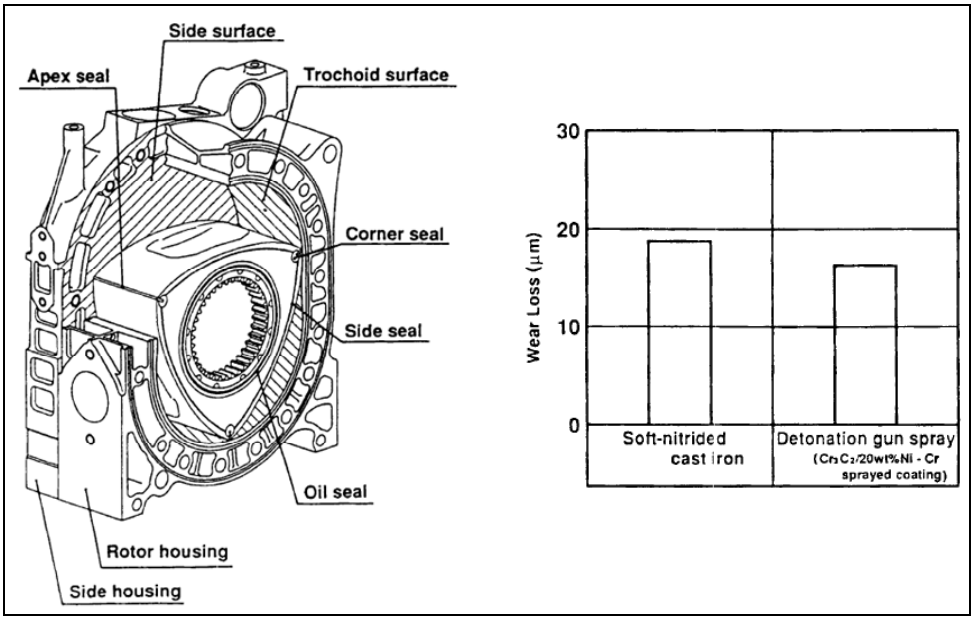

Figure 62. Cermet coating: shaded area (left) and result of reciprocating wear rig test (right) (*17*).

Figure 63 (*78*) shows a new cut-off seal of the Mazda RENESIS engine, which is located between the rotor's dual oil seal and side seal. The goal of this sealing is to eliminate blow-by of gases between the intake and exhaust ports via the slight gap between the oil seals and side seals on the side of the rotor, and to impede carryover of exhaust gas to the next intake cycle. The wedge-shaped side seal is optimized to remove any carbon buildup in the side seal and is more congruent to its opposed frictional surface for better sealing efficiency.

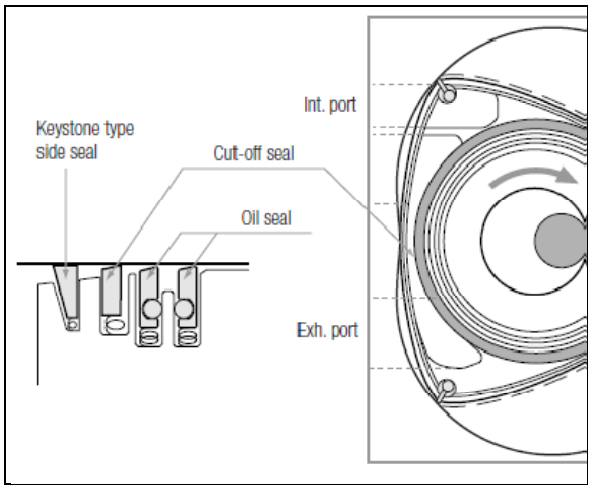

Figure 63. Mazda RENESIS cut-off seal (*78*).

Unlike large-scale rotary engines that have complex sealing mechanisms to separate the three operating chambers, small-scale engines have more difficulty implementing numerous sealing components because of relatively difficult assembly. Therefore, few and relatively simple seals are used for apex sealing. Consequently, the ratio of mass leakage to mass throughput is not constant as the size of the engine is decreased. As a result, sealing has been one of the main issues in the development of macro- (*90*), mini- (*38*, *89*), and microscale (*35*, *38*, *91*) rotary engines. The miniscale rotary engine is about the size of a penny from hardened steel and aluminum. Its displacement is 0.348 cc (348 mm^3). The microscale rotary engine is constructed primarily of silicon (Si) and silicon carbide (SiC), and its displacement is as small as 0.00008 cc (or 0.08 mm^3). Figure 64 compares the specification of the mini and microscale rotary engines (*38*).

	Mini-Rotary Engine	Micro-Rotary Engine	
Rotor Diameter	13 mm	1 mm	2.4 mm
Engine Depth	9 mm	0.3 mm	0.9 mm
Displacement	348 mm^3	0.08 mm^3	1.2 mm^3

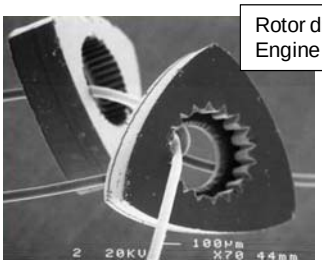

Figure 64. Mini- and microscale rotary engine comparison (*38*).

For small-scale engines, side sealing is not used but relies on tight tolerances (i.e., high smooth finish of the rotor face and housing face) (*18*), which are limited by manufacturing technology. The electrical discharge machining can produce tolerances ranging from 0.003 to 0.2 mm depending on the manufacturing approach (*40*). Leakage problems in the MEMS rotary engine, in which the minimum tolerance is extremely important to maintain minimum CR, has been a limiting factor for an acceptable efficiency. A fluid analysis showed that a necessary distance is about 2 μm between the rotor and the housing of the engine. A minimum CR should be maintained over the characteristic time of 2 ms at a shaft speed of 40,000 rpm. A mechanical analysis is needed to ensure that the apex seals will maintain the required minimum distance by integrating a spring-loaded apex design. For microscale rotary engines, minimizing the leaks is limited with the conventional techniques, but scaling effects may help the sealing. On the microscale, the effects of fluid viscosity dominate and thus could reduce leakage (*91*). If a target gap tolerance cannot be met with the manufacturing approach, more viscous fluid may be used for better sealing (*91*).

Tight sealing is needed to prevent gas leaks during the compression stroke and the combustion event. However, the tight sealing increases the frictional losses. It was estimated that the seal friction accounts for about 25% of rotary engine friction (*47*). An analysis of the apex seal friction showed that the friction increases as displacement decreases to the 1/3 power of the displacement in equation 2. However, the friction due to the face seals decreases as displacement decreases by the 1/3 power of the displacement for a constant gap between rotor and end plates (equation 3). f is a normalized friction and V_d is the displacement volume. Sprague et al. (*40*) performed a motoring friction test on 0.367-, 5-, and 500-cc rotary engines and found that the friction decreased as the engine size was reduced. This result suggests that the side seal friction is the dominant friction loss mechanism for small-scale rotary engines.

$$f_{apex} \propto \frac{1}{V_d^{1/3}} \qquad \text{for apex seal} , \tag{2}$$

and

$$f_{side} \propto V_d^{1/3} \qquad \text{for side seal} . \tag{3}$$

New apex seal designs, such as those shown in figure 65, have been introduced in the past to reduce friction loss (*92*). The three-piece apex seals allow for sliding with low friction over the treated-chrome-alloy-plated housing inner surface. The three-piece seal design with two leaf springs decreases seal mass through reduced thickness. This arrangement provides the area contact rather than the line contact between the seal and rotor. The reduced thickness of both apex and side seals could decrease friction with the housing by reducing the seal area on which the normal force is applied on the housing, which causes friction.

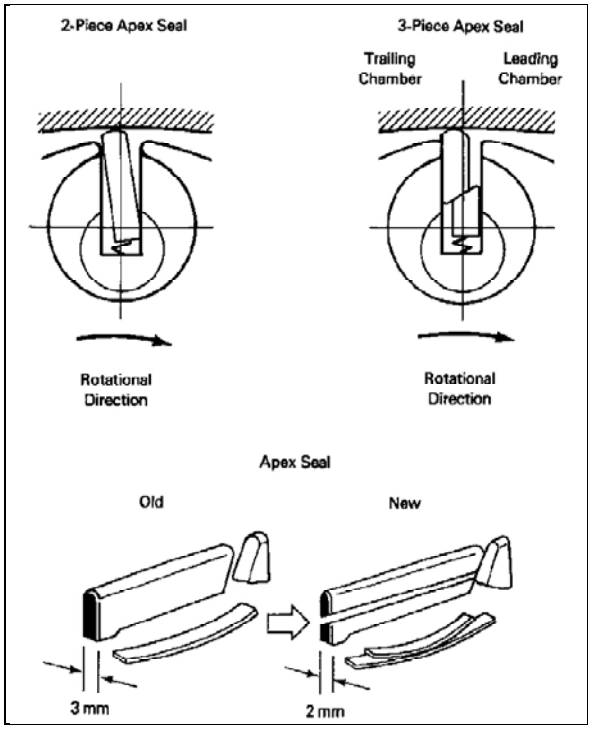

Figure 65. Design improvements in the apex seals of the Mazda RX-7 rotary engine (*92*).

4.5 Heat Loss and Flame Quenching

Flame quenches at a certain distance from its source as it propagates. The flame quenching distance is defined as a minimum distance from the wall as the flame propagates, below which the flame is quenched by the wall (*93*). As an example, figure 66 (*94*) shows a flame quenching distance and flame front. The quenching distance is the "dead space" between the flame front and the wall, which determines the thickness of the unburned layer on the wall. Flame quenching occurs because of thermal losses and radical destruction at the walls (*95*). Heat loss

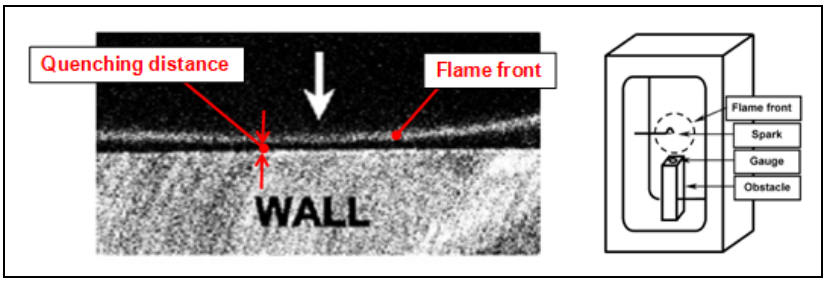

Figure 66. Picture showing quenching distance and flame front (*94*).

has more influence on flame quenching than fuel-air mixture quality (*22*). In other words, the flame quenches not because of the nonavailability of sufficient fuel near the walls but because of heat loss to the cold walls. A minimum quenching distance is determined by the ratio of the heat loss to the walls to heat generated by the combustion reaction, as shown in equation 4 (*93*), where α is the thermal diffusivity ($=\lambda/\rho_0 c_p$), ρ_0 is the combustible mixture density, c_p is the specific heat, ϕ_0 is the stoichiometric mole fraction of the combustible mixture, $\bar{r}$ is the reaction rate, T_q is the lowest temperature for flame propagation, T_f is the flame temperature, and T_0 is the wall temperature. The thermal quenching distance for methanol at standard temperature and pressure is 2 mm (*96*). Figure 67 shows the quenching distance for a premixed methane (CH_4)-air mixture combustion measured with respect to pressure and equivalence ratio in a constant volume chamber (*94*). The result shows that the quenching distance decreases exponentially as the chamber pressure increases. The richer mixture shows a shorter quenching distance compared to the leaner mixture. In the same manner, the thermal quenching distance in an actual engine is decreased because of high temperature and high pressure in the combustion chamber (*96*).

$$d = \sqrt{\frac{4\alpha\rho_0}{\phi_0 \bar{r}}\left(\frac{T_q - T_0}{T_f - T_0}\right)} \propto \sqrt{\frac{\alpha}{\bar{r}}}. \qquad (4)$$

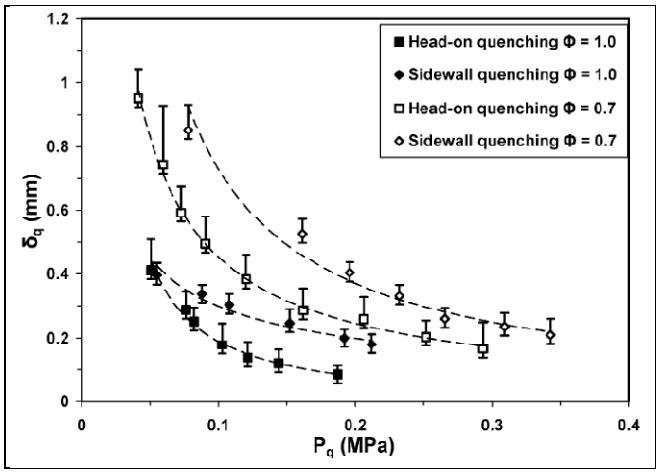

Figure 67. Quenching distance with respect to pressure and equivalence ratio (*94*).

In rotary engines, the maximum heat losses occur at top center where both the temperature and the gas velocity are high because of changes in density by combustion (*22*). The heat transfer coefficient of the Woschni correlation (*97*) is proportional to the rotor width, B, and gas velocity, w, as shown in equation 5 (*40*, *51*).

$$h_c \propto B^{-0.2} w^{0.8} . \quad (5)$$

Heat transfer decreases as the engine size is decreased because of reduced gas velocity, but it increases as the rotor width decreases. The Woschni correlation was made based on the assumption of the turbulent convective heat transfer because large-scale engines were used (*51*). However, the Reynolds number (Re) of a small rotary engine, such as the 1.5 cc engine, ranges from 4200 at 8000 rpm to 7800 at 15000 rpm, which is outside the laminar flow but not fully turbulent (*40*). Unlike in a reciprocating engine in which the Re is defined as $Re = (\rho SB)/\mu$, the Re in a rotary engine used in the literature is $Re = (\rho Dv)/\mu$, where *S* is the piston mean speed, *B* is the bore, *D* is the intake port or tube diameter, *v* is the velocity at the intake port, and ρ and μ are intake mixture density and dynamic viscosity, respectively. Therefore, the Woschni correlation overestimates the heat transfer coefficients with small-scale engines. Also, for the small-scale engines the total heat loss is higher because of high surface-area-to-volume ratio as the engine size is reduced. Consequently, flame quenching is more likely to occur as the engine size is reduced (*40*).

Since the geometry of the rotary engine is significantly different from that of a piston engine, Lee and Schock (*98*) developed the equations to estimate heat transfer coefficients in the combustion chamber of a naturally aspirated single-rotor 649-cc OMC stratified-charge rotary engine, as shown in equations 6 and 7.

$$h = 19.402 \times T_b^{-0.538} P^{0.3593} v^{0.9794} \text{ for unburned gas region,} \quad (6)$$

and

$$h = 6.2315 \times T_b^{-0.45} P^{0.0689} v^{1.4327} \text{ for burned gas region,} \quad (7)$$

where T_b is the bulk gas temperature, P is the chamber pressure, and v is the local gas velocity. The local gas velocity is assumed to be equal to the local rotor tip speed. These correlations have no engine geometry involved but the engine speed. Since we know that the engine speed increases as the engine size is reduced, the heat transfer coefficient will increase. However, the measured T_b and P would be decreased because of the increased heat loss. Hence, the total heat transfer would be increased as the engine size is reduced. The correlation has about a 27% error near the intake and exhaust ports because of low crank angle resolutions used to acquire chamber pressure. Furthermore, these correlations may be engine specific, not universal.

The following two equations (8 and 9) for the Nusselt number are expressed in terms of temperature ratio and overall flow Reynolds number. T_f is the film temperature (*98*). The Reynolds number decreases as the engine size is reduced. Also, the turbulent Reynolds number

($v'l_0/\nu$) is reduced because the integral length scale (l_0) is decreased, where v' is the turbulent intensity and ν is kinematic viscosity. The integral length scale is typically the size of the engine chamber diameter. For example, the bore diameter is the integral length for a reciprocating engine. Since mixing is enhanced by turbulence, attaining adequate mixing is becoming an important factor for small-scale engines.

$$\mathrm{Nu} = 0.3311 \left(\frac{\mathrm{T_b}}{\mathrm{T_f}}\right)^{-4.552} \mathrm{Re}^{0.7387} \quad \text{for unburned gas region,} \tag{8}$$

and

$$\mathrm{Nu} = 13.865 \left(\frac{\mathrm{T_b}}{\mathrm{T_f}}\right)^{-3.28} \mathrm{Re}^{0.3906} \quad \text{for burned gas region.} \tag{9}$$

For rotary engines, flame quenching is one of the main reasons for lower combustion efficiency. Since a rotary engine has a relatively high surface-to-volume ratio and a narrow and long combustion chamber, it experiences more heat loss than an equivalent reciprocating engine. Flames adjacent to relatively cool rotor and chamber surfaces are extinguished, which results in a thin layer of unburned hydrocarbons on the surfaces. Radicals that lead to and sustain combustion by chain carrying and chain branching reactions diffuse to the walls and recombine to form stable species by surface reactions (i.e. radical quenching). Radical quenching is dominant when the wall temperature is relatively high. Surface material has no effect on quenching distance below 500 K, but a large radical quench effect is observed near 1300 K. Flame quenching in the rotary engine is more serious in the trailing edge, where the rotor and the housing are in close proximity. The small clearance and high heat transfer rate during the expansion stroke reduce the temperature and pressure; thus, the flame is not able to propagate against gas motion, which is induced by the squish flow. This can lead to higher unburned hydrocarbon emissions for a premixed Wankel engine but may not be a serious issue for a stratified-charge engine because end gases are almost pure air.

Yamamoto and Muroki (*88*) showed that the BSFC could be decreased by 3% at light loads and 9% at high loads with the stratified-charge rotary engine. The study by Giovanetti et al. (*99*) shows that the stratified-charge rotary engine has the lowest ISHC, as shown in figure 68. However, the overall heat loss can still lead to lower combustion efficiency or more required ignition energy for the stratified-charge engine.

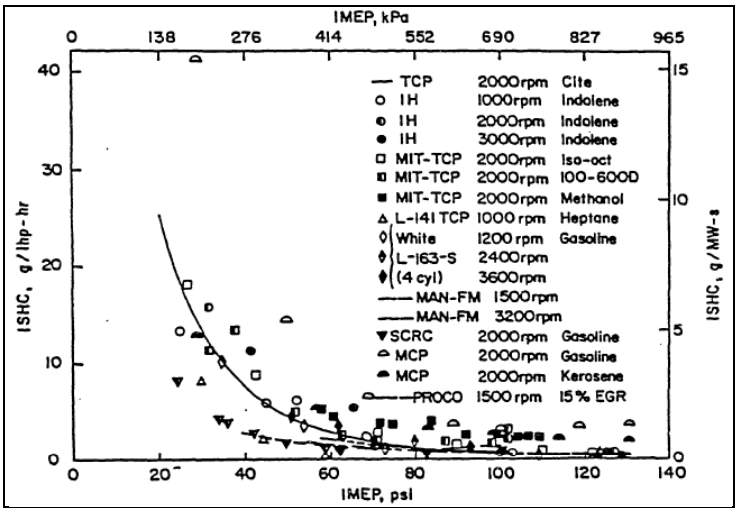

Figure 68. ISHC vs. IMEP for stratified-charge engines (*99*).

Several researchers (*5*, *59*, *88*) have shown that maintaining high surface temperatures can significantly reduce fuel consumption, particularly at light loads. High wall temperatures are favored for higher efficiency but can lead to overheating of the rotor, rotor bearing, and eccentric shaft. The overheated engine parts would result in diminished volumetric efficiency because of the increased temperature of the fresh charge mixture (*81*). Thus, various technologies have been developed to maintain the chamber wall temperatures of rotary engines by minimizing the heat transfer, mainly in the areas of surface coatings with high thermal insulation and wear-resistant materials, such as ceramics (*100*).

Moller (*100*) used Zirconia as a thermal barrier coating (TBC) and PS-200 as the wear coating to reduce heat transfer to the walls. It is critical to achieve uniform coating on the surfaces, so they used computer-controlled plasma spraying and various grinding and honing methods. The results show that the TBC coating significantly improved the efficiency of the engine by reducing heat loss and maintaining higher surface and combustion chamber temperatures. The use of the TBC on both the side walls and the rotor face of the titanium rotor (lower thermal conductivity [19–22.5 W/m-K]) compared to an iron rotor (72.7 W/m-K) reduced the fuel consumption by 16.1%. The PS-200 (solid lubricant) wear coating improved the durability of the engine.

Other approaches used to reduce the overheating of rotor and rotor bearing were oil-cooled rotor (OCR), charge-cooled rotor (CCR), and liquid- and charge-cooled rotor (LCCR), as shown in figure 69 (*81*). The OCR was in engines for high-power density, while the CCR was used for simplicity. The LCCR uses an additional circuit through a hollow eccentric shaft to control the rotor and rotor bearing temperatures. The OCR has a liquid cooling system in the engine housings such as rotor housing, front housing, and rear housing. This cooling system was used in the production engines, such as Mazda and John Deere. The CCR design is preferred for light duty applications because of its simplicity. However, its cooling efficiency is lower than the

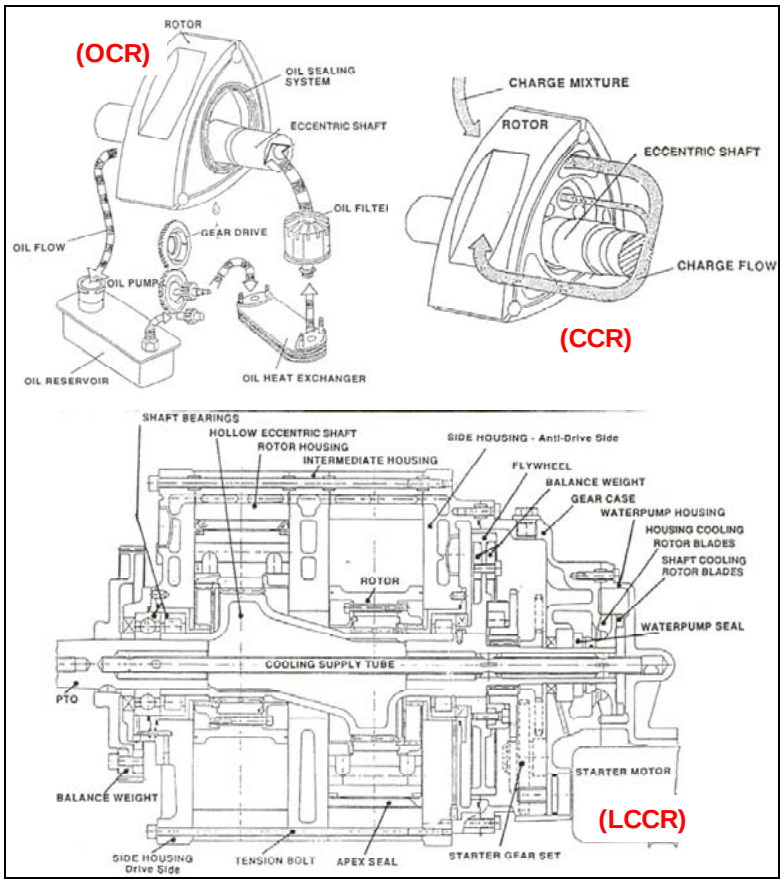

Figure 69. Schematic showing OCR, CCR, and LCCR (*81*).

OCR. Typically, the performance of the CCR engine is about 20% lower than the OCR engine (*81*). The LCCR was designed to improve the drawback of the CCR engine, namely, the thermal load on the engine shaft imposed by the blow-by gas escaping the side seal system. The shaft cooling system used in the LCCR engine compensates the additional thermal loading on the shaft. The LCCR seems slightly less efficient than the OCR, but its manufacturing cost is significantly lower than the latter design.

4.6 Turbocharging and Supercharging

A turbocharged stratified-charge rotary engine is of special interest because a turbocharger allows higher power density and better efficiency (*8, 56*), particularly at higher loads and high altitudes, as shown in figure 70 (*14*). As the engine load is increased, the equivalence ratio for a naturally aspirated engine reaches to the region where $\phi > 0.7$, which is usually associated with less efficient combustion. Turbocharging delivers higher airflow, leading to lower equivalence ratios, particularly at higher loads. This delays the onset of the lower combustion efficiency with respect to engine load; therefore, the low BSFC region becomes broader, moves downward, and shifts to higher engine loads (*8*).

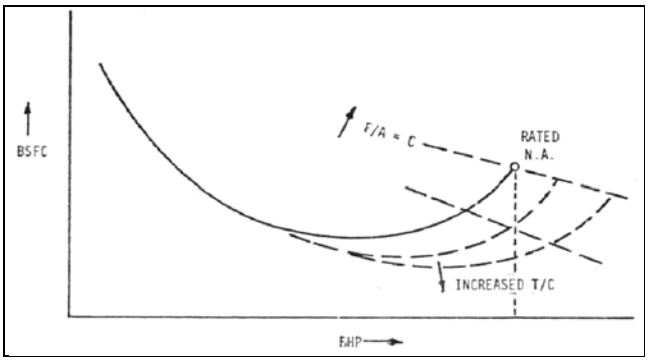

Figure 70. Theoretical turbocharging effects on BSFC (*14*).

In addition, turbocharging allows lean operation through higher airflow, which gives higher combustion efficiency in a broader operating region as well as lower specific heat rejection (*101*). This will lead to higher thermal efficiency. ISFC is almost inversely proportional to thermal efficiency except for extremely lean conditions, as shown in figure 71 (*14*). The figure clearly shows that operating at leaner conditions is more efficient if lean operation is achievable. As load increases, turbocharging can provide higher airflow accordingly, which allows leaner combustion at higher loads, leading to higher thermal efficiency. The trend in figure 71 (*14*) can predict BSFC at higher loads as the engine load is extended through turbocharging. The minimum lean limit fuel-air ratio is when increased fueling does not increase engine load at a specific boost pressure.

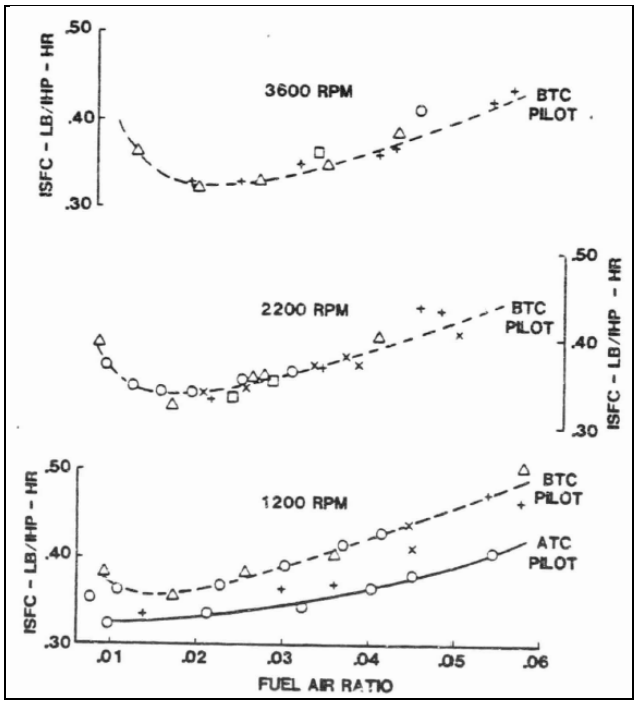

Figure 71. ISFC vs. fuel-air ratio for five different RC1-350 rotary engines (CR = 8.5:1) (*14*).

Most of all, the rotary engine has no intake and exhaust valves, which would eliminate flow restrictions and dynamic limitations. This feature leads to an increase in available exhaust energy. This exhaust energy for a turbocharger is particularly beneficial for the stratified-charge rotary engine because the engine can be boosted to a higher level without preignition. Higher boost pressures lead to higher peak firing pressures; therefore, the major parts of the engine such as rotor, rotor housing, and main bearing should be reinforced to withstand the increased peak firing pressure (*2*). Another important task when a turbocharger is employed is the optimization of the engine-turbocharger matching. The turbocharger should be matched to the engine so that the turbocharger delivers the required air quantity with optimal efficiency (*8*).

Figure 72 shows that turbocharging significantly decreases fuel-air ratio throughout the operating regime, particularly at higher loads (*14*). Specific fuel consumption also significantly decreased with turbocharging, particularly at higher loads, compared to the naturally aspirated engine.

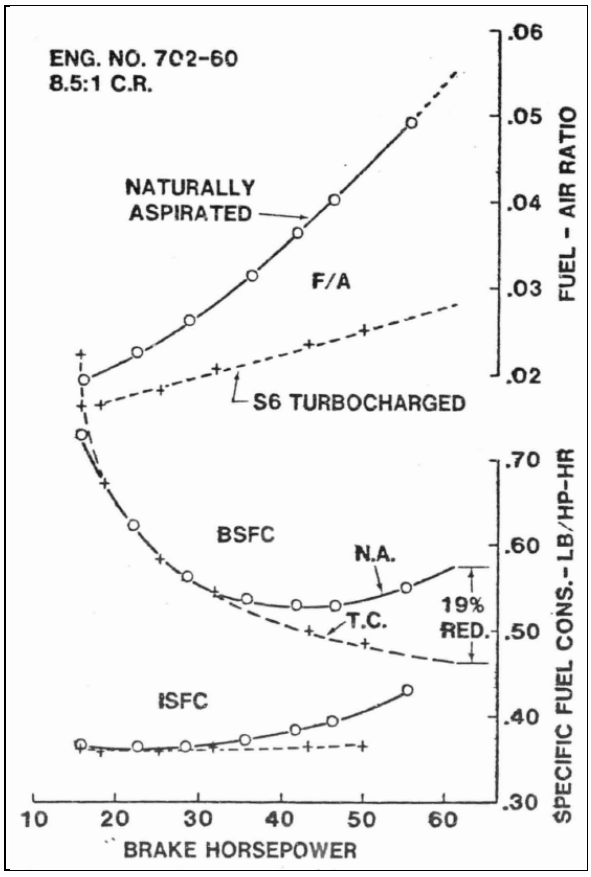

Figure 72. Fuel-air ratio and specific fuel consumption (SFC) vs. brake horsepower for RC1-60 SCRE at 4000 rpm with peripheral intake ports (CR = 8.5:1) (*14*).

Jones et al. (*14*) used turbocharging to compare dual side ports with peripheral ports. The results show that the specific "late-opening" side ports performed worse than the peripheral intake ports with higher overlap. Optimization of the side port timing was not made in this study; therefore, further research should be conducted to make a reasonable comparison with the peripheral ports.

Jones et al. also used a reduced CR (6:1) to evaluate a wider-range operation with turbocharging to avoid exceeding the peak firing pressure. Figure 73 shows that the effect of turbocharging on fuel-air ratio and specific fuel consumption is relatively larger than the CR (*14*). However, the effect of the CR on the peak firing pressure and metal temperature is huge, as shown in figure 74 (*14*). This result indicates that a lower CR is better with turbocharging. However, it should be noted that a higher CR can be used with turbocharging when the engine is operated at leaner conditions, which will lead to even higher thermal efficiency.

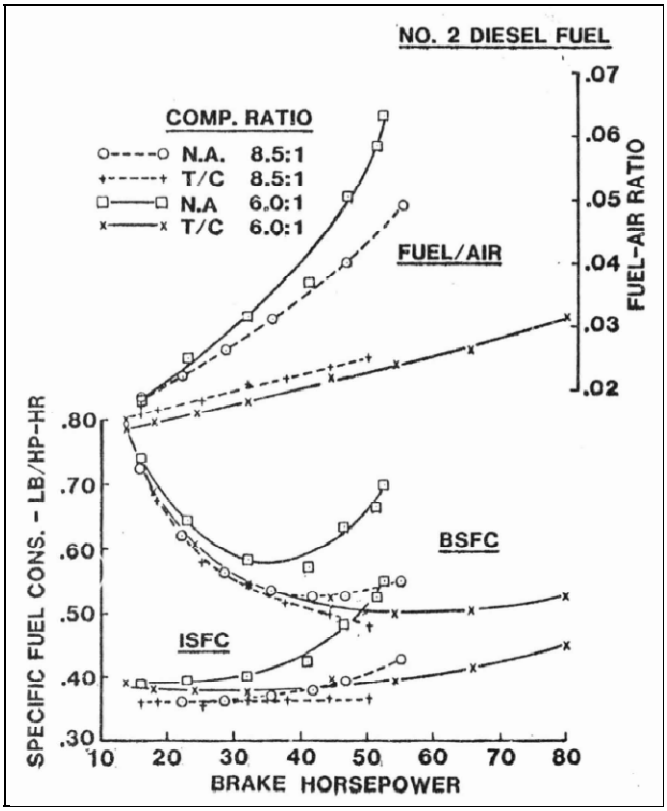

Figure 73. Fuel-air ratio and SFC vs. brake horsepower for RC1-60 SCRE at 4000 rpm with peripheral intake ports for two different CRs (*14*).

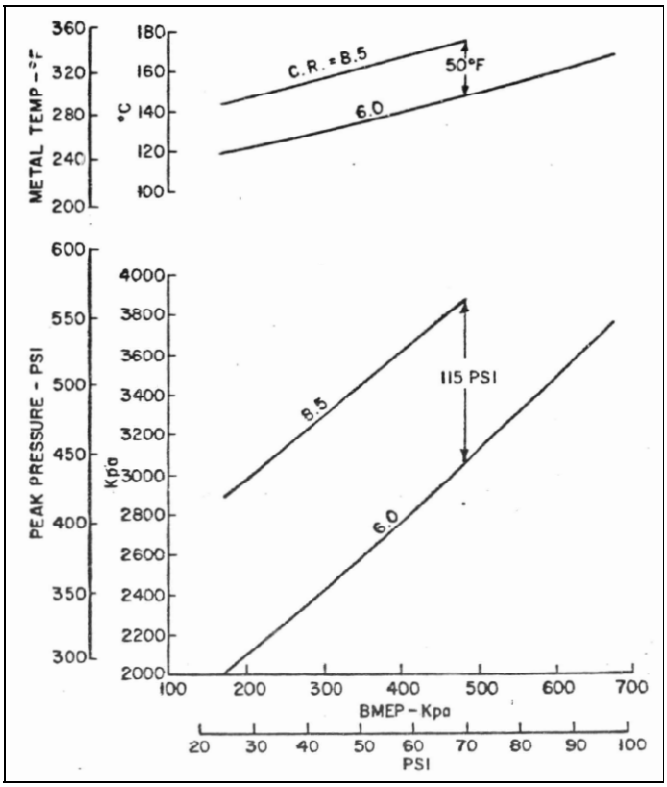

Figure 74. Peak firing pressure and metal temperature for SCRI-60T at 5000 rpm with peripheral intake ports for two different CRs (*14*).

Figure 75 (*52*) shows the effect of the intake/exhaust pressure ratio on indicated power, ISFC, exhaust temperature, and IMEP, which are the results of the computer simulation of the John Deere 1007R direct-injection stratified charge rotary engine. As the intake/exhaust pressure ratio increases, so does the engine performance compared to the naturally aspirated conditions.

Schock et al. (*102*) showed that a supercharged engine delivers higher vorticity in the intake than in a naturally aspirated engine, which enhances turbulent flow pattern during the compression stroke. Also, flow reversal was reduced in the supercharged engine. However, the blow-by loss along the surface of the housing was higher than in the naturally aspirated engine.

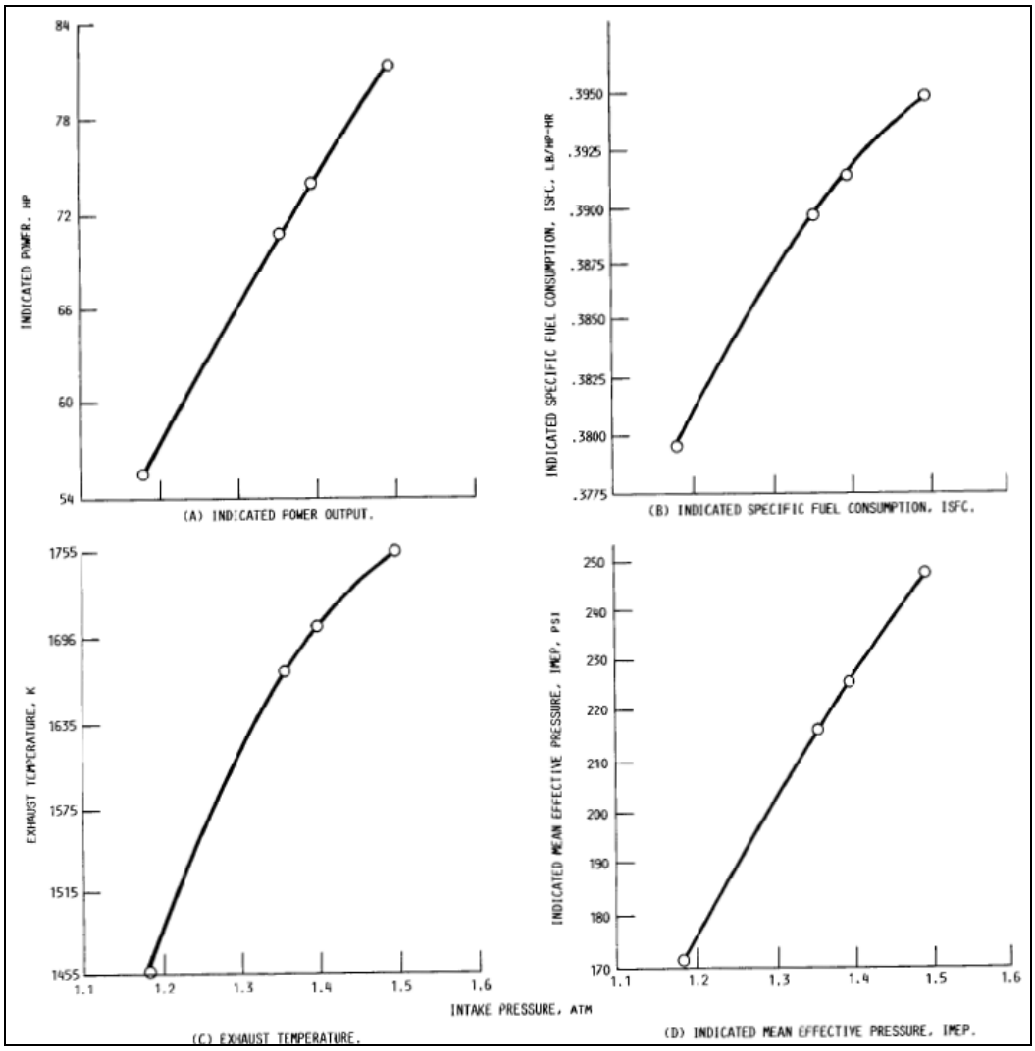

Figure 75. Effect of intake/exhaust pressure ratio (1007R rig engine, 4000 rpm, 890 kPa BMEP, exhaust pressure = 1.074 atm) (*52*).

5. Conclusions and Recommendations

This report reviewed heavy-fueled rotary engines to understand the current status of the rotary engine combustion technologies and to gain insight into technology gaps that need further research and development to improve fuel economy, power density, multifuel capability, engine startability (particularly at low temperature), and flexibility of operation in a broader range of speeds and loads of rotary engines. Recently, a rotary engine was considered one of the most promising powerplants for UAV and ground vehicles because of its high power density, compact size, light weight, and low vibration, which are becoming more important in advanced vehicles.

Rotary engines have not been thoroughly researched and developed with both experiments and simulation, particularly for heavy-fueled rotary engines, compared to the reciprocating engines. Therefore, there are significant opportunities to improve its efficiency and performance by implementing advanced fuel systems, ignition systems, control systems, sealing technologies, and system optimization.

Improving engine efficiency requires improved combustion efficiency, reduced cooling and exhaust losses, and reduced friction loss while maintaining combustion noise level below a threshold. Combustion efficiency can be improved by lean operation (i.e., $\lambda > 1$) and more complete combustion of the delivered fuel. This requires a thorough understanding of fuel spray; fuel-air mixture formation; and ignition, combustion, and emissions formation processes. A rotary engine is inherently limited for a high CR because of its geometric shape of the trochoid (i.e., small displacement volume). It needs to have external ignition sources, such as a spark or glow plug, to increase the combustion efficiency. Fuel stratification is deemed one of the best ways to achieve almost pure air near the leading and trailing sides of the combustion chamber while maintaining flammable fuel-air mixture near the spark or glow plug for efficient ignition. Lean operation can be achieved by using a turbocharger or supercharger, which will deliver higher airflow.

More complete combustion would also reduce exhaust loss by reducing unburned and incomplete combustion gases. Cooling heat loss can be reduced by optimally controlling combustion rate to reduce combustion chamber temperature and by implementing low thermal conductivity materials on the inner surfaces of the combustion chamber. Friction loss can be reduced by optimizing the seal loading and by using lower friction materials for the seals while minimizing seal wear. Friction loss can also be reduced by decreasing the seal area.

Sealing has been one of the major problems of the rotary engines. Leaks through the seals lead to lower volumetric efficiencies (both real and effective), thus decreasing engine performance. One of the major issues with the leaks is reduced effective CR, which deteriorates the ignition of the fuel-air mixture. It was shown that even modest reduction in the leakage area could result in a significant improvement in performance. The major seal factors include seal loading and wear (both the seal and the housing surface) because there are almost no gaps in the apex and side seals. Several areas have been researched and developed to reduce leakage and wear, which include new seal materials, coating materials, spray methods, different seal designs, and the addition of a new seal (i.e., cutoff seal).

Advanced 3-D in-cylinder engine simulation of a rotary engine would enable detailed investigation of air flow in the combustion chamber (including squish flow), fuel-air mixing, ignition, and combustion processes. The currently available advanced 3-D CFD software includes KIVA3v (*103, 104*), CONVERGE* (*105*), and AVL FIRE (*106*) among others. Use of

*CONVERGE is a trademark of Convergent Science, Inc.

these tools would help achieve improved charge air utilization, optimized fuel-air mixing, and combustion. The 3-D CFD simulation can also be used to optimize the location of injector, spark or glow plugs, and the number of spark or glow plugs.

Optimization of engine combustion should be performed together with turbocharging as well as fuel injector and combustion chamber designs and fuel injection strategies. These optimization efforts can be made by using advanced design of experiment and optimization tools. For the last decade, the dramatically evolving turbocharger and supercharger technologies have been driven by the development of advanced diesel engines. Engine controllers have also improved tremendously because of the rapid computer evolution, particularly for the last decade. All these advanced subsystems and control strategies have never been applied to rotary engines until now. Particularly, the development of small rotary engines is primitive because demand was low, and all these efforts until now have been made by small companies, unlike the light to heavy-duty diesel engines made by larger companies.

The following areas are required for further research and development of multifuel capable rotary engines:

- Combustion chamber design optimization, which includes rotor pocket (or recess) shape, depth, width, length, location, and pocket (or recess) volume for improved fuel-air mixing.
- Optimization of housing geometry, which includes eccentricity (e) and rotor radius (R). CR should be considered when this optimization is performed.
- Use of advanced fuel injection system with high-pressure common rail.
- Optimization of fuel injector, which includes spray angle, angle between injector holes, nozzle size, number of nozzles, and injector location.
- Fuel injection strategies, which include injection timing, multiple injections (preinjection timing, quantity, and separation time), injection pressure, and injection rate shapes.
- Spark or glow plug ignition system optimization, which includes the number of spark or glow plugs, ignition energy, spark or glow duration, spark or glow plug voltage, spark gap geometry, and the location of the spark or glow plugs. Also, various other ignition systems can be evaluated including new spark plugs (i.e., microelectrode, four-electrode wide-gap spark, or pulse plug), new glow plug, and plasma ignition.
- Spark or glow plug ignition timing optimization for various speeds and loads ranges.
- Intake and exhaust port designs for optimized intake and exhaust flow, which include peripheral and side ports. Develop ideas to implement the concepts of Atkinson and Miller cycles.
- Optimization of injector and/or spark or glow plug recess depth from the housing surface.

- Apex and side seal designs to minimize leaks and wear, which include the use of different materials and contact area. Especially, the apex seal needs improved durability.
- Methods to minimize combustion chamber heat loss to minimize flame quenching, which include the use of low thermal conductivity materials for a rotor, such as ceramic and titanium.
- Optimization of local charge stratification near spark plug or glow plug in the rotary engine.
- Use of advanced turbocharger or supercharger, which includes turbocharger or supercharger matching and optimization.
- Combustion sensing methods for closed-loop combustion control by using an in-cylinder pressure sensor, ion sensor, accelerometer, or speed sensor.

6. References

1. Mazda. *The Mazda RX-8*; Mazda media report, 2002.
2. Walker, J. W.; Mount, R. E. *The Stratified Charge Rotary Engine*; John Deere Review, John Deere Rotary Division: Waterloo, IA, 1986.
3. Alterdyne. 20–80 kW Rotary Engine Generator Sets. *Alterdyne Product Catalog* **2006**.
4. LML Korea Co., Ltd. *Wankel Rotary Engine Generator and Jatropha Bio-Diesel Combination Project*; Seoul, South Korea, 2008.
5. Jones, C. An Update of Applicable Automotive Engine Rotary Stratified Charge Developments. Society of Automotive Engineers International (SAE), SAE 820347, 1982.
6. Jones, C.; Lamping, H. Curtiss-Wright's Development Status of the Stratified Charge Rotating Combustion Engine. Society of Automotive Engineers International (SAE), SAE 710582, 1971.
7. Mount, R. *Advanced Propulsion Systems Study for General Aviation Aircraft*; NASA CR-212334; National Aeronautics and Space Administration: Cleveland, OH, 2003.
8. Willis, E. A.; McFadden, J. J. *NASA's Rotary Engine Technology Enablement Program - 1983 Through 1991*; SAE 920311/NASA-TM-105562; National Aeronautics and Space Administration: Cleveland, OH, 1992.
9. Mazda Web site. Hydrogen Rotary Engine. http://www.mazda.com/mazdaspirit/env/hybrid/hre.html (accessed 16 July 2010).
10. Widener, W. K. A Survey of Technology for Hybrid Vehicle Auxiliary Power Units; TFLRF No. 311, interim report; Southwest Research Institute: San Antonio, TX, 1995.
11. Edmunds Web site. Volt II - A $5,000 Battery Pack and a Rotary Engine Range Extender? http://blogs.edmunds.com/greencaradvisor/2010/05/volt-ii---a-5000-battery-pack-and-a-rotary-engine-range-extender.html (accessed 16 July 2010).
12. Rotapower Web site. The World's Most Advanced and Cleanest Hybrid Engine for Electric Cars Is Ready for Production. http://www.rotapower.net/Rotapower2010 (accessed 16 July 2010).
13. Griffis, C.; Wilson, T.; Schneider, J.; Pierpont, P. Unmanned Aircraft System Propulsion Systems Technology Survey; DOT/FAA/AR-09/11; U.S. Department of Transportation, Federal Aviation Administration: Washington, DC, 2009.

14. Jones, C.; Ellis, D. R.; Meng, P. R. *Multi-Fuel Rotary Engine for General Aviation Aircraft*; NASA-TM-85428; National Aeronautics and Space Administration: Cleveland, OH, 1983.

15. Kagawa, R.; Okazaki, S.; Somyo, N.; Akagi, Y. A Study of a Direct-Injection Stratified-Charge Rotary Engine for Motor Vehicle Application. Society of Automotive Engineers International (SAE), SAE 930677, 1993. .

16. McCoy, C. D.; Réville, J.; Limtiaco, J.; Hopcroft, M.; Pisano, A. P. *Fuel-Flexible Engines for Portable-Power Applications*; final report for contract W911NF-07-1-0432; U.S. Army Research Office: Research Triangle Park, NC, 2009.

17. Shimizu, R.; Tadokoro, T.; Nakanishi, T.; Funamoto, J. Mazda 4-Rotor Rotary Engine for the Le Mans 24-Hour Endurance Race. Society of Automotive Engineers International (SAE), SAE 920309, 1992.

18. Liu, Y.; Li, W.; Yang, C.; Song, R. Design and Test of Small-Scale Rotary Engine Power System. *Proceedings of MNC2007, MicroNanoChina07, MNC2007-21194*, Hainan, China, 2007.

19. Yamamoto, K. *Rotary Engine*; Sankaido Co., Ltd.: Tokyo, Japan, 1981.

20. Izweik, H. T. CFD Investigations of Mixture Formation, Flow and Combustion for Multi-Fuel Rotary Engine. Ph.D. Dissertation, Brandenburg Technical University at Cottbus, Libya, 2009.

21. Ohkubo, M.; Tashima, S.; Shimizu, R.; Fuse, S.; Ebino, H. Developed Technologies of the New Rotary Engine (RENESIS). Society of Automotive Engineers International (SAE), SAE 2004-01-1790, 2004.

22. Norman, T. J. A Performance Model of a Spark Ignition Wankel Engine: Including the Effects of Crevice Volume, Gas Leakages, and Heat Transfer. M.S. Thesis, Massachusetts Institute of Technology, Cambridge, MA, 1983.

23. Niedzwiecki, R. W. *Small Engine Technology Programs*; 19920013289; National Aeronautics and Space Administration: Cleveland, OH, 1987.

24. Irion, C. E.; Mount, R. E. *Stratified Charge Rotary Engine Critical Technology Enablement Volume I*; NASA Contractor Report 189106: National Aeronautics and Space Administration: Cleveland, OH, 1992.

25. Roberts, J. M. Heat Release Estimation and Prediction of Wankel Stratified-Charge Combustion Engine. M.S. Thesis, Massachusetts Institute of Technology, Cambridge, MA, 1985.

26. Jandhyala, A. S.; Paliwal, R.; Varun, G. S. An Insight Into the Methodology of the Hydro Wankel Cell. Proceedings of the ASME Heat Transfer/Fluids Engineering Summer Conference, Charlotte, NC, 2004.

27. Jandhyala, A. S.; Muffakham, J. A Design of the Hydro Wankel Cell. Fédération Internationale des Sociétés d'Ingénieurs des Techniques de l'Automobile (FISITA): Barcelona, Spain, 2004.

28. Alaküla, M.; Jonasson, K.; Andersson, C.; Simonsson, B. Hybrid Drive Systems for Vehicles: Part 1 System Design and Traction Concepts. Course material for the course "Hybrid Drive Systems for Vehicles" given by the Royal Institute of Technology (KTH), Chalmers University of Technology (CTH) and Lund University (LTH), 2006.

29. Ganesan, V. *Internal Combustion Engines*; McGraw-Hill, Inc.: New Delhi, India, 2007.

30. Mazda Web site. Miller-Cycle Engine. http://www.mazda.com/mazdaspirit/env/engine /miller.html (accessed 13 January 2011).

31. Epstein, A. H.; Senturia, S. D.; Anathasuresh, G.; Ayon, A.; Breuer, K.; Chen, K-S.; Ehrich, F. E.; Gauba, G.; Ghodssi, R.; Groshenry, C. Power MEMS and Microengines. International Conference on Solid-State Sensors and Actuators, Chicago, IL, June 1997.

32. Jiang, K. C.; Prewett, P. D.; Ward, M. C. L.; Tian, Y.; Yang, H. Design of a Micro-Wankel Rotary Engine for MEMS Fabrication. *Proceedings of SPIE*, 2001; Vol. 4407.

33. Fu, K.; Knobloch, A.; Martinez, F.; Walther, D. C.; Fernandez-Pello, A. C.; Pisano, A. P.; Liepmann, D. Design and Fabrication of a Silicon-Based MEMS Rotary Engine. *Proceedings of 2001 ASME International Mechanical Engineering Congress and Exposition (IMECE)*, New York, NY, 11–16 November 2001; IMECE2001/MEMS-23925, 2001.

34. Heppner, J. D.; Walther, D. C.; Pisano, A. P. Leakage Flow Analysis for a MEMS Rotary Engine. *Proceedings of the ASME International Mechanical Engineering Congress and Exposition*, Washington, DC, 15–21 November 2003; Micro-Electromechanical Systems Division Publication (MEMS), Vol. 5, Micro-Electro-Mechanical Systems (MEMS), IMECE2003-41868; pp 327–334.

35. Martinez, F. C.; Knobloch, A. J.; Pisano, A. P. Apex Seal Design for the MEMS Rotary Engine Power System. *Proceedings of 2003 ASME International Mechanical Engineering Congress and Exposition (IMECE)*, IMECE2003-42071, Washington, DC, 2003, 157–162.

36. Jacobson, S. A.; Epstein, A. H. An Informal Survey of Power MEMS. The International Symposium on Micro-Mechanical Engineering (ISMME), ISMME2003-K18, Tsuchiura and Tsukuba, Japan, 2003.

37. Knobloch, A. J.; Wasilik, M.; Fernandez-Pello, C.; Pisano, A. P. Micro Internal-Combustion Engine Fabrication With 900 mm Deep Features via DRIE. *Proceedings of 2003 ASME International Mechanical Engineering Congress and Exposition (IMECE),* IMECE2003-42558, Washington, DC, 2003.

38. Walther, D. C.; Pisano, A. P. MEMS Rotary Engine Power System: Project Overview and Recent Research Results. *Proceedings of the 4th International Symposium on MEMS and Nanotechnology,* 2003; pp 227–234.

39. Lee, C. H.; Jiang, K. C.; Jin, P.; Prewett, P. D. Design and Fabrication of a Micro Wankel Engine Using MEMS Technology. *Microelectronic Engineering* **2004**, *73–74*, 529–534.

40. Sprague, S. B.; Park, S.-W.; Walther, D. C.; Pisano, A. P.; Fernandez-Pello, A. C. Development and Characterization of Small-Scale Rotary Engines. *International Journal of Alternative Propulsion* **2007**, *1* (2–3), 275–293.

41. Moller International. *A Powerful New Engine,* 2001. http://www.moller.com/ and http://www.sti.nasa.gov/tto/spinoff2001/t2.html (accessed 9 March 2011).

42. Donaldson, P. Heavy-Fuel Engines (HFE): Fuelling Competition. *Unmanned Vehicles* **August and September 2009**, *14* (4), 22–25.

43. UAV Engine, Ltd. Product Catalog. AR741-38 hp for Small Surveillance UAVs, 2010.

44. Cubewano, Ltd. Product Catalog. Sonic Range – UAV Engines, 2010.

45. Oron, H. UAV Engines in the Next Decade - Turbine Engines, Piston Engines and the Newly Combat Proven Rotary Engine. A Lecture at the 6th Symposium on Jet Engines and Gas Turbines, Haifa, Israel, 16 November 2006.

46. Tomorrow's Technician Web site. Chapter 1: Rotary Engine Operation: Structure and Working Principles of the Rotary Engine. http://www.tomorrowstechnician.com (accessed 9 March 2011).

47. Weston, K. C. *Energy Conversion – EBook*. The University of Tulsa: Tulsa, OK, 1992.

48. Jean, G. V. Army's Shadow Unmanned Aircraft Receiving Upgrades for Longer Missions. *National Defense Magazine* [Online] **February 2010**, http://www.nationaldefensemagazine .org/archive/2010/February (accessed 9 March 2011).

49. Froede, W. G. The NSU-Wankel Rotating Combustion Engine. Society of Automotive Engineers International (SAE), SAE 610017, 1961.

50. Abraham, J.; Magi, V. *Effects of Ignition Cavity Flows on the Performance of a Stratified-Charge Rotary Engine: Initial 3-D Predictions*; University of Minnesota Supercomputer Inst Res Report, UMSI 93/262; University of Minnesota/University of Reggio: Minneapolis, MN/Calabria, Italy, 1993.

51. Heywood, J. B. *Internal Combustion Engine Fundamentals*; McGraw-Hill, Inc.: New York, 1988.

52. Nguyen, H. L. *Performance and Combustion Characteristics of Direct-Injection Stratified-Charge Rotary Engines*; NASA-TM-100134; National Aeronautics and Space Administration: Cleveland, OH, 1987.

53. Eiermann, D.; Nuber, R.; Breuer, J.; Soimar, M.; Gheorghiu, M. An Experimental Approach for the Development of a Small Spark Assisted Diesel Fueled Rotary Engine. Society of Automotive Engineers International (SAE), SAE 930683, 1993.

54. Muroki, T.; Moriyoshi, Y.; Takagi, M. Combustion Characteristics of a Direct Injection Stratified Charge Rotary Engine Using Spark Ignition and Pilot Flame Ignition Systems. Society of Automotive Engineers International (SAE), SAE 2002-32-1791, 2002.

55. Abraham, J.; Bracco, F. V. 3-D Computations to Improve Combustion in a Stratified-Charge Rotary Engine - Part II: A Better Spray Pattern for the Pilot Injector. Society of Automotive Engineers International (SAE), SAE 892057/SAE Trans., 1989; Vol. 98.

56. Meng, P. R.; Rice, W. J.; Schock, H. J.; Pringle, D. P. Preliminary Results on Performance Testing of a Turbocharged Rotary Combustion Engine. Society of Automotive Engineers International (SAE), SAE 820354, 1982.

57. Muroki, T.; Moriyoshi, Y. Combustion Characteristics of Spark-Ignition and Pilot Flame Ignition Systems in a Motored Wankel Stratified Charge Engine. *Journal of Automobile Engineers* **2000**, *214*, 949–955.

58. Muroki, T.; Moriyoshi, Y.; Takagi, M.; Suzuki, K.; Imai, M. Research and Development of a Direct Injection Stratified Charge Rotary Engine With a Pilot Flame Ignition System. Society of Automotive Engineers International (SAE), SAE 2001-01-1844, 2001.

59. Burley, H. A.; Meloeny, M. R.; Stark, T. L. Sources of Hydrocarbon Emissions in Rotary Engines. Society of Automotive Engineers International (SAE), SAE 780419, 1978.

60. Balles, E. N.; Ekchian, J. A.; Heywood, J. B. Fuel Injection Characteristics and Combustion Behavior of Direct-Injection Stratified Charge Engine. Society of Automotive Engineers International (SAE), SAE 841379, 1984.

61. Jones, C. A New Source of Lightweight, Compact, Multiful Power for Vehicular Light Aircraft and Auxilliary Applications-The John Deere SCORE Engine. The 33rd ASME International Gas Turbine and Aeroengine Congress and Exposition, ASME 88-GT-194, ASME Paper 88-GT-271, Amsterdam, the Netherlands, 1988.

62. Mount, R. E.; LaBouff, G. A. Advanced Stratified-Charge Rotary Engine Design. Society of Automotive Engineers International (SAE), SAE 890324, 1989.

63. Shih, T. I-P.; Yang, S. L.; Schock, H. J. *A Two-Dimensional Numerical Study of the Flow Inside the Combustion Chamber of a Motored Rotary Engine*; NASA-TM-87212; National Aeronautics and Space Administration: Cleveland, OH, 1986.

64. Nagao, A.; Ohzeki, H.; Niura, Y. Present Status and Future View of Rotary Engines. *Proceedings of the International Symposium on Alternative and Advanced Automotive Engines*, Vancouver, British Columbia, Canada, 1987; 183–201.

65. Kamo, R.; Yamada, T. Y.; Hamada, Y. Starting Low Compression Ratio Rotary Wankel Diesel Engine. Society of Automotive Engineers International (SAE), SAE 870449, 1987.

66. Abraham, T.; Wey, M. J.; Bracco, F. V. Pressure Non-Uniformity and Mixing Characteristics in Stratified-Charge Rotary Engine Combustion. Society of Automotive Engineers International (SAE), SAE 880624, 1988.

67. Abraham, J.; Bracco, F. V.; Epstein, P. 3-D Computations to Improve Combustion in a Stratified-Charge Rotary Engine - Part IV: Modified Geometries. Society of Automotive Engineers International (SAE), SAE 930679, 1993.

68. Yasuaki, H.; Kouichi, Y. An Experimental Investigation on Air-Fuel Mixture Formation Inside a Low-Pressure Direct Injection Stratified Charge Rotary Engine. Society of Automotive Engineers International (SAE), SAE 930678, 1993.

69. Ma, H. L.; Kuo, C. H.; Chen, C. C. Chamber Contour Design and Compression Flow Calculations of Rotary Engine. *Journal of C.C.I.T.* **May 2010**, *39* (1), 35–50.

70. Jones, C.; Lamping, H. D.; Myers, D. M.; Loyd, R. W. An Update of the Direct Injected Stratified Charge Rotary Combustion Engine Developments at Curtiss-Wright. Society of Automotive Engineers International (SAE), SAE 770044, 1977.

71. Abraham, J.; Bracco, F. V. Fuel-Air Mixing and Distribution in a Direct-Injection Stratified-Charge Rotary Engine. Society of Automotive Engineers International (SAE), SAE 890329, 1989.

72. Hoffman, T.; Mack, J.; Mount, R. *Two Rotor Stratified Charge Rotary Engine (SCRE) Engine System Technology Evaluation*; NASA-CR-195395; National Aeronautics and Space Administration: Cleveland, OH, 1994.

73. Mashayek, F. STTR Phase I: *Electrostatic Atomizing Fuel Injector for Small Scale Engines*; Report No. EES-DD0010; U.S. Army Research Office: Research Triangle Park, NC, 2008.

74. Kinetic BEI. Introducing Micro Fuel Injectors for Small Heavy Fuel Engines. Micro Fuel Injection Product Sheet 2-10 R3; South Elgin, IL, 2010.

75. Kinetic BEI. Introducing Micro Fuel Pumps for Small Heavy Fuel Engines. Micro Fuel Pump product sheet 2-10 R3; South Elgin, IL, 2010.

76. Husted, H. L.; Piock, W.; Ramsay, G. Fuel Efficiency Improvements From Lean, Stratified Combustion With a Solenoid Injector. Society of Automotive Engineers International (SAE), SAE 2009-01-1485, 2009.

77. Yi, J.; Wooldridge, S.; Coulson, G.; Hilditch, J.; Iyer, C. O.; Moilanen, P.; Papaioannou, G.; Reiche, D.; Shelby, M.; VanDerWege, B.; Weaver, C.; Xu, Z.; Davis, G.; Hinds, B.; Schamel, A. Development and Optimization of the Ford 3.5L V6 EcoBoost Combustion System. Society of Automotive Engineers International (SAE), SAE 2009-01-1494, 2009.

78. Tomorrow's Technician Web site. Technical Highlights of the RENESIS Rotary Engine, Tomorrow's Technician training material, 2007. http://www.tomorrowstechnician.com /Issue/ (accessed 9 March 2011).

79. Willis, E. A.; McFadden, J. J. *Rotary Engine Technology*; NASA Report 1991010801; National Aeronautics and Space Administration: Cleveland, OH, 1991.

80. Abraham, J.; Bracco, F. V. 3-D Computations to Improve Combustion in a Stratified-Charge Rotary Engine - Part III: Improved Ignition Strategies. Society of Automotive Engineers International (SAE), SAE 920304/SAE Trans., 1992; Vol. 101.

81. Eiermann, D.; Nuber, R.; Soimar, M. The Introduction of a New Ultra-Lite Multipurpose Wankel Engine. Society of Automotive Engineers International (SAE), SAE 900035, 1990.

82. Andersson, P.; Tamminen, J.; Sandströ, C. E. Piston Ring Tribology: A Literature Survey; Research Notes 2178; VTT Tiedotteita, 2002.

83. Eberle, M. K.; Klorap, E. D. An Evaluation of the Potential Gain From Leakage Reduction in Rotary Engines. Society of Automotive Engineers International (SAE), SAE 730117, 1973.

84. Nguyen, H. L.; Addy, H. E.; Bond, T. H.; Lee, C. M.; Chun, K. S. Performance and Efficiency Evaluation and Heat Release Study of a Direct-Injection Stratified-Charge Rotary Engine. Society of Automotive Engineers International (SAE), SAE 870445, 1987.

85. Kohno, T.; Ito, R.; Morita, M.; Mizuno, N. Analysis of Light-Load Performance in Rotary Engines. Society of Automotive Engineers International (SAE), SAE 790435, 1979.

86. Knoll, J.; Vilmann, C. R.; Schock, H. J., Stumpf, R. P. A Dynamic Analysis of Rotary Combustion Engine Seals. Society of Automotive Engineers International (SAE), SAE 840035, 1984.

87. Lamping, H. D.; Galliers, M. W.; Wolosin, S. M. Rotary Combustion Engine Trochoid Coatings and Seals. Society of Automotive Engineers International (SAE), SAE 741043, 1974.

88. Yamamoto, K.; Muroki, T. Development on Exhaust Emissions and Fuel Economy of the Rotary Engine at Toyo Kogyo. Society of Automotive Engineers International (SAE), SAE 780417, 1978.

89. Fu, K.; Knobloch, A. J.; Martinez, F. C.; Walther, D. C.; Fernandez-Pello, C.; Pisano, A. P.; Liepmann, D.; Miyasaka, K.; Maruta, K. Design and Experimental Results of Small-Scale Rotary Engines. *Proceedings of International Mechanical Engineering Congress and Exposition*, New York, NY, 2001.

90. Ansdale, R. F. *The Wankel RC Engine: Design and Performance*; A. S. Barnes & Company: London, 1969.

91. Martinez, F. C.; Knobloch, A. J.; Pisano, A. P. Apex Seal Design for the MEMS Rotary Engine Power System. *Proceedings of 2003 ASME International Mechanical Engineering Congress and Exposition (IMECE),* IMECE2003-42071, 2003; pp 157–162.

92. Tadokoro, A.; Tatsutomi, Y.; Ozeki, H.; Tadokoro, A. Present and Prospective Technologies of Rotary Engine. Society of Automotive Engineers International (SAE), SAE 870446, 1987.

93. Kuo, K. K. *Principles of Combustion*; John Wiley and Sons: Hoboken, NJ, 1986.

94. Boust, B.; Sotton, J.; Labuda, S. A.; Bellenoue, M. A Thermal Formulation for Single-Wall Quenching of Transient Laminar Flames. *Combustion and Flame* **2007**, *149*, 286–294.

95. Warnatz, J.; Maas, U.; Dibble, R.W. *Combustion*; Springer Berlin – Heidelberg: Berlin, Germany, 2006.

96. Borman, G. L.; Ragland, K. W. *Combustion Engineering*; McGraw-Hill, Inc.: Singapore, China, 1998.

97. Woschini, G. A Universally Applicable Equation for the Instantaneous Heat Transfer Coefficient in the Internal Combustion Engine. Society of Automotive Engineers International (SAE), SAE 670931/SAE Trans, 1967; Vol. 76.

98. Lee, C. M.; Schock, H. J. *Regressed Relations for Forced Convection Heat Transfer in a Direct Injection Stratified Charge Rotary Engine*; NASA-TM-100124; National Aeronautics and Space Administration: Cleveland, OH, 1988.

99. Giovanetti, A. J.; Ekchian, J. A.; Heywood, J. B. Analysis of Hydrocarbon Emissions Mechanisms in a Direct Injection. Society of Automotive Engineers International (SAE), SAE 830587, 1983.

100. Moller, P. S. *Evaluation of Thermal Barrier and Self-Lubricating Coatings in an Air-Cooled Rotary Engine*; NASA-CR-195445; National Aeronautics and Space Administration: Cleveland, OH, 1995.

101. Stokes, J.; Lake, T. H.; Osborne, R. J. A Gasoline Engine Concept for Improved Fuel Economy – The Lean Boost System. Society of Automotive Engineers International (SAE), SAE 2000-01-2902, 2000.

102. Schock, H.; Hamady, F.; Somerton, C. *Stratified Charge Rotary Engine Combustion Studies*; NASA-CR-197985; National Aeronautics and Space Administration: Cleveland, OH, 1989.

103. Amsden, A. A. *KIVA-3V: A Block-Structured KIVA Program for Engines With Vertical or Canted Valves*; DOE LA-13313-MS; Los Alamos National Laboratory: Los Alamos, NM, 1997.

104. Amsden, A. A. *KIVA-3V, Release 2, Improvements to KIVA-3V*; DOE LA-UR-99-915; Los Alamos National Laboratory: Los Alamos, NM, 1999.

105. Convergent Science Web site. CONVERGE™ CFD Software. http://convergecfd.com/ (accessed 13 June 2010).

106. AVL Web site. AVL FIRE® - Computational Fluid Dynamics (CFD) for Conventional and Alternative Powertrain Development. https://www.avl.com/fire (accessed 13 June 2010).

List of Symbols, Abbreviations, and Acronyms

2-D	two dimensional
3-D	three dimensional
AFR	air-fuel ratio
AGNI-3D	Sverdrup Technology CFD code name
bhp	brake horsepower (= BHP)
BMEP	brake mean effective pressure
BSFC	brake-specific fuel consumption
bTC	before top center
CA	crank angle
CCR	charge-cooled rotor
cermet	composite material composed of ceramic (cer) and metallic (met) materials
CFD	computational fluid dynamics
CI	compression ignition
cc	cubic centimeter
CR	compression ratio
DI-SCRE	direct-injection stratified-charge rotary engines
EGR	exhaust gas recirculation
e/R	eccentricity ratio
η_{Otto}	thermal efficiency of Otto cycle engine
ϕ	diameter, equivalence ratio
f	normalized friction
FIRE	AVL 3-D CFD program package
GDi	gasoline direct injection
h	hour
hp	horsepower

IMEP	indicated mean effective pressure
ISFC	indicated specific fuel consumption
ISHC	indicated specific hydrocarbon emissions
φ	working chamber leading angle
JP	jet propellant
K	trochoid constant (= R/e), Kelvin (a temperature unit)
K-ε	turbulent kinetic energy and its dissipation rate equations
KKM	Kreiskolbenmotor means “rotary engine” in German
kPa	kilopascal
kV	kilovolt
L	liters, leading
lb	pounds
LCCR	liquid- and charge-cooled rotor
LR	leading rectangular
LS	leading standard
MEMS	Micro Electro-Mechanical System
mJ	millijoule
ms	millisecond
NASA	National Aeronautics and Space Administration
NGK	Nihon Gaishi Kaisha
NSU	German manufacturer of cars, motorcycles, and pedal cycles—currently Audi
Nu	Nusselt number
OCR	oil-cooled rotor
OMC	Outboard Marine Corporation
OPEC	Organization of the Petroleum Exporting Countries
P	pressure
PFP	peak firing pressure

θ	rotor included angle, angle between holes
γ	specific heat ratio (= Cp/Cv)
R	rotor radius or generating radius
Re	Reynolds number
RENESIS	Rotary Engine's geNESIS (Mazda rotary engine, first production in 2004 Mazda RX-8)
rpm	revolution per minute
R26B	Mazda rotary engine model (V_d = 2622 cc, 522 kW @ 9000 rpm)
RX-7	Mazda sports car, equipped with a 1146 cc twin-rotor Wankel rotary engine
RX-8	Mazda sports car, successor to the RX-7
SCORE	stratified charged omnivorous rotary engine
SCRE	stratified-charge rotary engine
T	temperature, trailing
T_b	bulk gas temperature
TBC	thermal barrier coating
TC	top center
TDC	top dead center
T_f	film temperature
UAV	unmanned aerial vehicle
UEL	UAV Engine Ltd.
v	local gas velocity, cross-sectional velocity
V_d	displacement volume or stroke volume, droplet velocity
V_t	sum of the combustion chamber pocket (or recess) and spark plug hole volumes

NO. OF COPIES	ORGANIZATION
1 (PDF only)	DEFENSE TECHNICAL INFORMATION CTR DTIC OCA 8725 JOHN J KINGMAN RD STE 0944 FORT BELVOIR VA 22060-6218
1	DIRECTOR US ARMY RESEARCH LAB IMNE ALC HRR 2800 POWDER MILL RD ADELPHI MD 20783-1197
1	DIRECTOR US ARMY RESEARCH LAB RDRL CIM L 2800 POWDER MILL RD ADELPHI MD 20783-1197
1	DIRECTOR US ARMY RESEARCH LAB RDRL CIO MT 2800 POWDER MILL RD ADELPHI MD 20783-1197
1	DIRECTOR US ARMY RESEARCH LAB RDRL D 2800 POWDER MILL RD ADELPHI MD 20783-1197

NO. OF
COPIES ORGANIZATION

2 NASA GLENN
RDRL VT
P MEITNER
M VALCO
BLDG 21
CLEVELAND OH 44135-3191

1 NASA GLENN
RDRL VTP
W ACOSTA
BLDG 21
CLEVELAND OH 44135-3191

1 NASA GLENN
RDRL VTP
A KASCAK
BLDG 49
CLEVELAND OH 44135-3191

1 NASA GLENN
RDRL VTP
S MINTZ
BLDG 23
CLEVELAND OH 44135-3191

1 NASA GLENN
RDRL VTP
A OWEN
BLDG 142
CLEVELAND OH 44135-3191

ABERDEEN PROVING GROUND

2 DIR USARL
RDRL VTP
B HUFFMAN
BLDG 1120B
RDRL VTV
J GERDES
BLDG 517

INTENTIONALLY LEFT BLANK.